SYSTEMS TECHNOLOGY, INC.
Inglewood, California

TECHNICAL REPORT NO. 137-1

AN ANALYSIS OF TERMINAL FLIGHT PATH CONTROL IN CARRIER LANDING

TULVIO S. DURAND
GARY L. TEPER

AUGUST 1964

PERFORMED UNDER
CONTRACT NO. Nonr-4156(00)
FOR
OFFICE OF NAVAL RESEARCH
DEPARTMENT OF THE NAVY
WASHINGTON, D. C.

ABSTRACT

A mathematical model is formulated for the ship/FLOLS/pilot/aircraft system, considering deck motions and air turbulence inputs. Performance of this model in terms of terminal conditions in the vertical plane (ramp clearance, impact velocity, dispersion of the touchdown point) and aircraft longitudinal motions in the groove prior to touchdown is consistent with and validated by actual performance. The terminal dispersions are statistically combined to yield probabilities of potential ramp strikes, landing gear failures, and bolters, which, when put through a simplified pilot/LSO decision model, yield probabilities of successful pass, bolter rate, and accident rate. Again, these rates are consistent with actual experience and are used as criteria for evaluating various competing systems.

The effects on landing performance of variations in piloting technique, FLOLS stabilization methods, intensity and spectral form of ship motions, and gust inputs are computed. The variations tested and their resulting relative performance are described. Tentative conclusions are drawn from the analysis relating to possible improvements to the present operational recovery system.

FOREWORD

The study documented in this report was jointly sponsored by the Office of Naval Research and the Bureau of Naval Weapons under Contract Nonr 4156(00). Mr. G. Flohil of the Office of Naval Research was the contract monitor, and Mr. Tulvio Durand was the project engineer for Systems Technology, Inc.

The authors gratefully acknowledge the assistance of their colleagues on certain technical specialties: Mr. David H. Weir on ship motion characteristics; Mr. Walter A. Johnson on FLOLS kinematics; Mr. Robert L. Stapleford on adjoint method computations; and Mr. Irving Ashkenas on virtually all aspects of the problem. The authors are additionally indebted to Mr. G. Flohil (ONR) and LCDR T. Porter (BuWeps) for their efforts in obtaining reports useful to this project, and for their and Mr. Charles H. Cromwell III's (BuWeps) review of the draft report and suggested clarifying improvements.

CONTENTS

FIGURES

TABLES

NOMENCLATURE

$A^{h_B}_{q_s}$	Range-dependent beam vertical translation due to ship motion, q_s
$B^{h_B}_{q_s}$	Range-independent beam vertical translation due to ship motion, q_s
C	Generalized constant
CVA	Attack carrier class
db	Decibel $\equiv 20 \log_{10} \lvert\ \rvert$; db (power) $\equiv 10 \log_{10} \lvert\ \rvert$
F, f	Function of
FLOLS	Fresnel lens optical landing system
h	Altitude
h_B	Beam height
h'_B	Beam height with compensated-meatball system
h'_ϵ	Pilot-interpreted altitude error using FLOLS (see Fig. 1, p. 3)
h_R	Vertical motion of the ramp
Δh_R	Aircraft's height error when passing the ramp (see Eq A-9, p. 77)
h_{TD}	Vertical motion of the touchdown point
Δh_{TD}	Aircraft's height error when passing the nominal touchdown point (see Eq A-10, p. 77)
j	$\sqrt{-1}$
K	Open-loop gain; the frequency-invariant portion of a transfer function as $s \rightarrow 0$, particularized by subscript
K_p	Pilot's gain
K_{δ_p}	Pilot's gain in $q \rightarrow \delta$ loop
L_R	Ship dimension (see Fig. A-4, p. 78)
LSO	Landing safety officer
NH	Without heave compensation

$N_{q_{i\delta_e}}$, $N_{q_{i\delta_T}}$	Numerator of q_i/δ_e or q_i/δ_T transfer function, particularized by substituting motion quantity involved for q_i
$N_{q_{iu_g}}$, $N_{q_{iw_g}}$	Numerator of gust transfer function, particularized by substituting motion quantity involved for q_i
$N_{\delta_e\delta_T}^{q_i q_j}$	Coupling numerator, particularized by substituting motion quantities involved for q_i, q_j
P	Probability function, particularized by subscript
q	Generalized motion quantity
R	Range
RMS, rms	Root mean square value
s	Laplace operator, $\sigma + j\omega$
t	Time
u	Linear perturbed velocity along the X axis
U_o	Linear steady-state velocity along X axis
U_R	Ground speed of approaching aircraft (see Eq A-12, p. 79)
U_s	Ship's forward speed
V_I	Impact velocity
ΔV_I	Aircraft's impact velocity in excess of nominal (see Eq A-11, p. 77)
w	Linear perturbed velocity along Z axis
W	Natural wind speed
WOD	Wind-over-deck speed
WH	With heave compensation
W.N.	White noise
x	Distance along angled deck
x_m	Distance from FLOLS to apparent meatball (see Fig. 1, p. 3)
Δx_{TD}	Aircraft's error along the angled deck at impact
Y_p	Pilot's describing function (see Eq 1, p. 7)

Y_R	Ship dimension (see Fig. A-4, p. 78)
Y_{TD}	Ship dimension (see Fig. A-4, p. 78)
z	Generalized variable
α	Angle of attack
β_o	FLOLS beam angle relative to the deck
γ	Flight path angle
δ	Control deflection
Δ	Incremental change
$\Delta(s)$	Denominator of airframe transfer functions; characteristic equation when set equal to zero
ϵ	Error
ζ	Damping ratio
θ	Pitch angle
σ	Real part of Laplace operator, s
σ	Standard deviation, root mean square value
τ	Time constant
φ	Roll angle
Φ	Power spectral density
ψ_d	Deck angle to ship centerline (see Fig. A-4, p. 78)
ω	Frequency, rad/sec
α, θ, h, u, w	Pertaining to control of the variable indicated, as in A_θ, K_{p_h}, etc.
α, δ_e, δ_T, q, u, u_g, w, w_g	Indicates partial derivative, e.g., $M_w = \partial M/\partial W$, $Z_{\delta_T} = \partial Z/\partial \delta_T$

Special Subscripts

a	Aircraft	M	Margin
B	Beam	o	Nominal, at t = 0
c	Command	p	Phugoid
e	Elevator	R	Ramp
ϵ	Error	REF	Reference
g	Gust	s	Ship
L	Lens or FLOLS	T	Throttle
min	Minimum	TD	Touchdown

Mathematical Signs

^{o}	Degree
∂	Partial derivative
$\doteq$	Approximately equals
$(\dot{})$	Time derivative
$(\bar{})$	Mean, nominal
$\lvert\ \rvert$	Magnitude
$\measuredangle$	Angle

Groove	The space envelope defined by the FLOLS beam
SPN-10	A radar-controlled automatic carrier landing system
Meatball	Image of the FLOLS source light as seen by the pilot of the approaching aircraft
Pass	An attempted landing
Bolter	Missed landing resulting from failure to engage an arresting wire (similar to a touch-and-go landing on a fixed field)
Waveoff	A landing attempt which is aborted prior to deck contact

SECTION I

STATEMENT OF THE PROBLEM AND BASIC APPROACH

Carrier landings are generally regarded as the most exacting of all routine airplane operations. The small dimensions of the carrier deck, its heaving, pitching, and rolling motions, and the rapid closure rates associated with the high landing speeds of contemporary high-performance aircraft combine to place an exceptional burden on the pilot. The penalties for error are high in terms of both human life and the cost of aircraft. The accident rate for carrier landings is excessive when compared to operations on fixed fields, and too often landings are limited by unfavorable environmental conditions. There is, then, a strong need for improved carrier landing aids and a concomitant need for some systematic way of confidently assessing the many proposed improvements without having to undertake long and costly developmental programs, build hardware, and conduct sea trials for each proposal.

The present study is directed to the development of a mathematical model capable of such assessments for the complete carrier/FLOLS/pilot/aircraft system and its environment. This first gross look at the problem is restricted to the vertical plane, and involves no considerations of lateral line-up. Further, only dynamic aspects of the problem are treated, as opposed to static geometry considerations (such as alternate landing deck arrangements, additional visual aids, etc.). These imposed limitations do not severely restrict the applicability of the present investigation or the possible evaluation of improvements, since approximately 80 percent of all carrier landing accidents (Ref. 1) and 25 percent of all landing attempts which result in either bolters or waveoffs (Ref. 2) are attributed to inadequate control in the vertical plane.

The specific approach taken in this study consists of three steps:

1. Formulation of a mathematical model of the elements and inputs representing the operational carrier landing system, as well as alternate competing dynamic systems.

2. Computation of terminal flight path landing dispersions due to separate and combined ship-motion and atmospheric-turbulence influences.

3. Integration of the measured dispersions into performance indices to facilitate comparison of the relative merits of competing systems.

The modeling, computation, and performance-assessment activities performed in the course of this work are described in the remaining portions of this section, preparatory to a discussion of results (Sections II and III), simplified analytic considerations (Section IV), and conclusions (Section V). The rudimentary descriptions given in the text to provide an uninterrupted flow of material are supported by appendices to which the reader is specifically referred. In spite of this stratagem the casual reader will perhaps find Sections III and IV too detailed and he should then skip to Section V.

A. SYSTEM MODELING

The real-life carrier landing operation involves many elements and inputs. These categorically consist of the snip and its responses to wave irputs, the optical landing aid providing a steady glide slope reference (FLOLS), the pilot and his control actions, the aircraft and its responses to atmospheric turbulence. These elements and their interplay are described in Fig. 1. The generic forms of these elements and evaluation variables are briefly discussed here with reference to Fig. 1, while their specific forms and numerics are given in Appendix A.

1. Ship and Wave Inputs

Of interest here are total deck vertical motions, which result from response to sea wave and swell wave excitation. Spectral representations of ship pitch, θ_S, heave, h_S, and roll, φ_S, were used to represent the combined wave input and ship dynamic characteristics. These motions and their velocities affect the FLOLS-commanded glide slope and directly contribute to terminal dispersions of aircraft height over the ramp, h_R, height over the intended touchdown point, h_{TD}, and impact velocity, V_I, as indicated by the beam-motion and terminal-error generic equations.

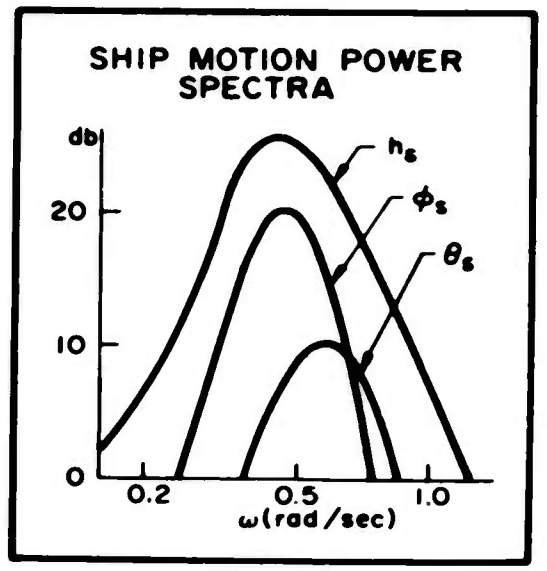

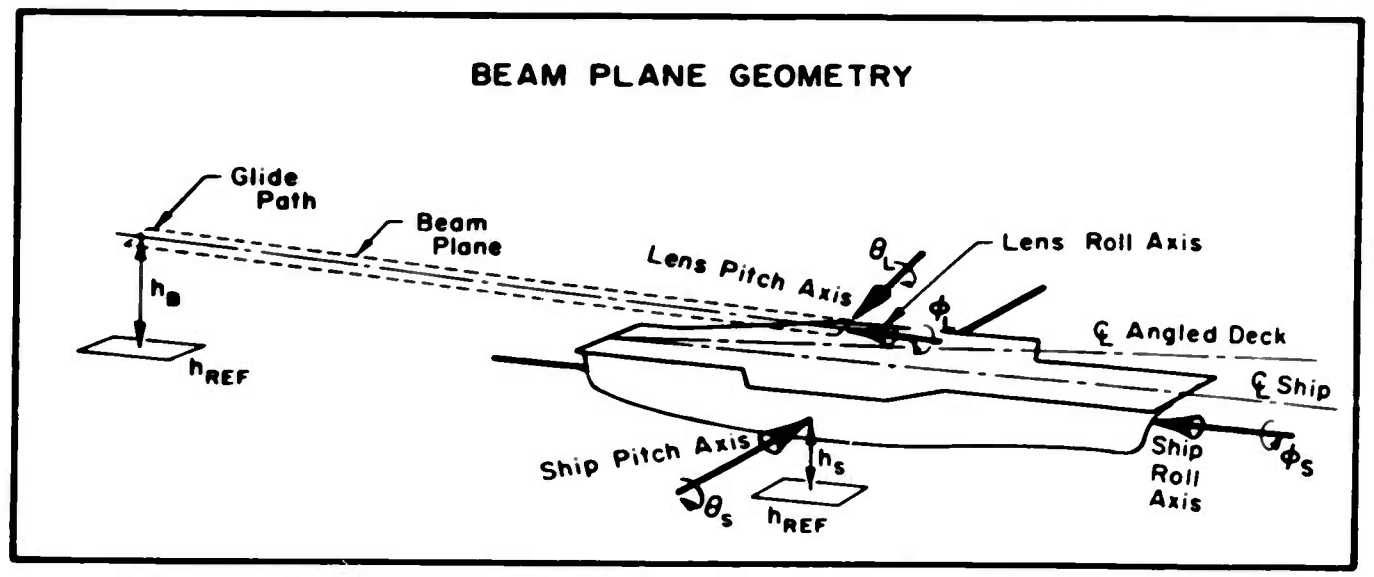

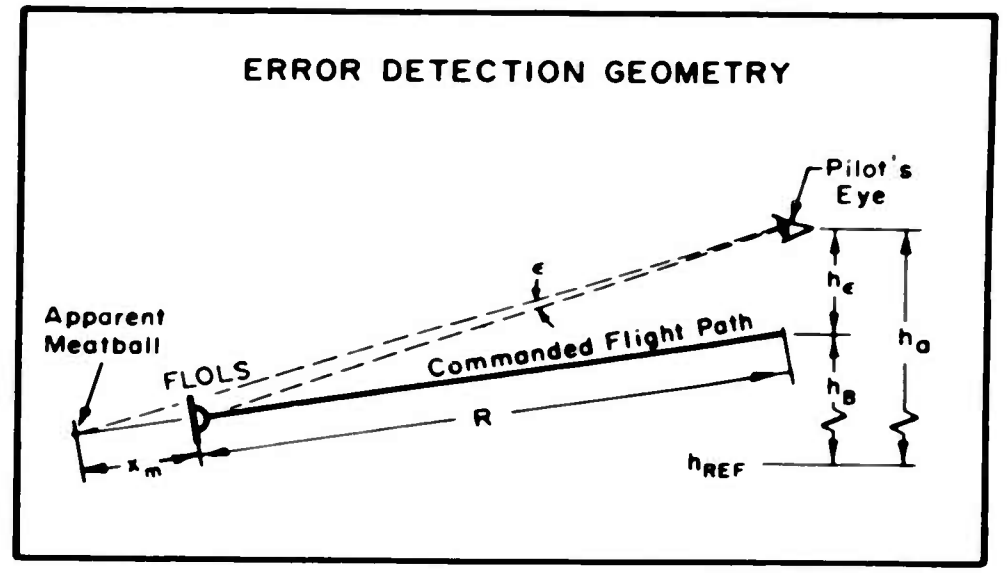

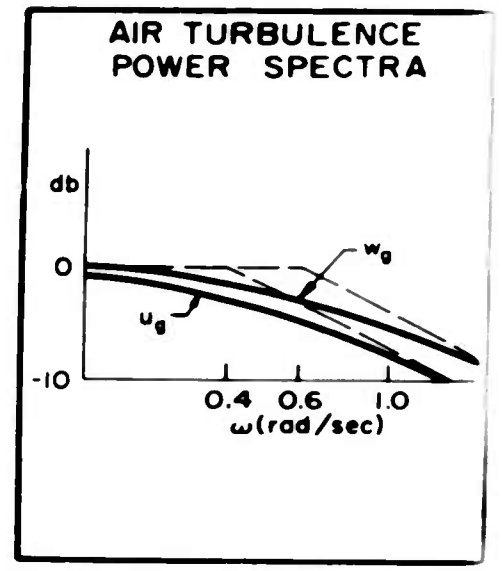

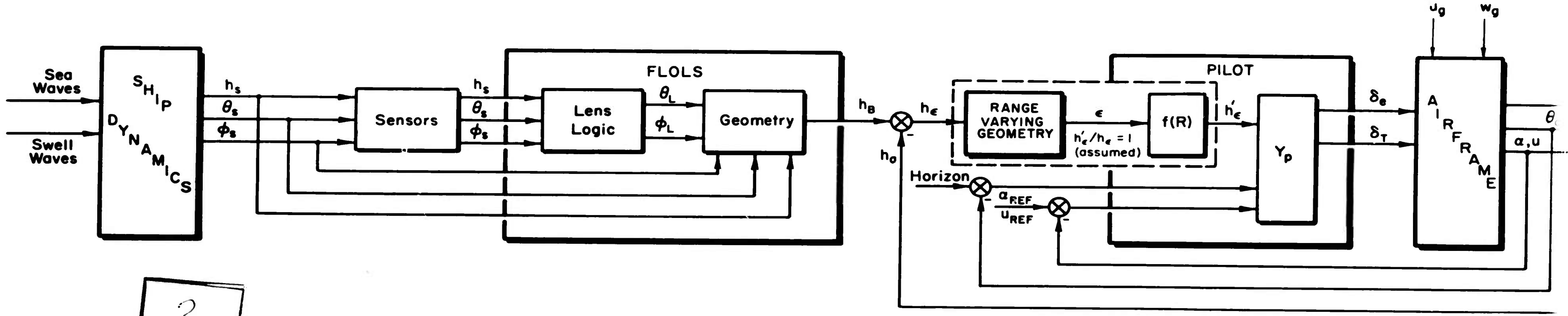

2 FRAMES

TERMINAL ERROR EQUATIONS

$$\Delta h_{TD} = h_a - (h_s - L_{TD}\theta_s - Y_{TD}\phi_s)$$
$$\Delta h_R = h_a - (h_s - L_R\theta_L - Y_R\phi_s)$$
$$\Delta V_I = \dot{h}_s - L_{TD}\dot{\theta}_s + U_R\theta_s + U_R\sin\psi_d\phi_s - \dot{h}_a$$

BEAM MOTION EQUATION

$$h_B = \underbrace{\left[h_s + C_1\theta_s + C_2\phi_s + C_3\phi_s\right]}_{\text{Beam Translation}} + \underbrace{\left[C_4\theta_s + C_5\phi_s + C_6\theta_L\right]}_{\text{Beam Rotation}} R$$

AIRCRAFT MOTION EQUATIO

$$q_a = \frac{q_a}{u}u_g + \frac{q_a}{w_g}w_g + \frac{q_a}{\delta_T}\delta_T + \frac{q}{\delta}$$

A

FIGURE I. CARRIER APPROACH AND LANDING SYSTEM BLOCK DIAGRAM

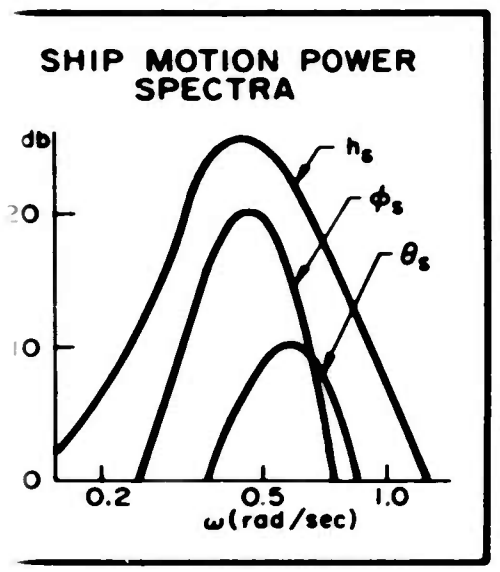

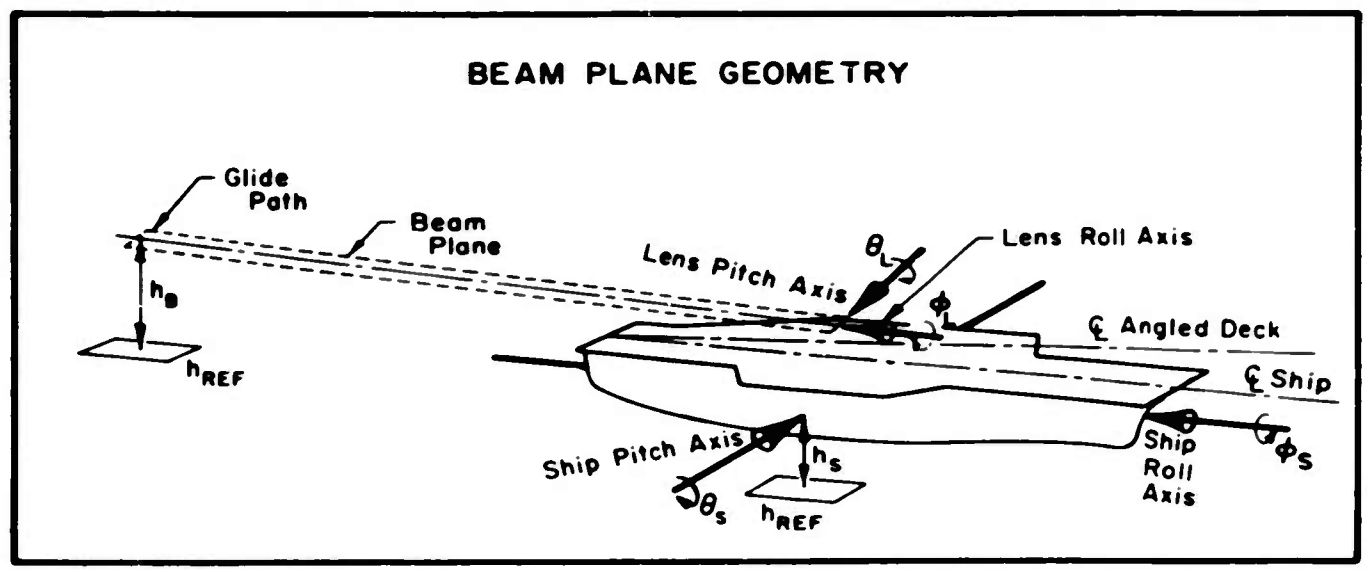

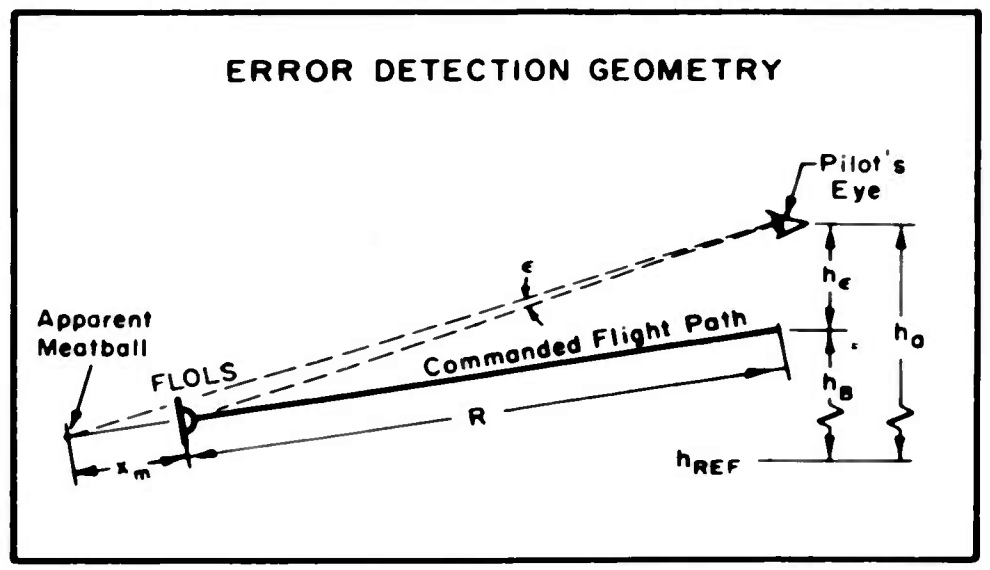

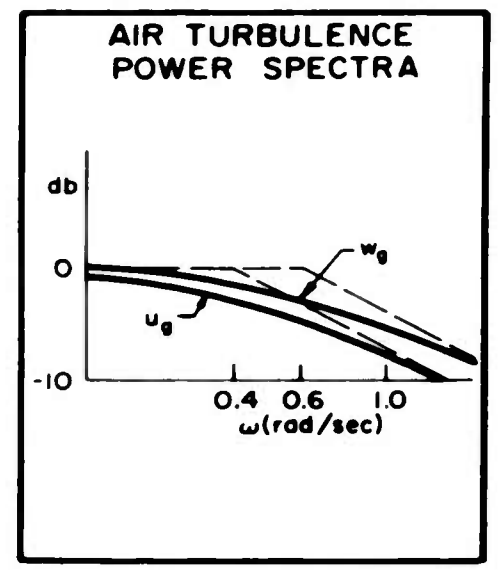

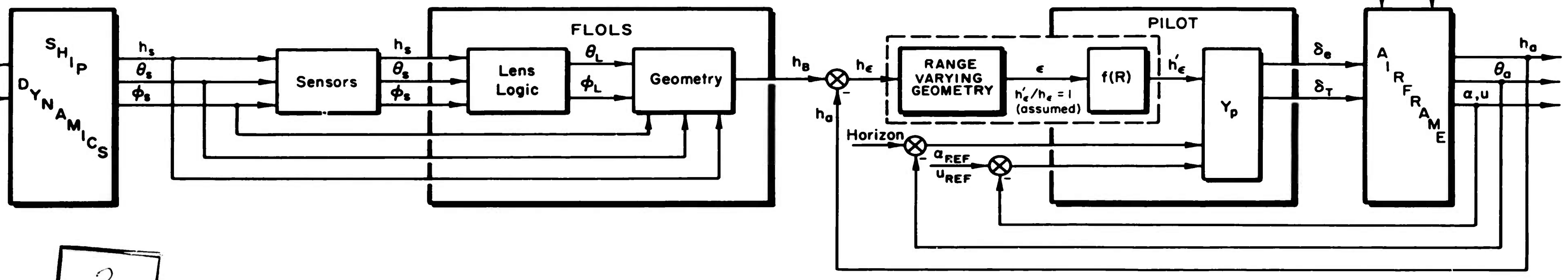

2 FRAMES

TERMINAL ERROR EQUATIONS

$$\Delta h_{TD} = h_a - (h_s - L_{TD}\theta_s - Y_{TD}\phi_s)$$
$$\Delta h_R = h_a - (h_s - L_R\theta_s - Y_R\phi_s)$$
$$\Delta V_I = \dot{h}_s - L_{TD}\dot{\theta}_s + U_R\theta_s + U_R\sin\psi_d\phi_s - \dot{h}_a$$

BEAM MOTION EQUATION

$$h_B = \underbrace{\left[h_s + C_1\theta_s + C_2\phi_s + C_3\phi_s\right]}_{\text{Beam Translation}} + \underbrace{\left[C_4\theta_s + C_5\phi_s + C_6\theta_L\right]}_{\text{Beam Rotation}} R$$

AIRCRAFT MOTION EQUATION

$$q_a = \frac{q_a}{u}u_g + \frac{q_a}{w_g}w_g + \frac{q_a}{\delta_T}\delta_T + \frac{q_a}{\delta_e}\delta_e$$

B

FIGURE I. CARRIER APPROACH AND LANDING SYSTEM BLOCK DIAGRAM

Measured motion spectra of the Essex carrier operating in a dominant swell condition (Ref. 3) were used for the majority of evaluations; the rms magnitudes of motions involved, $\sigma(\theta_S) = 1^\circ$, $\sigma(h_S) = 5.5$ ft, and $\sigma(\varphi_S) = 2.2^\circ$, correspond to upper limits of normal aircraft launch and recovery operations. Computed Forrestal motion spectra for Sea State 6 and similar computed spectra for severe swell conditions were also utilized in separate evaluations. Other variables, such as deck geometry, ship speed and heading, and wind-over-the-deck, received only limited consideration in evaluations of landing performance (Section III). Maximum performance improvement accruing from pitch stabilization and, separately, from perfect prediction of ship motions are also considered and discussed in Section II.

2. FLOLS

The Fresnel Lens Optical Landing System is used to provide a steady glide slope reference in the presence of deck motion. Lens pitch, θ_L, and roll, φ_L, servos correspondingly rotate and vertically translate the commanded beam in opposition to measured deck movements according to the lens logic used. Several forms of logic or stabilization schemes were investigated, and the characteristics of each in terms of commanded flight path (i.e., "roger" meatball path) are as follows:

a. **Angle-stabilized.** Maintains a constant angle relative to the horizon; path translates with vertical motion of the intended touchdown point (heave, plus vertical motion of touchdown point induced by pitch and roll).

This stabilization method resembles some early visual glide slope stabilization schemes (Refs. 4 and 5) which proved inferior to later and presently used methods. Beam translation control, φ_L, has been added here to synchronize beam motion with the motion of the touchdown point in an attempt to improve on previous results.

b. **Point-stabilized.** Path translates with heave, and rotates about a point 2500 ft aft of the ship (FLOLS location) due to pitch/roll-induced vertical motion of the FLOLS.

The point-stabilized FLOLS is currently in fleet use (Ref. 6), and utilizes just the pitch servo for stabilization; the roll servo is used only for static setting of beam tilt angle to accommodate variations in hook-to-eye distances of different aircraft types.

c. **Line-and-point-stabilized.** Path translates with ship heave. Ship pitch and roll motions are completely removed from the visually indicated path.

This stabilization method is undergoing sea trial evaluations (Refs. 7 and 8), and is sometimes referred to as the two-degree-of-freedom system or line-stabilized system. Both pitch and roll servos are utilized to effect beam stabilization.

d. **Compensated meatball (point-stabilized).** Path motions are identical to those described for the point-stabilized scheme. Phasing of path motion is advanced in time to effectively provide lead equalization.

This compensation scheme was evolved in the course of this work and is somewhat similar to that used in the SPN-10 automatic landing system during its deck-chasing mode (Ref. 9, last 10 sec before touchdown). Schematically, it may be represented by the point-stabilized FLOLS with a lead filter inserted between the FLOLS and pilot/aircraft blocks to advance the phase of h_B in time. In practice, the filter function is applied to the servo inputs to produce the equalized beam motion; both pitch and roll servos are utilized as opposed to the pitch servo alone for the conventional point-stabilized FLOLS.

In addition, beam stabilization against ship heave motions was considered in conjunction with the first three methods listed above, producing a total of seven FLOLS stabilization configurations subsequently evaluated. The beam plane geometry used corresponds to an operational CVA-64 carrier installation (Refs. 6 and 10); basic beam angle setting is important to the landing performance and is considered in the relative performance assessments, Section II.

3. Pilot/Aircraft

The pilot and aircraft elements are treated together, since only their combined closed-loop characteristics affect system performance. The control actions of the pilot in compensatory tracking tasks are describable in conventional servo theory terms. Roughly speaking, this makes the pilot's error-sensing and control-actuating functions equivalent to those of an autopilot. This equivalence is not generally demonstratable in the point-by-point sense, but is observable in the short-time average sense and results in an effectively linear model of the pilot's combined linear and nonlinear control behavior. That is, the pilot's measured quasi-linear

output/input characteristics account for over 90 percent of the pilot's total control power. The remaining 10 percent or so is principally due to time-variation and sampling characteristics and, to a lesser extent, threshold and saturation nonlinearities. The sum total of all measured quasi-linear characteristics when fitted by a simple general mathematical form and augmented by "rules" which explain how the form is to be adjusted (i.e., what numerical values are appropriate) in given control situations becomes a pilot model. Pilot modeling activities of this nature have been in process now for over a decade. Their status prior to 1958 is comprehensively recapitulated in Ref. 11; and Ref. 12 furnishes a recent up-dating based on currently available literature. In addition, Ref. 13 describes preliminary results of a very extensive series of measurements undertaken in 1961 and continuing at present. These results support and extend the applicability of the quasi-linear pilot models in current use.

Early applications of the pilot model to the study of aircraft handling qualities were limited to simple single-loop control situations (Refs. 14, 15, 16, and 17). The pilot/vehicle performance thereby predicted was successfully validated in simulation experiments and flight tests (Refs. 16, 17, and 18). This experience provided the foundation for the analysis of the multiple-loop, multiple-input piloted control situations which occur in carrier landing (Ref. 19), and the predictions based on these analyses were successfully validated in the simulator experiments of Ref. 20. These two efforts, directed at clarifying the dynamic factors limiting the minimum selected approach speed, have considerable bearing on the pilot/aircraft models used in the present study, and applicable detailed results are summarized below.

Considering only longitudinal control, there are two possible pilot outputs, throttle and elevator, and four probably useful inputs, altitude (relative to the desired glide path), airspeed, angle of attack, and pitch attitude. Of the possible loops available, the only one that, for certain, is always closed is the pitch attitude loop, $\theta \rightarrow \delta_e$. There are several justifications for this:

a. It is the only loop useful in controlling short-period motions.

b. It is a powerful way to increase phugoid damping because it effectively provides altitude rate damping (for phugoid motions, where $\alpha \doteq$ constant, $\dot{h} = U_o\gamma \doteq U_o\theta$).

c. There is ample evidence from time histories of carrier approach that the pilot in fact does this.

d. The pilot gets benefits a and b, regardless of how he chooses to control altitude or airspeed, merely by controlling his pitch attitude relative to the horizon.

All other possible loops, viz,

$$h \rightarrow \delta_T \text{ and/or } \delta_e$$
$$u \text{ or } \alpha \rightarrow \delta_T \text{ and/or } \delta_e$$

were considered and analyzed in varying detail in conjunction with the basic $\theta \rightarrow \delta_e$ loop. The gain of the altitude loop was considered invariant with time or range ($h'_\epsilon/h_\epsilon = 1$) despite the increasing optical gain of the FLOLS system as range is reduced. This amounts to assuming—consistent with flight experience—that the pilot decreases his control gain as the ramp is approached. Note, however, that even with the fixed-gain altitude loop, an over-all time- or range-variant system still results when considering the rotational components of FLOLS beam motion. The pilot describing function used in these analyses was of the form:

$$Y_p = K_p e^{-\tau s} \frac{(T_L s + 1)}{(T_I s + 1)(T_N s + 1)} \qquad (1)$$

where

τ = pilot reaction time

T_N = pilot neuromuscular lag (his actuator lag) time constant

K_p = pilot gain

T_L = pilot-adopted lead time constant

T_I = pilot-adopted lag time constant

} Pilot sets these as required by system

The general criteria used to set gains and lead or lag time constants are those described in Ref. 19. The pilot model can be considerably simplified in the present instance, since flight path control problems in the approach are low frequency in nature; that is, they are associated with the closed-loop phugoid motions of the aircraft. Because the phugoid frequencies are about 0.2 rad/sec, pilot reaction time, τ, and neuromuscular lag, T_N, will contribute only slightly in this region and need not be

included in the pilot model. Also, lag equalization is generally not helpful here and the pilot cannot easily develop effective lead from the information content of the meatball display. Accordingly, the pilot transfer functions in the low frequency region can be approximated by pure gains (proportional control) for the purpose of this investigation:

$$Y_p = K_p \qquad (2)$$

The results of previous multiple-loop analyses have shown that:

a. On the front side of the drag curve, elevator-only control (θ and $h \rightarrow \delta_e$) gives adequate closed-loop performance with minimal adaptation on the pilot's part. Throttle is not required except as initial trim for the glide slope. Ref. 21 points out that this is the natural way to fly the approach.

b. On the back side of the drag curve,

(1) Assuming that the only information available is by reference to the FLOLS display (altitude error and attitude), the pilot can theoretically stabilize and control the system by controlling attitude with elevator and altitude with throttle ($\theta \rightarrow \delta_e$, $h \rightarrow \delta_T$). The resulting closed-loop performance is marginal (but probably adequate) in terms of response or bandwidth. But as speed is progressively reduced, the achievement of even this marginal performance eventually becomes essentially impossible.

(2) Assuming additional information is available through suitable angle of attack or airspeed displays, the pilot can use elevator for height and attitude control, and throttle to hold angle of attack or airspeed constant (θ and $h \rightarrow \delta_e$; u or $\alpha \rightarrow \delta_T$). Essentially, the throttle manipulations involved in this mode of operation reverse the "back side" effect of an increase in drag as speed decreases to an "effective front side" net decrease in drag as speed decreases. Thus the pilot gets good longitudinal response, and there is, theoretically, no controllability limit as speed is reduced as long as he is able to maintain thrust required with the throttle. This mode of operation can provide much tighter (i.e., faster-responding by a factor of 2 or 3) control of altitude than can the simpler process of Item (1) above.

The control technique used by pilots additionally depends on the particular phase of approach in question. Considering the approach in four chronological portions, pilot control activities are expected to be as follows:

a. **Approach to the glide slope beam.** During this phase the pilot is primarily concerned with trimming the aircraft at the proper approach speed (or angle of attack), and with maintaining a somewhat constant altitude. Altitude need not be

controlled precisely because, regardless of its value, interception of the FLOLS beam always occurs at 0.75° (beam width is 1.5°) below the nominal glide slope and is routinely handled in essentially a programmed fashion. The simpler $h \rightarrow \delta_T$ method of operation is adequate for the loose altitude control required here, especially since it maintains airspeed sufficiently well.

b. **Acquisition of glide slope beam.** On interception of the FLOLS beam, two programmed control actions are observed, both triggered by the appearance of the meatball. The first is a throttle retardation, using the rpm indicator, to reduce thrust to approximately that required for trim on the glide slope; the second is the establishment of a new pitch attitude consistent with glide slope and indexed angle of attack. Notice that there is again no particular requirement for very fast response in altitude and that the direct control of sink rate with throttle is the simplest possible procedure.

c. **Beam-following.** After transition and within that range where there is sufficient resolution in the optical system to permit compensatory tracking of the meatball (typically a range of 4000 to 5000 ft), the pilot is vitally concerned with maintaining the proper flight path in order not to exceed beam limits. Altitude controlled by throttle may give, at best, marginally satisfactory performance, depending on aircraft type, approach speed, and severity of atmospheric turbulence and ship motions. The more precise altitude tracking by elevator control may be necessary here, either with or without airspeed (or angle of attack) controlled with throttle, depending on divergence rate, if any, and the time-to-go.

d. **Approaching the ramp.** The last 10 sec or so of the approach are by far the most critical of any of the previous phases. Any upset of a "roger meatball" condition due to burble encounter or severe deck motion must be corrected most expeditiously. Altitude response to throttle is, in most cases, too slow; recourse to elevator control of flight path is then necessary.

Piloting technique can thus be generalized according to two broad regions of the approach. The first, concerning gross corrections such as setting up the descent path, is best represented by pilot control of attitude with elevator and altitude with throttle. The second, involving vernier flight path corrections in approaching the ramp (i.e., small adjustments in altitude or sink rate), is representable by elevator control of both attitude and altitude ($\theta, h \rightarrow \delta_e$). For the short times of interest (10 sec or less) the use of throttle to control airspeed or angle of attack even when below

minimum drag speed is immaterial; however, for completeness, u or $\alpha \rightarrow \delta_T$, similar to flight control with an autothrottle (Ref. 22), is added. Both altitude control techniques were modeled and separately applied to the complete approach. This was done in conjunction with the typical dynamics of an F4D-1 aircraft* at slightly less than minimum drag speed; with forms and numerics taken directly from previous analyses (Ref. 19) and validation experiments (Ref. 20). Also, for both techniques, the pilot gains used in all pertinent loop closures were systematically varied to check performance sensitivity to these variations in a rough-air environment.

In addition to the technique variables above, environmental and operational variables involving (1) the effect of loss of horizon and (2) the relative merits of "meatball-chasing" versus "meatball-averaging" were also investigated. The first of these conservatively represents night flying and was conveniently modeled by substituting elevator control of angle of attack for normally controlled pitch attitude. This substitution takes into account the fact that without a horizon reference the pilot can still maintain control of short-period motions (e.g., through vertical acceleration cues), but he cannot readily control the phugoid. Elevator control of angle of attack very accurately simulates these conditions, since at short-period frequencies $\Delta\alpha \doteq \Delta\theta$, thus providing equivalent pitch attitude control; whereas at phugoid frequencies $\Delta\alpha \doteq 0$. This analogy infers that with no real horizon, such as on a dark moonless night, the pilot does not detach himself from his primary head-up concern to look down at the artificial horizon.

"Meatball-chasing" and "meatball-averaging" refer respectively to the pilot's compensatory tracking or averaging of apparent meatball motions. Such motions are due to unstabilized components of the FLOLS beam and flight path perturbations. Of the two, the pilot can at best only average out the higher frequency beam motions induced by ship pitch and heave. Aircraft flight path motions occur predominantly at low frequencies and the cyclical nature of these motions is not readily discernible, therefore

*Because the phugoid mode dominates the closed-loop flight path response, the dynamics selected here represent a wide variety of aircraft.

not averaged. Thus, "meatball-averaging" refers to filtering of the remaining (unstabilized) FLOLS beam motion, i.e., the "roger meatball" path motions previously described for the various FLOLS stabilization configurations. The Navy currently advocates the averaging technique and is taking steps to implement it by development of FLOLS stabilization systems which cut down beam motion (Ref. 8). Modeling of such behavior is straightforward since the compensatory-tracking pilot model essentially simulates tracking of beam motion. Meatball "averaging" is simulated by use of the completely stabilized FLOLS, i.e., the line-and-point-stabilized configuration with added stabilization against heave motion.

4. Atmospheric Turbulence

Random air gusts as well as ship-induced air turbulence contribute significantly to the over-all difficulty of maintaining accurate flight path control. Vertical and horizontal air turbulence components with spectral forms and intensities appropriate to the speed and altitude of carrier landing (Ref. 23) were simulated with the filter forms shown in Fig. 1. Low frequency components of these spectra simulate uncorrelated carrier-induced burble effects to some extent. However, water tunnel tests of a pitching carrier model (Ref. 24) in progress during the course of this work have indicated a strong correlation of the wake field with the pitching motions of the deck. The importance of such coupling influences on carrier landing is uncertain, since quantitative measurements of the correlated wake field have not yet been made; but results presented in Section II, obtained with the uncorrelated air-turbulence forms, indicate a fair consistency with actual performance experience. It seems, then, that the simple uncorrelated gust forms, which were deemed realistic by the pilots in previous simulations (Ref. 20), account in gross fashion for the total influence of combined ship-induced and random air turbulence. This inference should be more closely scrutinized in future investigations, especially in conjunction with pilot precognitive (i.e., "learned") control techniques through which he may more successfully cope with the burble.

Variations were made to the air turbulence model in spectral break points (both high and low frequency) as well as in intensities to represent

calm, moderate, and severe conditions, corresponding to like conditions of ship motions.

B. LANDING ANALYSIS

The nature of the landing problem concerns the flight path control to terminate in engagement of one of the arresting wire pendants while maintaining safe margins of ramp clearance and landing gear structural limits. The geometry representing this "terminal control" problem is illustrated in Fig. 2. Three probability distribution functions are illustrated, separately representing rms values of height dispersion over the ramp, $\sigma(\Delta h_R)$, height dispersion over the intended touchdown point, $\sigma(\Delta h_{TD})$, and sink rate dispersion at the intended touchdown point, $\sigma(\Delta V_I)$. The nominal values of the distributions are set by basic arrestment geometry, including deck configuration (wire spacing and layout), location of the FLOLS and its basic beam angle, β_o, relative to the deck, and aircraft glide path, γ_o, which in turn is related to the beam angle, aircraft approach speed, U_o, and wind-over-the-deck, $U_s + W$. These interrelations are described subsequently. The desired nominal values ($\bar{h}_R$, $\bar{V}_I$, $\bar{X}_{TD}$) are seldom obtained in practice because of motions of the ramp and touchdown point, as well as rough-air-induced flight path deviations.

Statistical height and velocity differences between aircraft and deck, referred to as dispersions, were computed from the mathematical models of elements and inputs previously described. Various computational methods were considered to contend with the multiple inputs, the complex transfer functions of the elements, and the time-varying nature of certain FLOLS configurations. Three methods were utilized in this study: adjoint analog, real-time analog, and digital computations. The adjoint analog (Ref. 25) is basically an analog computer method for directly obtaining rms spectra of terminal conditions for linear systems with or without time-varying elements; it was utilized for the majority of the evaluations discussed in Section II. The real-time computation was principally used to check the adjoint-computed data, and to obtain time histories of aircraft motions in the groove prior to reaching the ramp. Finally, digital computations were selectively employed for checks of the first two methods,

AIRCRAFT MOTION MEASUREMENTS	
Terminal	Continuous
$\sigma(h_a)$	$h_a(t)$
$\sigma(u)$	$u(t)$
$\sigma(a)$	$a(t)$
$\sigma(\theta)$	$\theta(t)$
$\sigma(\theta - \theta_s)$	$\theta(t) - \theta_s(t)$

FIGURE 2. DEFINITION OF MEASURED DISPERSIONS

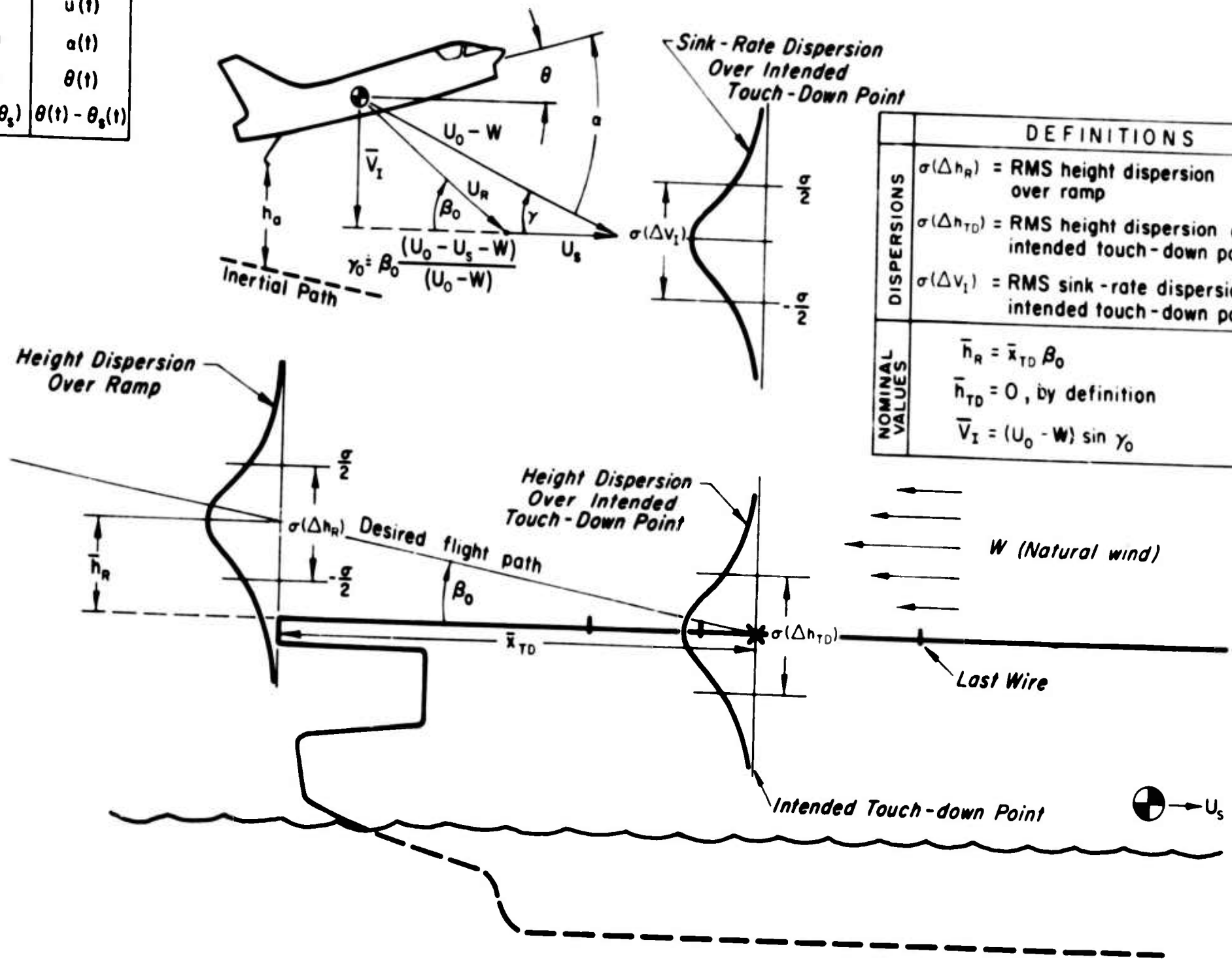

	DEFINITIONS
DISPERSIONS	$\sigma(\Delta h_R)$ = RMS height dispersion over ramp
	$\sigma(\Delta h_{TD})$ = RMS height dispersion over intended touch - down point
	$\sigma(\Delta V_I)$ = RMS sink - rate dispersion at intended touch - down point
NOMINAL VALUES	$\bar{h}_R = \bar{x}_{TD} \beta_0$
	$\bar{h}_{TD} = 0$, by definition
	$\bar{V}_I = (U_0 - W) \sin \gamma_0$

and to approximate the time-varying elements of certain FLOLS configurations with equivalent constant-coefficient systems; such simple approximations enhance the understanding of the important elements influencing landing performance, as discussed in Section IV. The analog computer methods together with appropriate circuit schematics are described in Appendix B.

The procedure in all but the real-time computation consisted of separately evaluating the rough-air-induced and ship-motion-induced dispersions. This is permissible because of the independence of atmospheric turbulence and ship motions, and is desirable because it considerably simplifies the computation procedure.

C. PERFORMANCE EVALUATIONS

To facilitate performance comparisons of competing systems, criteria were developed to integrate or weight the individual landing dispersions. That is, by suitably combining the dispersions with the basic arrestment geometry, probabilities of potential ramp strikes, gear failures, and bolters were obtained. The mechanics of this computation are illustrated in Fig. 3. Previously described Δh_R and ΔV_I distribution functions are replotted here, and the Δh_{TD} dispersion is converted to an equivalent fore-aft dispersion of the hook touchdown point by the basic flight path angle, $1/\gamma_o$. Available margins are computed as the difference in maximum permissible and nominal operating values of these functions, and the probabilities of exceeding said margins are computed from the area integral of margin exceedances (shaded areas). This computation is a standard routine applicable to Gaussian or normal distribution functions; the assumed normality in the present instance is supported by actual dispersion measurements (Ref. 26 and 27).*

*Later statistical analyses by Hoy (Ref. 33) of the Ref. 26 data in combination with other data questioned this normality. He concluded, however, that while some landing distributions are not highly normal in the precise statistical sense, they are in fact so in a practical engineering sense.

FIGURE 3. DEFINITION OF MARGINS AND PROBABILITIES USED IN ASSESSING RELATIVE PERFORMANCE

$$P_{h_{LSO}} = 1 - F\left[\frac{(h_{LSO})_M}{\sigma(h_{LSO})}\right]$$

$P_{V_{LSO}}$, $P_{X_{LSO}}$ } Of same form as $P_{h_{LSO}}$

$$(h_R)_M = \bar{h}_R$$
$$(V_I)_M = \left[(V_I)_{ultimate} - \bar{V}_I\right]$$
$$(X_{TD})_M = X_{Last\ Wire} - \bar{X}_{TD}$$

$$P_{h_R} = 1 - \frac{1}{\sqrt{2\pi}}\int_{-\infty}^{\frac{(h_R)_M}{\sigma(\Delta h_R)}} e^{-z^2/2}dz = 1 - F\left[\frac{(h_R)_M}{\sigma h_R}\right]$$

P_{V_I}, $P_{X_{TD}}$ } Of same form as P_{h_R}

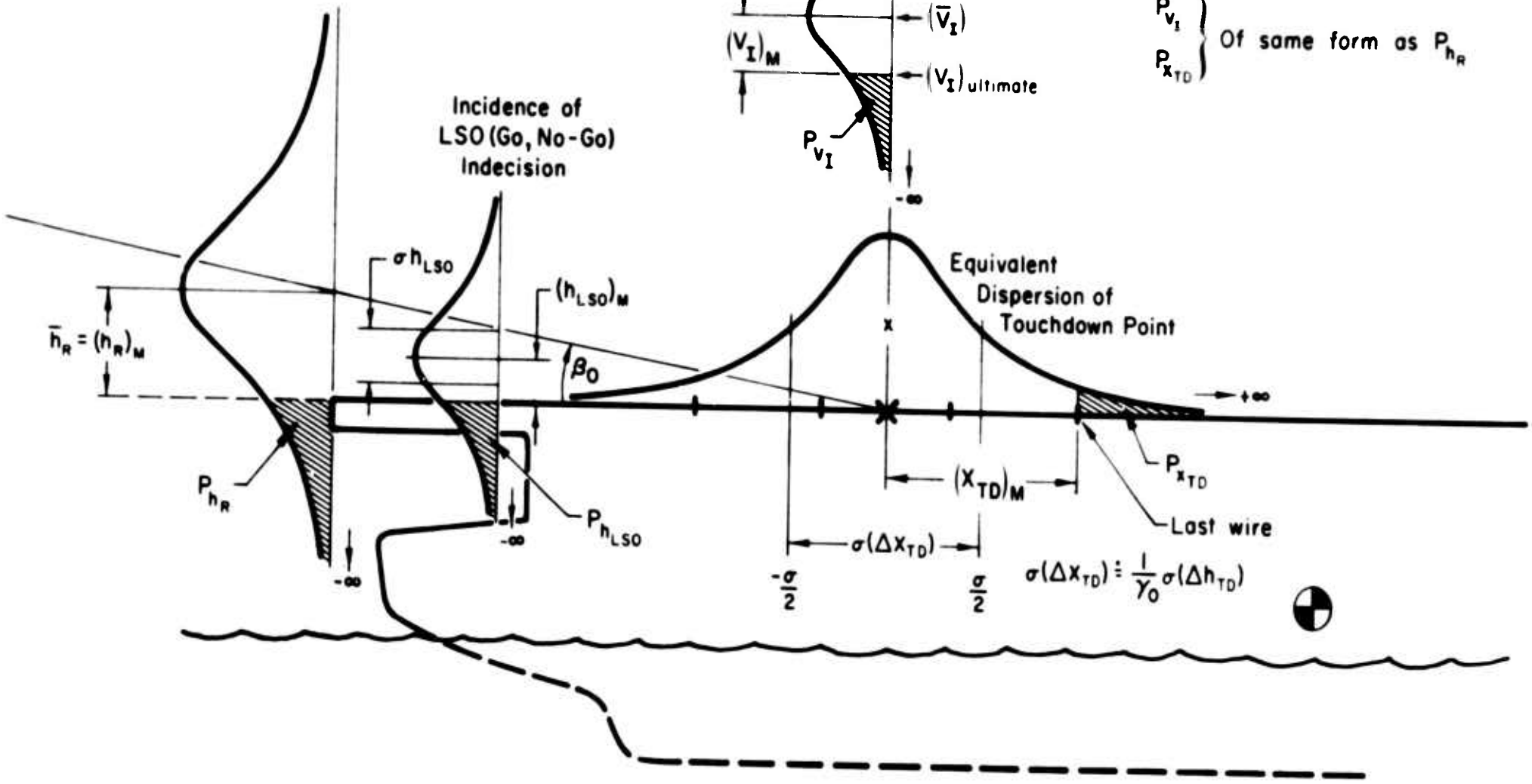

The product of unshaded areas represents the combined probability of a successful pass, and its reciprocal gives the minimum number of passes required for a successful landing. Conversely, the shaded areas P_{h_R}, P_{V_I}, and $P_{X_{TD}}$ separately represent probabilities of ramp strike, gear failure, and bolter which would result if waveoffs or aborted landings were not permissible. In actual operations a Landing Safety Officer (LSO) monitors the pass and, on the basis of anticipated terminal conditions, decides whether to let the landing proceed. The pilot similarly adjudges the pass, and will in many instances initiate a voluntary waveoff. This combined pilot/LSO decision model is represented by the hypothesized (LSO) normal error distribution function shown. The distribution function is illustrated in conjunction with control of ramp dispersion and relates to the incidence of LSO indecision (or wrong decision) in waving off an approaching aircraft. The value of this function is greatest at that height value, $(h_{LSO})_M$, considered by the LSO to be a desirable safe margin in clearing the ramp; the $\sigma(h_{LSO})$ parameter relates to the magnitude of error in LSO-predicted aircraft height over the ramp (i.e., as predicted 2 or 3 sec before crossing the ramp, after which the landing is committed). The shaded area, $P_{h_{LSO}}$, represents the probability of the LSO not waving off an approaching aircraft which is about to hit the ramp. In later computations of absolute accident rate, the pilot/LSO decision function was assumed to effectively prevent 90 percent (Ref. 27) of otherwise probable individual ramp strikes and gear failures, i.e., $P_{h_{LSO}} = P_{V_{LSO}} = 0.1$. For performance comparison of competing systems, relative accidents are more simply computed from the ratios of their corresponding probabilities directly, since the pilot/LSO multiplicative function cancels and does not, therefore, affect the relative performance of competing systems. The basic beam angle, β_o, was separately idealized for each system variation to effectively equate the computed probabilities P_{h_R} and P_{V_I} and thereby minimize the total accident rate. An ideal basic beam angle, $\beta_o = 4^o$, resulted with the conventional system for all environmental conditions tested.

A sample calculation of the performance indices just described is given in Appendix C, which demonstrates the process of converting the computed landing dispersions into equivalent probable passes per landing, accidents, and combined minimum bolters and waveoffs.

SECTION II

SUMMARY OF RESULTS

A. BEAM MOTION CHARACTERISTICS OF THE FLOLS CONFIGURATIONS

Table I summarizes the commanded path characteristics, control logic, and resultant rms beam motion in space for the seven FLOLS stabilization methods considered (each of the first three are shown with and without heave stabilization). The path characteristics are repeated here for easy identification of configuration, while the control logic shows the manner in which the FLOLS servos are used. The rms beam motions are computed from the beam motion equation of Fig. 1 using Essex motion spectra defined in Appendix A. The following observations are made from Table I:

1. Resultant beam motion is nearly equal for configurations without heave compensation (NH), and is not significantly affected by the range from FLOLS location at which it is measured. This indicates that all stabilization methods are highly effective in removing beam rotational components induced by ship pitch and roll.

2. Stabilizing the beam against ship heave effectively removes the major portion of remaining beam motion, and consequently appears desirable for obtaining an immobile glide path in space.

The latter observation is significant in view of recent interest in reducing beam motion, as revealed by contemplated changes to the presently operational point-stabilized FLOLS. These changes consider more optimum points in space for stabilizing the beam (Refs. 28 and 29) and converting to the line-and-point-stabilization scheme (Ref. 7). However, Table I shows that neither of these two approaches seems to significantly reduce beam motion (i.e., a more optimum stabilization point would at best approach the level of motions of Configuration 3NH) for the ship motions considered here. For seas lacking significant swells, where heave motion is small relative to pitch (as discussed in Section III), the line-and-point

TABLE I

BEAM MOTION CHARACTERISTICS FOR VARIOUS FLOLS STABILIZATION CONFIGURATIONS

CONFIG.	CHARACTERISTICS OF COMMANDED PATH (Flight Path Corresponding to "Roger" Meatball)	FLOLS CONTROL EQUATIONS (Lens Pitch and Roll* Control for CVA 64 Class)	HEAVE** STAB.	RESULTANT RMS BEAM MOTION • IN INERTIAL SPACE, $\sigma(h_B)/\sigma(\theta_s)$ (ft/deg)			
				At Touchdown	At Ramp	At 2500 Ft	At 5000 Ft
1	ANGLE-STABILIZED: Constant angle relative to horizon; path translates with vertical motion of deck touchdown point.	$\theta_L = 0.98\theta_s - 0.14\varphi_s$ $\varphi_L = -0.4\theta_s + 0.83\varphi_s$	NH	6.6	6.6	6.6	6.6
			WH	5.0	5.0	5.0	5.0
2	POINT-STABILIZED: Path translates with heave and rotates about a point 2500 ft aft of ship due to ship pitch/roll-induced vertical motion of FLOLS	$\theta_L = 1.0\theta_s - 0.1\varphi_s$ $\varphi_L = 0$	NH	6.04	6.02	5.5	5.8
			WH	2.27	2.19	0	2.66
3	LINE-AND-POINT STABILIZED: Path only translates with ship heave. Pitch and roll influences are completely removed.	$\theta_L = 0.98\theta_s - 0.14\varphi_s$ $\varphi_L = -0.935\theta_s + 0.91\varphi_s$	NH	5.5	5.5	5.5	5.5
			WH	0	0	0	0
4	COMPENSATED-MEATBALL: Path motion identical to that of Configuration 3. Phasing of path motion is advanced in time to provide effective lead compensation.	$\theta_L = 0.95\left(\frac{\frac{s}{0.19}+1}{\frac{s}{0.2}+1}\right)\theta_s - 1.12\left(\frac{\frac{s}{1.32}+1}{\frac{s}{0.2}+1}\right)\varphi_s$	NH	6.04	6.02	5.5	5.8
		$\varphi_L = (-1.71h_s - 1.89\theta_s + 1.9\varphi_s)\left(\frac{-\frac{s}{4.2}+1}{\frac{s}{0.2}+1}\right)$	WH	Not analyzed			

*For compensation against ship heave, add term $\Delta\varphi_L = 0.85h_s$ (deg/ft)

**NH No heave compensation
WH With heave compensation

•For $\sigma(\theta_s) = 1^o$, $\sigma(h_s)/\sigma(\theta_s) = 5.5$ ft, $\sigma(\varphi_s)/\sigma(\theta_s) = 2.2^o$

method would yield a more considerable reduction in beam motion than that shown in Table I.

Beam stabilization against ship heave, which appears highly desirable on the basis of Table I, has a special problem of its own. This relates to the lateral beam tilt required to offset heave motions (0.85° per foot of heave) and the vertical flight path errors induced by such tilting when lateral line-up is not precisely maintained. Also, as shown subsequently, heave stabilization additionally increases the magnitudes of landing dispersions when the pilot is tracking beam motion. These considerations offset the otherwise desirable stable-beam properties obtainable.

B. LANDING DISPERSION SENSITIVITY TO SHIP AND BEAM MOTIONS

A summary of computed landing dispersions and terminal aircraft motions for the FLOLS configurations and piloting techniques considered is given in Table II. Before discussing these results, a few notes detailing the evaluation background are necessary.

1. These data were obtained using the Essex ship motion spectra (defined in Appendix A) as inputs to the adjoint-simulated FLOLS/pilot/aircraft system.

2. For the fixed ratios of $\sigma(h_s):\sigma(\theta_s):\sigma(\varphi_s)$ corresponding to a given set of motion spectra, the dispersions can be normalized and scaled with respect to any motion quantity. In Table II they are presented in terms of $\sigma(\theta_s)$, since θ_s is the most significant of the motion quantities involved and is sometimes used to demarcate "severe," "moderate," and "calm" conditions.

3. Initial conditions simulated glide slope intercept at 5000 ft aft of the carrier. This range was determined in preliminary evaluations to adequately represent quiescent dispersion conditions (i.e., transients due to initial beam conditions have died out; see Section III, Item E).

4. The dispersions shown represent the combined correlated effects of deck vertical motion and resultant aircraft motion from the pilot's following the beam in smooth air. Rough-air inputs are considered separately in Item C of this section.

TABLE II

DISPERSION SENSITIVITIES TO SHIP* AND BEAM MOTIONS

PILOTING TECHNIQUE	DISPERSION SENSITIVITY		ANGLE-STABILIZED		POINT-STABILIZED		LINE-AND-POINT-STABILIZED		COMPENSATED MEATBALL
			1(NH)	1(WH)	2(NH)	2(WH)	3(NH)	3(WH)	4(NH)
$\theta,h \rightarrow \delta_e$, $u \rightarrow \delta_T$	Landing dispersions	$\frac{\sigma(\Delta h_R)}{\sigma(\theta_s)}$ (ft/deg)	10.5 (1.3)	12.1 (1.3)	7.3 (2.0)	9.0 (2.0)	6.9 (1.3)	7.7 (1.3)	5.0 (2.4)
		$\frac{\sigma(\Delta h_{TD})}{\sigma(\theta_s)}$ (ft/deg)	9.8 (0.3)	10.6 (0.3)	5.9 (1.5)	6.6 (1.5)	6.1 (0.2)	6.6 (0.2)	2.9 (1.6)
		$\frac{\sigma(\Delta V_I)}{\sigma(\theta_s)}$ (ft/sec/deg)	8.0 (1.2)	8.1 (1.2)	5.4 (0.5)	5.7 (0.5)	5.7 (1.1)	5.8 (1.1)	4.0 (1.1)
	Terminal aircraft motions	$\frac{\sigma(u)}{\sigma(\theta_s)}$ (ft/sec/deg)	1.5 (1.06)	1.0 (1.06)	1.4 (0.5)	— (0.5)	0 (0)	0 (0)	1.4 (0.5)
		$\frac{\sigma(w)}{\sigma(\theta_s)}$ (ft/sec/deg)	2.5 (0.8)	2.0 (0.08)	2.5 (1.5)	— (1.5)	0 (0)	0 (0)	2.5 (1.5)
		$\frac{\sigma(\theta)}{\sigma(\theta_s)}$ (deg/deg)	—	—	1.05 (0.3)	— (0.3)	— (0)	0 (0)	1.05 (0.3)
$\theta \rightarrow \delta_e$, $h \rightarrow \delta_T$	Landing dispersions	$\frac{\sigma(\Delta h_R)}{\sigma(\theta_s)}$ (ft/deg)	8.8 (1.3)	8.6 (1.3)	8.7 (1.1)	8.4 (1.1)	8.6 (1.3)	7.7 (1.3)	Not analyzed
		$\frac{\sigma(\Delta h_{TD})}{\sigma(\theta_s)}$ (ft/deg)	6.8 (0.3)	6.6 (0.3)	6.8 (0.2)	6.5 (0.2)	6.8 (0.2)	6.6 (0.2)	
		$\frac{\sigma(\Delta V_I)}{\sigma(\theta_s)}$ (ft/sec/deg)	5.9 (1.1)	5.9 (1.1)	5.9 (1.3)	— (1.3)	5.9 (1.1)	5.8 (1.1)	
	Terminal aircraft motions	$\frac{\sigma(u)}{\sigma(\theta_s)}$ (ft/sec/deg)	0.5 (0)	0.1 (0)	0.15 (0.15)	0.15 (0.15)	0.1 (0)	0 (0)	
		$\frac{\sigma(w)}{\sigma(\theta_s)}$ (ft/sec/deg)	—	—	0.07 (0.07)	0.07 (0.07)	0 (0)	0 (0)	
		$\frac{\sigma(\theta)}{\sigma(\theta_s)}$ (deg/deg)	—	—	0	—	0 (0)	0 (0)	

*$\sigma(h_s)/\sigma(\theta_s) = 5.5$ ft/deg; $\sigma(\varphi_s)/\sigma(\theta_s) = 2.2$ deg/deg; also, numbers enclosed in parentheses correspond to dispersions due to ship roll only

5. Two sets of values are given in Table II: the total dispersion due to combined ship pitch, heave, and roll, and that due to ship roll alone (in parentheses). Note that the roll-induced dispersion components could have been safely neglected in most instances, since they are small compared to the total dispersion value. For example, Configuration 3NH with respect to the dispersion parameter $\sigma(\Delta h_R)$ for $\sigma(\theta_s) = 1^\circ$:

Total dispersion..... $\sigma(\Delta h_R) = 6.9$ ft

Dispersion component due to roll..... $\sigma(\Delta h_R)_{\varphi_s} = 1.3$ ft

Dispersion component due to pitch/heave... $\left[\sigma(\Delta h_R)^2 - \sigma(\Delta h_R)^2_{\varphi_s}\right]^{1/2} = 6.77$ ft

1. Altitude Controlled by Elevator (θ,h$\rightarrow\delta_e$, u$\rightarrow\delta_T$)

FLOLS configurations with heave stabilization (WH) yield higher landing dispersions than their corresponding heave-unstabilized (NH) configurations. As shown in the analyses of Section IV, the heave-induced beam motion permits the pilot to control aircraft motions partially in phase with deck motions and thereby reduce dispersions at the ramp and touchdown point. The amount of aircraft synchronism with deck motion is dependent on the pilot/aircraft phase lags and FLOLS beam-phasing relative to deck motion, both of which are discussed in Section IV. Note that the dispersions for Configuration 3WH are just the rms values of deck motions, i.e., the aircraft perfectly follows an inertial path without deviation; this set of data is later used to relate the merits of pilot's averaging of ship-induced beam motions.

Based on relative magnitudes of landing dispersions, the angle-stabilization scheme renders poorest performance, while the compensated-meatball system seems best. The two remaining configurations, 2NH and 3NH, yield performance comparable to one another.

Terminal aircraft motions are least pronounced with the line-and-point-stabilization method, because of correspondingly less beam motion associated with this configuration. Note also that terminal aircraft motions are identical for Configurations 2NH and 4NH, since corresponding magnitudes of beam motion are also identical, as noted previously in Table I.

2. Altitude Controlled with Throttle ($\theta \rightarrow \delta_e$, $h \rightarrow \delta_T$)

Values of both landing dispersions and terminal aircraft motions indicate insignificant differences between the various FLOLS configurations considered. The relatively slower-responding $h \rightarrow \delta_T$ method of aircraft altitude control is incapable of following beam motions (effectively filtering these); consequently the aircraft follows an almost inertial flight path in all cases, as noted by near-zero values of aircraft motions (see below). The resulting dispersion values are effectively due to motions of the deck alone. This altitude control method is then particularly well suited to the beam-motion-averaging technique advocated by the Navy.

C. LANDING DISPERSION SENSITIVITY TO AIR TURBULENCE

This evaluation involved only the pilot/aircraft portion of the over-all system shown in Fig. 1, since rough-air-induced dispersions are independent of the ship/FLOLS-induced dispersions. Using vertical and horizontal components of random disturbances, described in Appendix A, resulting aircraft rms motion sensitivities for the two piloting techniques are summarized in Table III both for individual u_g, w_g inputs and for their total combined $\sigma(u_g) = \sigma(w_g)$ effects. Considering a maximum gust intensity level of $\sigma(\text{gust}) = 3$ ft/sec as typical of severe turbulence for carrier landing operations (Ref. 14), corresponding values of aircraft dispersions are three times the sensitivity values shown.

Conclusions drawn from Table III are as follows:

1. For severe atmospheric turbulence the piloting technique $\theta \rightarrow \delta_e$, $h \rightarrow \delta_T$ yields unsatisfactory performance for control near the ramp, i.e., the one sigma value of aircraft altitude dispersion exceeds the nominal ramp clearance ($\bar{h}_R \doteq 16$ ft). Consequently this piloting technique must be abandoned in favor of the faster-responding altitude control with elevator ($\theta, h \rightarrow \delta_e$, $u \rightarrow \delta_T$) when approaching the ramp.

2. Since the pilot has no foreknowledge of the atmospheric turbulence severity associated with burble encounter, it seems probable that vernier altitude corrections in the vicinity of the ramp are always performed with elevator control, regardless of actual turbulence conditions.

TABLE III

DISPERSION SENSITIVITIES TO AIR TURBULENCE

PILOTING TECHNIQUE.....	$\theta, h \rightarrow \delta_e$, $\delta_T \rightarrow \delta_T$			$\theta \rightarrow \delta_e$, $h \rightarrow \delta_T$		
AIR TURBULENCE PARAMETER*.....	u_g	w_g	Total for $\sigma(u_g) = \sigma(w_g)$	u_g	w_g	Total for $\sigma(u_g) = \sigma(w_g)$
$\frac{\sigma(\Delta h_R) = \sigma(\Delta h_{TD}) = \sigma(h_a)}{\sigma(\text{gust})}$ (ft/fps)	1.0	1.4	1.7	5.3	6.0	8.2
$\frac{\sigma(\Delta V_I) = \sigma(w)}{\sigma(\text{gust})}$ (fps/fps)	0.42	0.44	0.61	0.87	0.84	1.2
$\frac{\sigma(u)}{\sigma(\text{gust})}$ (fps/fps)	—	—	(0.58)**	—	—	(0.5)**
$\frac{\sigma(\theta)}{\sigma(\text{gust})}$ (deg/fps)	—	—	(0.38)**	—	—	(0.38)**

*σ_g measured either in vertical or horizontal plane

**Approximate values determined from real-time simulation

3. While the dispersions associated with throttle control of altitude are excessive for terminal control, they are satisfactory for flight path control in early phases of the approach, including glide slope acquisition and beam-following at distant range from the carrier (since the FLOLS beamwidth of 1.5° allows an altitude error margin of approximately ±100 ft at a range of 1.5 miles from the carrier).

4. Since landing performance is exclusively dependent on terminal dispersions, the appropriate piloting technique to consider in this regard is altitude control with elevator. Accordingly, only those data obtained with $h \rightarrow \delta_e$ control are utilized in subsequent evaluations of landing performance.

Dispersion sensitivities to air turbulence for altitude-to-elevator control with simulated loss of horizon reference are given in Table IV. To obtain these results, elevator control of angle of attack was substituted for previously and similarly controlled pitch attitude, at a gain yielding the same closed-loop short-period frequency. The values of Table IV are a factor of 2 greater than the corresponding ($\theta, h \rightarrow \delta_e$, $u \rightarrow \delta_T$) values given in Table III. Thus the horizon reference ($\theta \rightarrow \delta_e$) plays an important role in reducing the effects of turbulent air on flight path control; and loss of this primary reference can considerably degrade landing performance. The extent of performance deterioration is treated subsequently.

D. LANDING DISPERSIONS DUE TO COMBINED SHIP MOTIONS AND ATMOSPHERIC TURBULENCE, AND COMPARISON WITH ACTUAL DISPERSIONS

Total landing dispersions are computed by combining ship-motion-induced and rough-air-induced dispersion components in a manner compatible with independent Gaussian functions. The dispersion sensitivities of Tables II and III are first scaled to represent calm, moderate, and severe operating conditions by the ship motion and air turbulence intensity scale shown in Table V. The latter scale was compiled from averages of estimates and measurements given in the literature. For example, it is generally regarded that a deck pitch amplitude of $\pm 1.5^{\circ}$ $\left[\sigma(\theta_s) \doteq 1^{\circ}\right]$ is an upper limit to safe continuance of carrier landing operations (Refs. 27 and 30). Also, severe turbulence conditions correspond to rms intensities of 2.5, to 3.0 ft/sec [Refs. 9 and 20. Note that total turbulence intensity, $\sigma(g)$,

TABLE IV

DISPERSION SENSITIVITIES TO AIR TURBULENCE
WITH SIMULATED LOSS OF HORIZON REFERENCE

PILOTING TECHNIQUE.....	$\alpha \rightarrow \delta_e$, $u \rightarrow \delta_T$, $h \rightarrow \delta_e$		
AIR TURBULENCE PARAMETER.....	u_g	w_g	Total for $\sigma(u_g) = \sigma(w_g)$
$\frac{\sigma(\Delta h_R)}{\sigma(\text{gust})} = \frac{\sigma(\Delta h_{TD})}{\sigma(\text{gust})} = \frac{\sigma(h_a)}{\sigma(\text{gust})}$ (ft/fps)	2.24	0.92	2.43
$\frac{\sigma(\Delta V_I)}{\sigma(\text{gust})} = \frac{\sigma(w)}{\sigma(\text{gust})}$ (fps/fps)	1.09	0.264	1.12

is $\sqrt{2}$ times greater than the individual $\sigma(u_g)$ or $\sigma(w_g)$ values shown in Table V.] The simultaneous occurrence of these maxima, as well as other combinations shown, is only conjectured to represent values typical of the condition described.

TABLE V

RMS SHIP MOTION AND AIR TURBULENCE INTENSITIES AS A FUNCTION OF ENVIRONMENTAL CONDITION

DISPERSION PARAMETER	CONDITION		
	Calm	Moderate	Severe
$\sigma(\theta_s)$* (deg)	0.25	0.5	1.0
σ(gust)** (ft/sec)	1.0	2.0	3.0

* $\sigma(h_s)/\sigma(\theta_s) = 5.5$ ft/deg; $\sigma(\varphi_s)/\sigma(\theta_s) = 2.2$ deg/deg

** With $\sigma(g)$ measured in either vertical or horizontal plane

Computed landing dispersions for the presently conceived operational landing system for the three environmental conditions described above are given in Table VI. Note that the selected FLOLS configuration, 3WH, represents the pilot's averaging of ship-induced beam motion as is currently advocated. Also given in Table VI are actual landing dispersion values obtained in normal-air operations in "calm" conditions (Ref. 26). Actual dispersions compare well with averaged computed values of "calm" and "moderate" conditions. The adjectives used in the environmental scale of Table III may be somewhat pessimistic in view of these results but, more important, the consistent ordering of computed and actual dispersions lends additional credence to the system modeling and performance evaluation activities thus far described.

E. RELATIVE PERFORMANCE OF COMPETING SYSTEMS AND COMPARISON WITH ACTUAL PERFORMANCE

The dispersions so far considered are converted into probable bolters, waveoffs, and accidents to facilitate comparison of the relative performance of competing landing systems. The process is illustrated in Appendix C

TABLE VI

COMPUTED DISPERSIONS VERSUS ENVIRONMENT FOR SYSTEM 3(WH) OF TABLE I
AND COMPARISON WITH ACTUAL DISPERSIONS

	COMPUTED DISPERSIONS*				ACTUAL DISPERSIONS** (Averages)
	Calm	Moderate	Severe	Avg. of Calm and Moderate	
$\sigma(h_R) = \left(\sigma(\Delta h_R)^2_{\theta_s} + \sigma(\Delta h_R)^2_{gust}\right)^{1/2}$ (ft)	2.57	5.15	9.23	3.86	3.43
$\sigma(V_I) = \left(\sigma(\Delta V_I)^2_{\theta_s} + \sigma(\Delta V_I)^2_{gust}\right)^{1/2}$ (ft/sec)	1.57	3.14	6.09	2.36	2.59
$\sigma(x_{TD}) = \frac{1}{\gamma_o}^{\dagger} \left(\sigma(\Delta h_{TD})^2_{\theta_s} + \sigma(\Delta h_{TD})^2_{gust}\right)^{1/2}$ (ft)	27.2	54.5	95.2	40.9	35.5 (at mean glide slope of 3°)

*From Tables II, III, and IV for piloting technique $\theta,h \rightarrow \delta_e$, $u \rightarrow \delta_T$

**Experienced pilots; calm sea; approximately 700 landings on CVA-61 by five aircraft types (Ref. 26)

†γ_o = 5/57.3 rad as determined from trigonometry of measured ramp clearance and touchdown point distance from ramp (Ref. 26)

with a sample calculation of these performance indices for the operational landing system. Table VII compares the calculated performance indices with actual values reported in the literature. Again, the computed rates, as well as idealized basic angle setting, β_o, are consistent with actual performance values, and thus form a reasonable basis for the ensuing comparisons.

TABLE VII

COMPARISON OF COMPUTED AND ACTUAL PERFORMANCE INDICES

PERFORMANCE PARAMETER	COMPUTED (See Appendix C)	ACTUAL
FLOLS basic angle, β_o (deg)	4.1 (ideal)	3.5 to 4.0 (Ref. 10)
Bolters and waveoffs per landing	0.22	0.26 (Ref. 2)
Hard landings and undershoots per 10,000 landings	1.25	3.0* (Refs. 24, 1)

*Includes all accident causal factors. Reference 1 indicates considerable variability in this evaluation, depending on computation ground rules.

Ten potential landing systems are constructed from different combinations of FLOLS stabilization configurations, piloting factors, and environmental variables; and their performance in terms of minimum bolters/waveoffs and accidents relative to the present operational landing system (System 1) are given in Table VIII.* The method of constructing the system variants is indicated by the "Applicable Data" and "Comments" columns. It should be noted that comparisons shown apply to relative accidents, bolters, and waveoffs due only to dispersions in ramp clearance, sink rate, and touchdown point. In practice, other causes, such as lateral-directional control problems, pilot error and fatigue, and equipment failures, are

*Note that relative accidents for "calm" conditions are not given; these could not be properly determined because the reference system value is approximately zero.

TABLE VIII

RELATIVE PERFORMANCE OF VARIOUS COMPETING SYSTEMS

SYSTEM		APPLICABLE DATA (CONFIGURATION)	IDEAL β_o*			BOLTERS AND WAVEOFFS RELATIVE TO SYSTEM 1			ACCIDENTS RELATIVE TO SYSTEM 1			COMMENTS
No.	Description		Calm	Moderate	Severe	Calm	Moderate	Severe	Calm	Moderate	Severe	
1	Point-stabilized FLOLS (operational system), beam-averaging	(3WH)	4.1	4.1	4.0	1.0	1.0	1.0	(0)	1.0	1.0	Mathematical model of the present CV approach and landing system
2	Point-stabilized FLOLS with beam-chasing	(2NH)	4.2	4.2	4.0	0.75	0.89	0.90	—	0.58	0.79	Aircraft motions and piloting effort increased relative to System 1
3	System 2 with added stabilization against heave motion	(2WH)	4.3	4.3	4.2	0.80	0.92	1.0	—	1.6	1.2	Minimum beam motion seen by pilot
4	Angle-stabilized FLOLS, beam-chasing	(1NH)	3.9	3.9	3.8	2.5	1.5	1.5	—	10.5	2.7	Beam and aircraft motions increased relative to System 1
5	Line-and-point-stabilized FLOLS, beam-chasing	(3NH)	4.0	4.0	3.8	0.94	0.97	0.95	—	0.64	0.83	Reduced beam motion relative to System 1; presently being evaluated in sea trials
6	Night landing with System 1; simulated loss of norizon	Dispersion values of Table IX (3WH)	4.2	4.2	4.0	2.0	1.4	1.2	—	5.7	1.5	Assumes loss of attitude reference; $\alpha \rightarrow \delta_e$ control is substituted
7	Compensated-meatball FLOLS (phase compensation of System 2)	(4NH)	4.3	4.3	4.1	0.21	0.56	0.57	—	0.026	0.20	Beam and aircraft motions of same amplitude as System 2
8	Ship pitch stabilizers with System 1; 100 percent effective stabilization	(3WH) $\sigma(\Delta h_R) = \sigma(\Delta h_{TD}) = \sigma(h_S)$	4.8	4.8	4.7	0.30	0.64	0.63	—	0.007	0.12	Assumed 100 percent effectiveness; i.e., $\sigma_S = 0$
9	Gust alleviation with System 1; 50 percent reduction of rough-air intensity	(3WH) 50 percent of Table III values	3.8	3.8	3.8	0.44	0.73	0.86	—	0.18	0.68	Theoretical potential from deck streamlining, etc.
10	Ship motion prediction; inertially fixed beam to theoretically ideal values	Dispersions due to rough air only (Table III)	5.1	5.1	5.1	0.02	0.27	0.30	—	—	0.0004	Theoretical equivalence to fixed-field landing; i.e., no deck motions

*Ideal from the standpoint of minimum probable accidents; ideal pilot and LSO models assumed throughout

responsible for a sizable percentage of the total performance indices. Such excluded factors will not affect the rank-order shown, but will affect net performance gains or losses indicated. Considering only vertical dispersion causual factors, significant observations relating to the merits of the evaluated potential systems are as follows (numbers in parentheses refer to the system number used in Table VIII):

1. Tracking ship-induced beam motion (meatball-chasing) with the point-stabilized FLOLS (2) results in slightly fewer accidents under moderate conditions than occur with the conventional beam-averaging technique (1). Opposing this apparent performance gain are the more pronounced aircraft motions incurred by meatball-chasing (approximately 50 percent greater excursions as indicated by combined dispersions from Tables II and III). Large altitude and angle of attack excursions in the groove are disconcerting to the LSO and prompt him to order a greater number of waveoffs. Also, increased aircraft pitch attitude excursions reduce ramp clearance and significantly increase the probability of an in-flight engagement.* These additional considerations, added to the greater pilot tracking effort involved, offset the small performance gain achievable with uncompensated meatball-chasing.

2. Of the other "conventional" FLOLS stabilization schemes considered (3, 4, and 5), none exceed the performance of the point-stabilized configuration (2) under similar beam-chasing conditions. With beam-averaging they all yield performance identical to System 1, but with varying amounts of pilot averaging effort, i.e., according to the amount of beam motion involved (see Item A of this section). The line-and-point-stabilized beam (5) shows no advantage, while heave stabilization (3) and angle-stabilized FLOLS (4) seem to seriously degrade performance.

3. Loss of horizon reference (6) results in significant deterioration of performance, in both bolters/waveoffs (maximum factor of 2 increase) and accidents (maximum factor of 5.7 increase). Night flying is represented by a seriously degraded horizon reference. The pessimistic indication of the model is validated by fleet experience during night operations, which shows a significant increase in accident rate over daytime operations.

4. Compensation of beam motions associated with the point-stabilized FLOLS (7) reduces accidents by as much as a factor of 40:1 and bolters by a maximum factor of 5:1. Such improvement is predicated on the pilot's tracking beam motions

*Wire pickup prior to landing-gear contact with the deck.

as in System 2, but now the beam motions are compensated through FLOLS servo equalization which effectively synchronizes aircraft and deck motions. Aircraft motions, here, are as large as for the uncompensated point-stabilized FLOLS (2), but in this instance constitute only a minor influence on total performance. This system appears, tentatively, to be fairly easy to implement. The only change to the currently operational system would be the (electronic) phasing of the beam motion.

5. Ship pitch stabilization (8) and air turbulence alleviation (9) possibilities tend to improve landing performance. However, their performance indices represent maximum derivable improvement assuming theoretically ideal implementation. Note that the performance gain with partial alleviation of air turbulence (9), as might be possible by streamlining the superstructure and/or by airborne gust alleviation (direct lift) devices, is less than that obtained with the easier implemented compensated-meatball system (7).

6. Ship motion prediction (10) indicates a large potential performance improvement; but at this time it should be considered strictly a theoretical gain, since the feasibility and operational consequences of prediction have not been established. Also, the attendant unreliability of added electronic equipment necessary for prediction and processing of guidance commands will tend to offset this theoretical performance gain.

7. The ideal beam angle, β_o, is fairly insensitive to environmental conditions or FLOLS stabilization concept employed. Reducing ship motion effects, e.g., Systems 8 and 10, does slightly increase the value of theoretically ideal β_o.

SECTION III

SUPPORTING DATA AND MISCELLANEOUS RESULTS

This section presents the results of the preliminary evaluations which aided in the selection of representative operating points for the modeled system elements described in Section I; they also give additional enlightenment in support of the tentative findings of Section II. Subsequent paragraphs will discuss the effects of variations in ship motion, air turbulence spectra, and pilot loop closure gains. Miscellaneous data on landing dispersion effects and aircraft altitude motions in the groove are also presented and briefly discussed.

A. VARIATIONS IN SHIP MOTION SPECTRA

Computed spectral representations of ship pitch and heave motions for a Forrestal class carrier were examined in the course of this work. These motion spectra data are computed (Ref. 24) for various sea states and swell conditions, and for different ship headings and speeds. Two sets of spectra representing maximum deck motion (i.e., having the most adverse effect on landing operations) were selected for evaluation, one representing ship motions in Sea State 6 and the other representing ship motions in a severe swell condition. These spectra and corresponding fitted analytical forms appropriate to the landing dispersion computation technique are described in Appendix A.

Direct digital rather than adjoint computations were used here in an attempt to develop a simple approximate analytic approach which could more directly explain the important elements of the complete time-varying problem. These computations, involving constant-coefficient approximations to time-varying elements, were first validated by checks against the adjoint-computed results using Essex motion spectra. The approximation is itself the subject of the separate discussion given in Section IV.

Landing dispersions incurred with the Forrestal motions were computed for only three of the original seven FLOLS configurations—the line-and-point

without heave stabilization (4NH), the point-stabilized with heave stabilization (3WH), and the point-stabilized without heave stabilization (3NH). The results are summarized in Table IX. In the first two rows of Table IX are given Sigma values of ship pitch/heave motions and landing dispersions due to separate ship operation in Sea State 6 (with no swells) and Sea State 0 (swell condition). Although uncorrelated, sea waves and swell waves seldom occur independently (Ref. 24), i.e., to the exclusion of one or the other; their combined motions and dispersions, given in the third row, more typically represent actual operating conditions. It should be noted that significant wave heights used correspond to 17 ft for the sea state and 15 ft for the swell condition. In the fourth row for comparison are values of dispersions digitally computed using previously described Essex ship motions. It may be seen from Table IX that:

1. For the same significant wave height, swell waves cause approximately five times greater ship heave motion, $\sigma(h_s)$, than do sea waves, while pitch motions, $\sigma(\theta_s)$, are approximately the same for both. Consequently, dispersions are more pronounced for the swell condition, especially for the completely stabilized beam (Configuration 3WH) or, equivalently, for pilot's averaging of the beam motion.

2. The ranking of the FLOLS stabilization system in order of their relative magnitudes of dispersion is the same regardless of wave input conditions or ship configuration. Therefore, the more complete rank-order results obtained using Essex data (Section II) seem sufficiently representative to be applicable also to Forrestal class carriers over a wide range of wave inputs and sea conditions.

B. VARIATIONS IN AIR TURBULENCE SPECTRA

Horizontal and vertical components of air turbulence, u_g and w_g, were used to represent the unsteady random-airflow field behind the carrier; these were simulated by passing white noise (W.N.) through a shaping filter of the form

$$\frac{u_g}{W.N.} \text{ or } \frac{w_g}{W.N.} = \frac{K_g s}{(\tau_1 s + 1)(\tau_2 s + 1)} \qquad (3)$$

Variations in both low and high frequency spectral breakpoints, τ_1 and τ_2, were evaluated for both piloting techniques to ascertain landing dispersion

TABLE IX

SEA STATE AND SWELL CONDITION EFFECTS ON SHIP MOTIONS
AND ON RESULTANT LANDING DISPERSIONS

PILOT CONTROL TECHNIQUE: $\theta,h \rightarrow \delta_e$, $u \rightarrow \delta_T$ IN SMOOTH AIR

SHIP CLASS	WAVE INPUT CONDITION AND RESULTANT RMS SHIP MOTIONS* (PITCH AND HEAVE)	LINE-AND-POINT WITH HEAVE STABILIZATION (Configuration 3WH)			LINE-AND-POINT NO HEAVE STABILIZATION (Configuration 3NH)			POINT NO HEAVE STABILIZATION (Configuration 2WH)		
		$\sigma(\Delta h_R)$	$\sigma(\Delta V_I)$	$\sigma(\Delta h_{TD})$	$\sigma(\Delta h_R)$	$\sigma(\Delta V_I)$	$\sigma(\Delta h_{TD})$	$\sigma(\Delta h_R)$	$\sigma(\Delta V_I)$	$\sigma(\Delta h_{TD})$
Forrestal	Sea State 6: $\sigma(\theta_s) = 0.75^o$; $\sigma(h_s) = 0.93$ ft	4.87	3.12	3.02	4.16	2.79	2.36	4.03	2.5i	2.05
	Swell condition: $\sigma(\theta_s) = 0.705^o$; $\sigma(h_s) = 4.41$ ft	6.93	4.38	5.64	3.89	4.00	3.68	3.49	3.55	3.12
	Combined Sea State 6 and swell condition: $\sigma(\theta_s) = 1.03^o$; $\sigma(h_s) = 4.52$ ft	8.46	5.39	6.35	5.69	4.88	4.37	5.34	4.35	3.74
Essex	Combined sea state and swell condition: $\sigma(\theta_s) = 1.0^o$; $\sigma(h_s) = 5.5$ ft	7.6	5.7	6.6	6.8	5.6	6.1	6.3	5.4	5.7

*Ship roll rms motion for both Essex and Forrestal is approximately 2^o, and is neglected since it does not appreciably affect terminal dispersions

sensitivities to the final selected value, and to permit extrapolation of previously described results to fit variations in the random-turbulence field (i.e., as might be incurred from changes in ship heading or speed, aircraft approach speed, natural wind, etc., although these data are not as yet available). Resulting aircraft motion dispersions in altitude, $\sigma(h_a)$, and vertical velocity, $\sigma(\dot{h}_a)$, are given in Figs. 4 and 5 for the case of altitude controlled with elevator, and in Figs. 6 and 7 for altitude controlled with throttle. Note that these results are plotted in sensitivity form, $\sigma(h_a)/\sigma_g$ or $\sigma(\dot{h}_a)/\sigma_g$, since the absolute dispersion value is linearly proportional to the rms turbulence intensity.

1. Altitude Controlled with Elevator (θ,h$\rightarrow\delta_e$, u$\rightarrow\delta_T$)

Figure 4 demonstrates very little aircraft dispersion sensitivity to low frequency attenuation over a wide range of $1/\tau_{u_1} = 1/\tau_{w_1}$ values, thus indicating little susceptibility to low frequency turbulence. The observed insensitivity is due to the high pilot/aircraft system bandwidth associated with elevator control of altitude, which permits effective tracking of low frequency disturbances. Representative values of $1/\tau_{u_1} = 1/\tau_{w_1} = 0$ were selected in the final spectral form for use in the dispersion evaluations described in Section II.

A slightly peaked response is noted in Fig. 5 for values of $1/\tau_{u_2}$ and $1/\tau_{w_2}$ in the vicinity of the closed-loop pilot/vehicle phugoid frequency ($\omega_p \doteq 0.5$ rad/sec), which is caused by resonance of the input with the phugoid mode. Values of $1/\tau_{u_2} = 0.4$ and $1/\tau_{w_2} = 0.6$ rad/sec were selected in the final spectral form as representative of the speed and altitude conditions of carrier approach (Ref. 23), which, as indicated, also induce maximum aircraft dispersions.

2. Altitude Controlled with Throttle ($\theta\rightarrow\delta_e$, h$\rightarrow\delta_T$)

For both low and high frequency attenuation, Figs. 6 and 7 indicate greater dispersion sensitivity to low frequency turbulence power than is true with elevator control of altitude. This results from the correspondingly lower (by a factor of 3 or so) system bandwidth associated with throttle control of altitude.

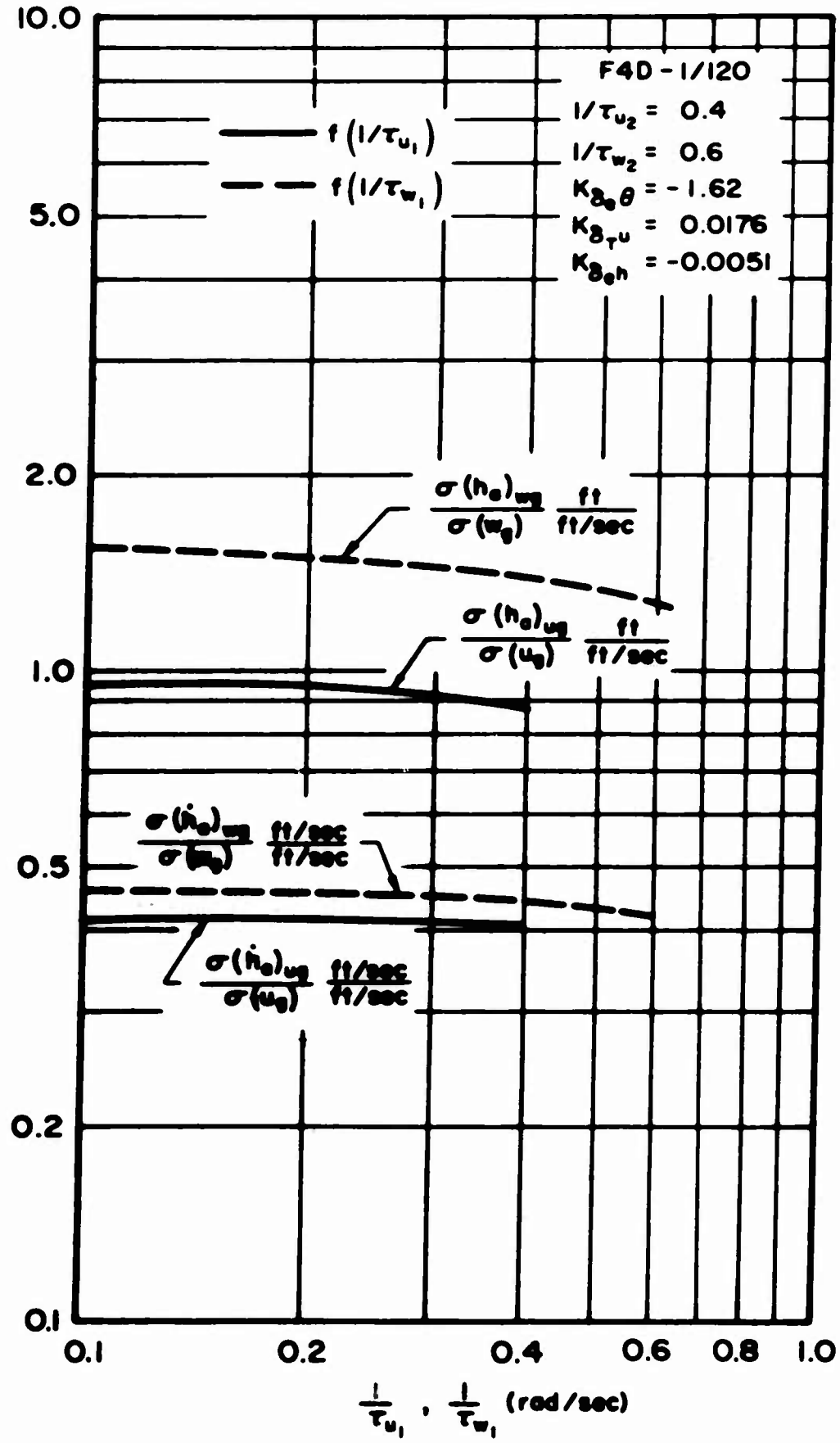

Figure 4. Sensitivity of Aircraft's Dispersions to Gust Spectrum Low Frequency Break Point; Dispersions due to Gusts with θ,h→δ_e and u→δ_T

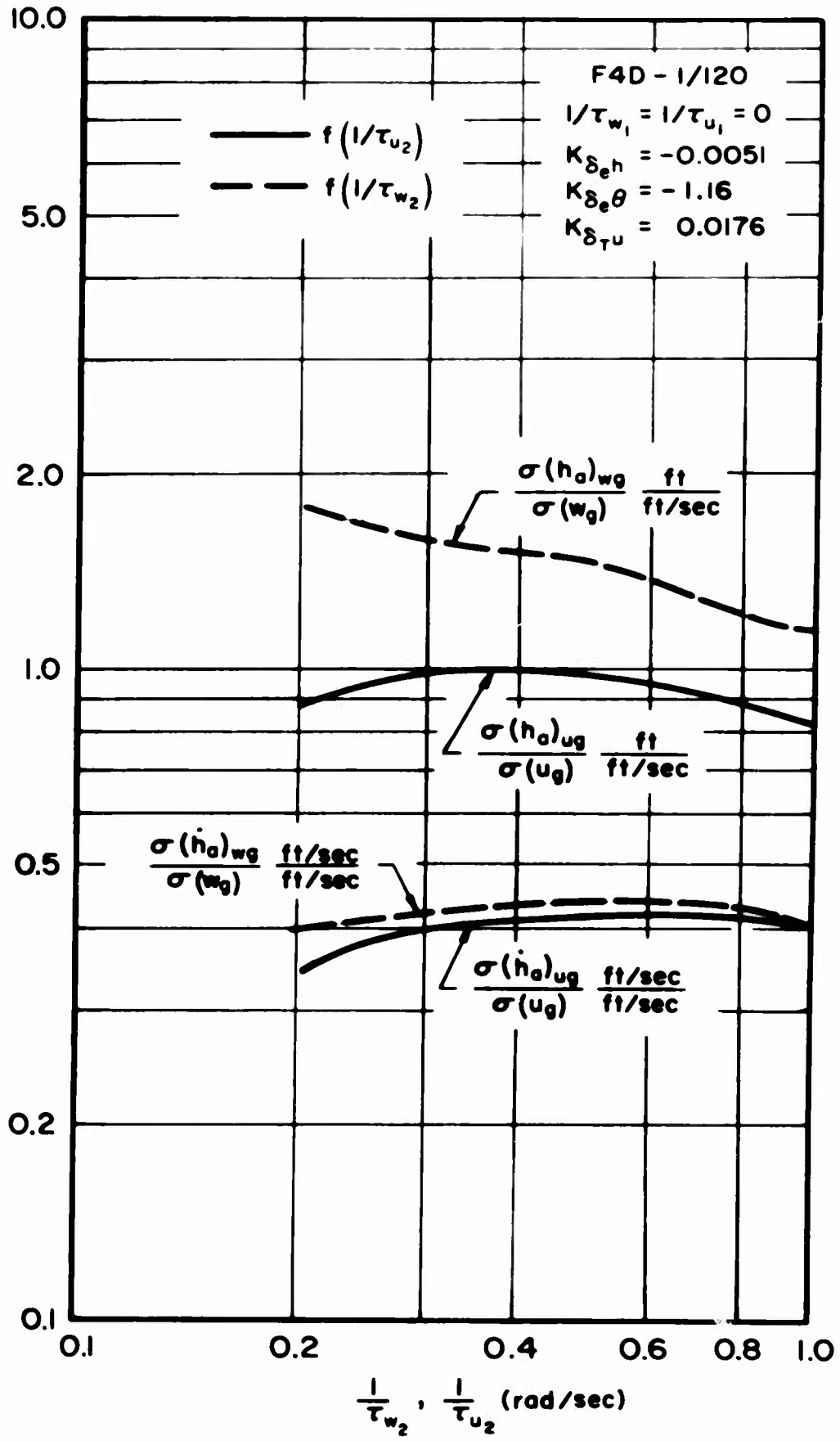

Figure 5. Sensitivity of Aircraft's Dispersions to Gust Spectrum High Frequency Break Point; Dispersions due to Gusts with $\theta, h \rightarrow \delta_e$ and $u \rightarrow \delta_T$

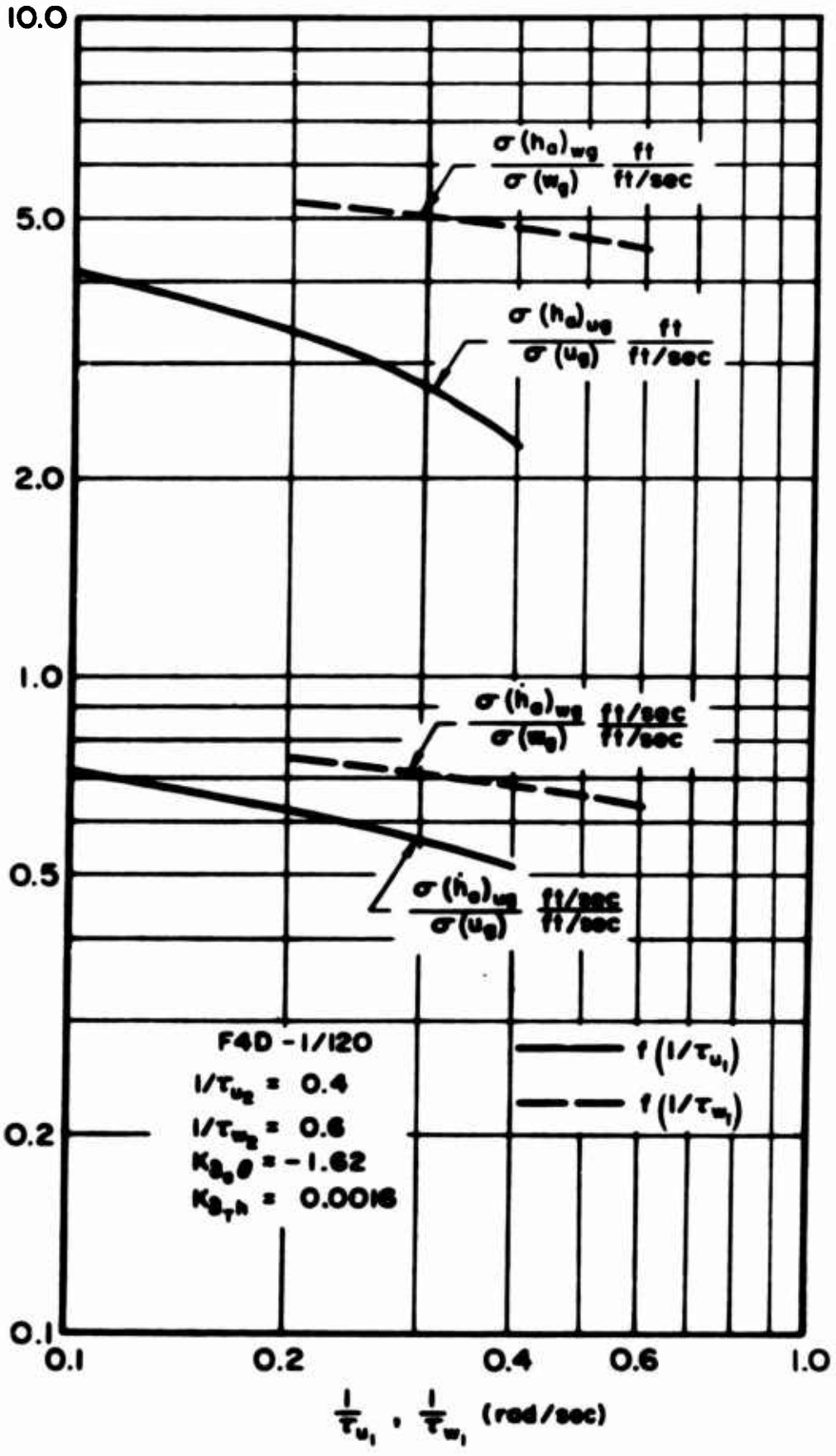

Figure 6. Sensitivity of Aircraft's Dispersions to Gust Spectrum Low Frequency Break Point; Dispersions due to Gusts with $\theta \rightarrow \delta_e$ and $\dot{h} \rightarrow \delta_T$

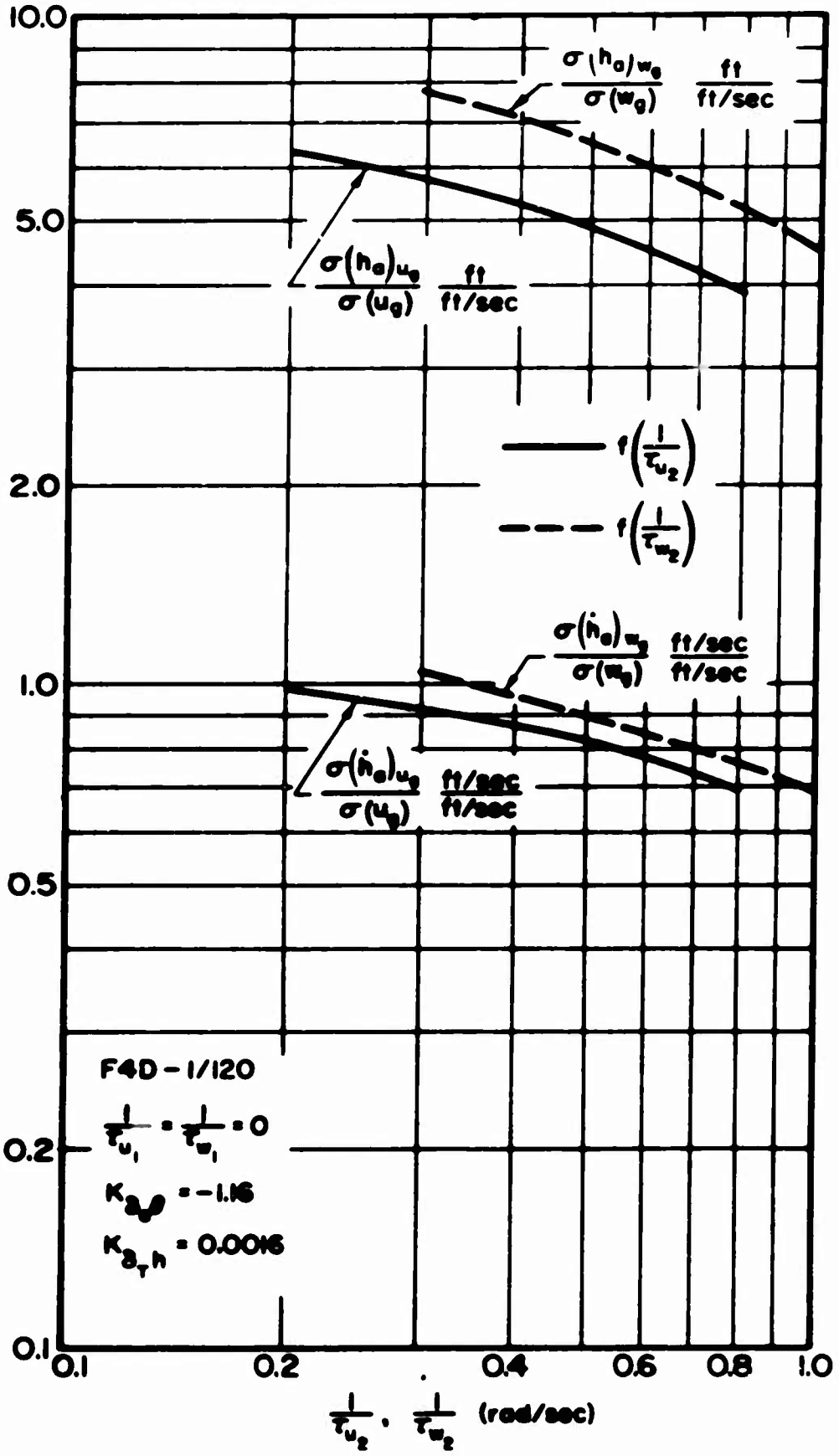

Figure 7. Sensitivity of Aircraft's Dispersions to Gust Spectrum High Frequency Break Point; Dispersions due to Gusts with $\theta \rightarrow \delta_e$ and $h \rightarrow \delta_T$

C. LANDING DISPERSION SENSITIVITY TO PILOT GAINS IN TURBULENT AIR CONDITIONS

Nominal gains for the loops closed by the pilot were selected on the basis of good low frequency performance and adequate stability margins as determined from previously discussed analyses. These nominal values were perturbed to discern resulting performance changes, considering only the air turbulence inputs. Resulting aircraft altitude and vertical velocity excursions are plotted in Fig. 8 for both piloting techniques as a function of separate loop-gain variations, i.e., only one gain varied at a time while holding other loop gains fixed at their nominal values.

For elevator control of altitude (Fig. 8a) there appears to be a moderate sensitivity of aircraft altitude dispersion as a function of altitude loop gain, $K_{\delta_{eh}}$, whereas vertical velocity dispersion, $\sigma(\dot{h}_a)$, is almost totally insensitive to pilot gain variations. It seems possible, therefore, to somewhat reduce the altitude dispersion by increasing $K_{\delta_{eh}}$, assuming the pilot tolerates the consequent loss of closed-loop damping (i.e., control may tend to get away from him). An autothrottle is desirable in this respect, since it provides increased phugoid damping (Ref. 22) necessary to operation at higher altitude-loop gains.

For altitude controlled with throttle (Fig. 8b) there is no performance improvement available by either increasing or decreasing pilot gains; further, the performance sensitivity about the nominal gain values is very small. Performance insensitivity to pilot gains is particularly useful in the early phases of the approach, for which resolution of the FLOLS indicated error is marginal (Ref. 32), i.e., altitude controlled with throttle permits considerable latitude in erroneously interpreted magnitude of flight path error. But the high level of dispersions render this control method inadequate for vernier altitude corrections in the vicinity of the ramp.

D. LANDING DISPERSION SENSITIVITY TO EQUALIZATION PARAMETERS FOR THE COMPENSATED-METBALL SYSTEM

A variable equalization network was inserted between the point-stabilized FLOLS and pilot/airframe system elements in the manner indicated at the bottom

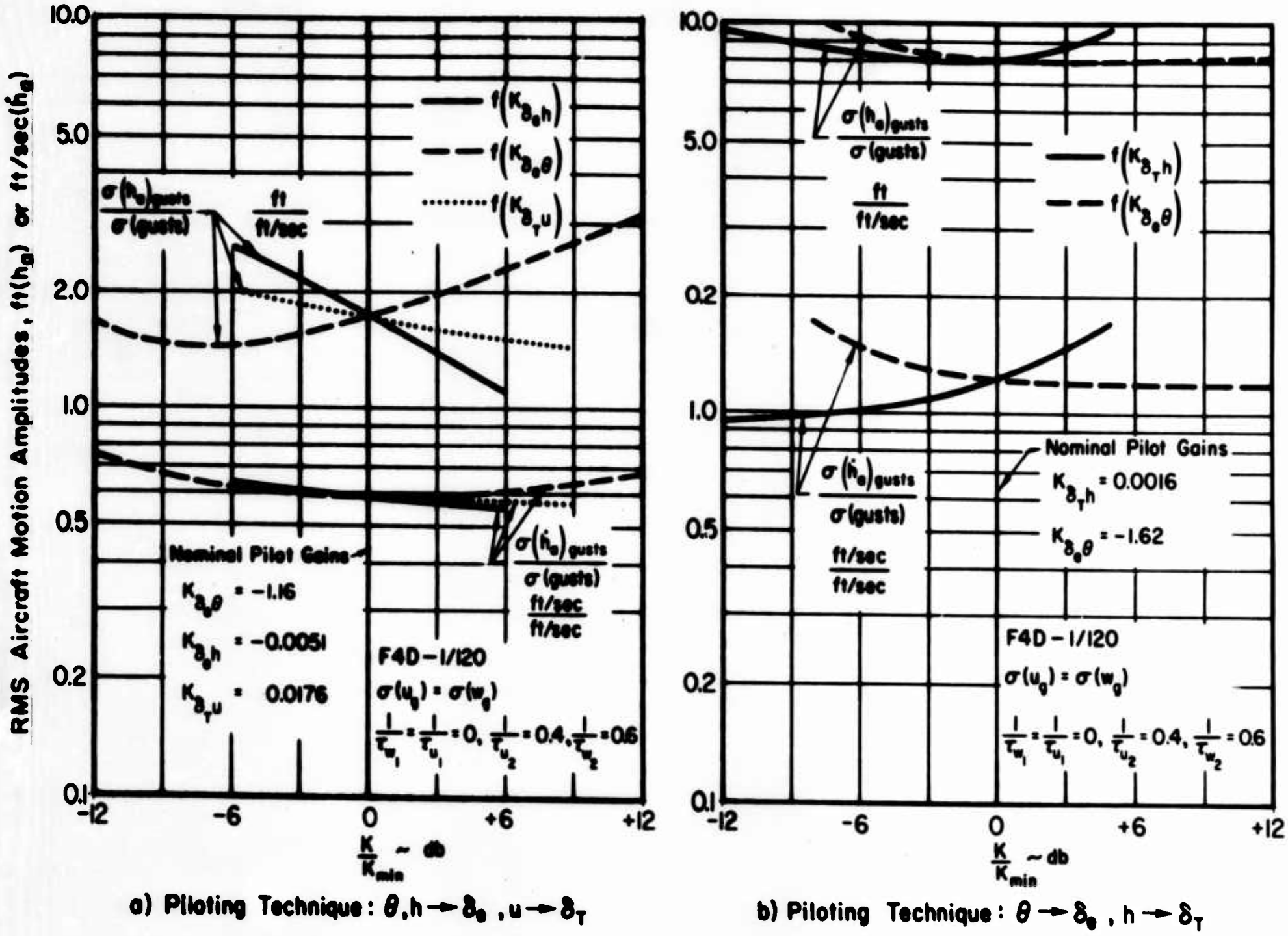

a) Piloting Technique: $\theta, h \rightarrow \delta_e$, $u \rightarrow \delta_T$

b) Piloting Technique: $\theta \rightarrow \delta_e$, $h \rightarrow \delta_T$

Figure 8. Altitude and Vertical Velocity Dispersion Sensitivity to Pilot Gains

of Fig. 9. This shaping filter effectively alters the phase and amplitude characteristics of the uncompensated beam motion, h_B, to produce aircraft motions more nearly in phase with the vertical movement of the ship, and thereby reduce landing dispersions. Using the Essex ship motion spectra [at amplitudes $\sigma(\theta_S) = 1^o$, $\sigma(h_S) = 5.5$ ft, and $\sigma(\varphi_S) = 2.2^o$] and the altitude-controlled-with-elevator piloting technique, resulting landing dispersions versus filter gain, K, and inverse time constant, $1/\tau$, are plotted in Fig. 9. Note that for $K \rightarrow 0$, resulting dispersions approach Table II values for meatball-averaging [e.g., Configuration 3WH; $\sigma(\Delta h_{TD}) = 6.6$ ft, $\sigma(\Delta h_R) = 7.7$ ft, $\sigma(\Delta V_I) = 5.5$ ft/sec]. The latter were obtained for beam intercept at $R_o = 5000$ ft, whereas the comparative data of Fig. 9 are mostly for $R_o = 2500$ ft. However both values yield comparable performance, as indicated by the $\sigma(\Delta h_{TD})$ dispersions so evaluated (Fig. 9).

Optimum filter values are indicated to be in the region of $1/\tau = 0.2$ and $K = 1.0$ for both Δh_{TD} and Δh_R dispersions, although somewhat higher values would further reduce ΔV_I. Dispersions corresponding to the above values of gain and inverse time constant were used in the performance evaluations for the compensated-meatball system described in Section II; also, the servo logic required to produce equivalent compensated-beam motion, h_B', given in Table I, is based on these values. No particular effort was made to obtain an optimum filter form, i.e., one that is relatively insensitive to changes in pilot/airframe and ship motion characteristics. The aim here was simply to examine the feasibility of beam compensation, and to roughly estimate performance gains realized. Note, for example, that equalization tends to increase the roll-induced component (dashed lines) of landing dispersions. It appears desirable, therefore, to stabilize the beam against ship roll in the conventional fashion without equalization (i.e., drop φ_S terms from the lens logic given in Table I for Configuration 4, and add term $\varphi_L = -0.16\varphi_S$, similar to Configuration 2).

E. ALTITUDE DEVIATION FROM THE NOMINAL FLIGHT PATH INCURRED BY TRACKING BEAM MOTION; COMPENSATED- AND UNCOMPENSATED-BEAM CONDITIONS

Aircraft rms altitude excursions in the groove induced by beam motions alone with the conventional point-stabilized FLOLS are shown in Fig. 10 as

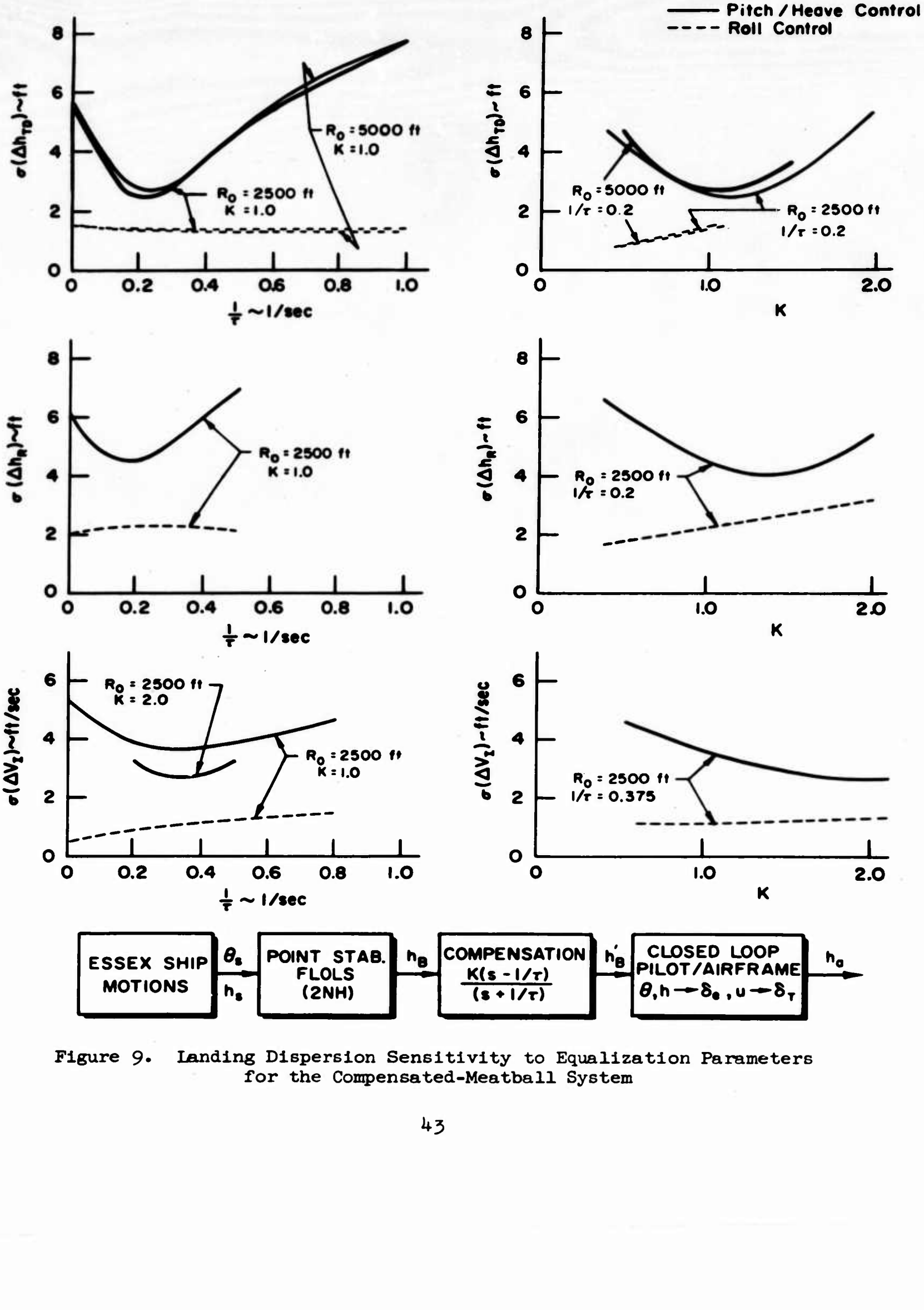

Figure 9. Landing Dispersion Sensitivity to Equalization Parameters for the Compensated-Meatball System

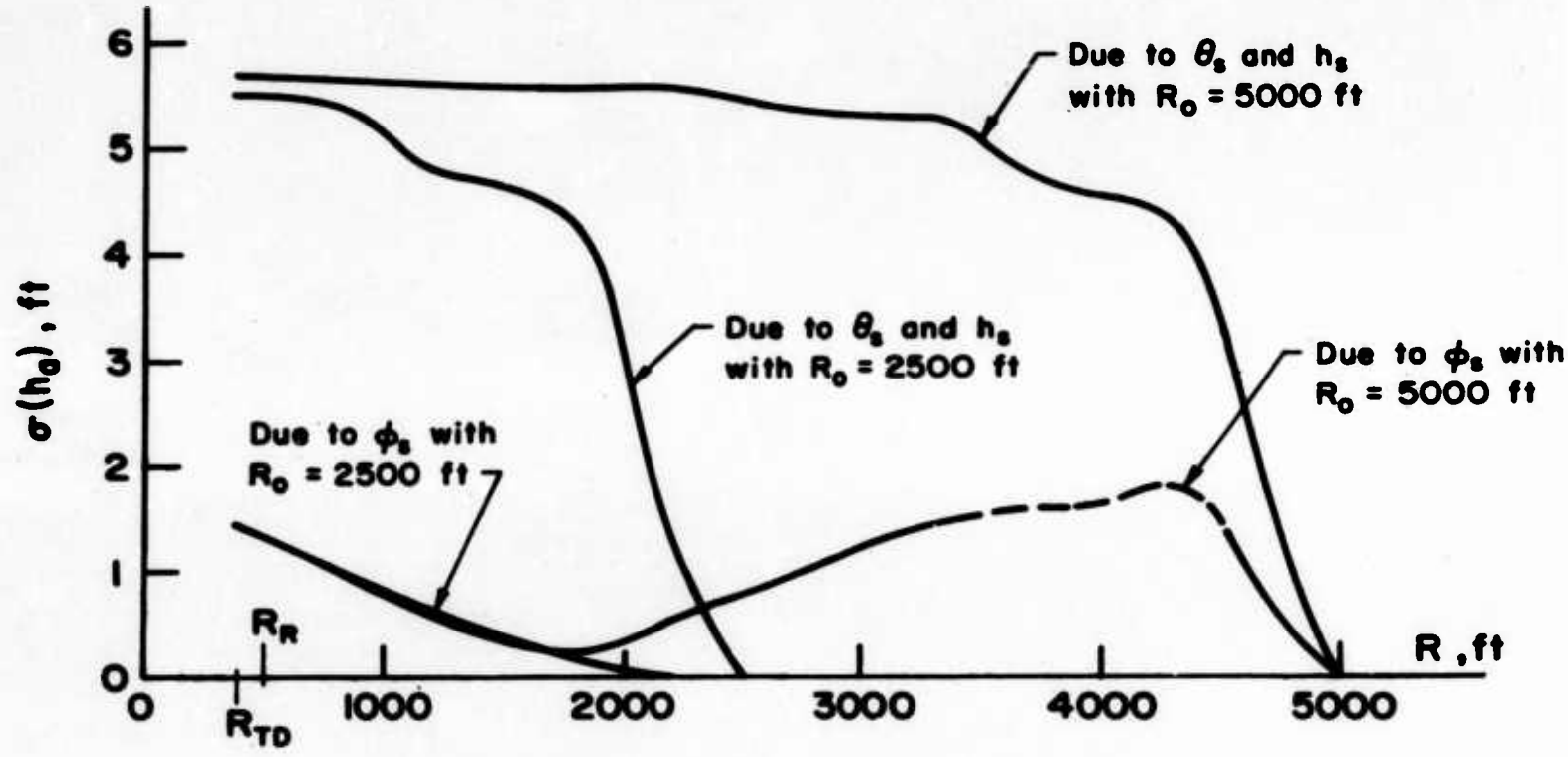

Point Stab. (2500 ft) Beam ; No Heave Stab.
$h \rightarrow \delta_e$, $u \rightarrow \delta_T$

Essex Motion Spectra
$\sigma(\theta_s)$ = 1.0 deg
$\sigma(h_s)$ = 5.5 ft
$\sigma(\phi_s)$ = 2.2 deg

Figure 10. Aircraft Altitude Excursions in the Groove Resulting from Pilot's Tracking the Uncompensated Beam

a function of range. Two initial ranges of beam-tracking are illustrated, R_o = 2500 and 5000 ft, both of which seem to have nearly identical transient conditions in establishing quiescent rms dispersion magnitudes. Thus, if the pilot is initially averaging beam motions, $\sigma(h_a) = 0$, and is then assumed to initiate tracking the beam at a range R_o, 10 sec or so later the aircraft altitude dispersions reach a quiescent rms value approximately equal to the rms beam motion in space [see Table I, $\sigma(h_B)$ values for Configuration 2NH].

Nearly identical altitude dispersion characteristics result with beam phase compensation (Fig. 11a) using compensation values K = 1 and $1/\tau = 0.2$ previously discussed. It is possible, however, to reduce altitude deviations by reducing the gain in the compensation network as indicated in Fig. 11b, but only at the expense of increased landing dispersions (see Fig. 9 and discussion).

Altitude excursions with either the uncompensated or compensated beam are small, being approximately equal to $\sigma(h_a)$ due to air turbulence alone, and probably would be unnoticed by the LSO until the aircraft is very close to the ramp. In the case of the uncompensated beam, resulting performance improvement is small, and is probably not worth the additional tracking effort involved. On the other hand, the performance gain with the compensated beam is substantial, so the additional incurred aircraft motion (approximately 50 percent greater excursions over beam-averaging conditions) is highly beneficial; these motions are also more nearly in phase with the deck and should, therefore, be less objectionable to the LSO. It is indicated, further, that the pilot should commence beam-tracking with the compensated system at least 5 to 10 sec from the ramp, which is consistent with adequate resolution of the FLOLS indicated error at that range. Prior to this range, the pilot may either average or track beam motion without much consequence to landing dispersions.

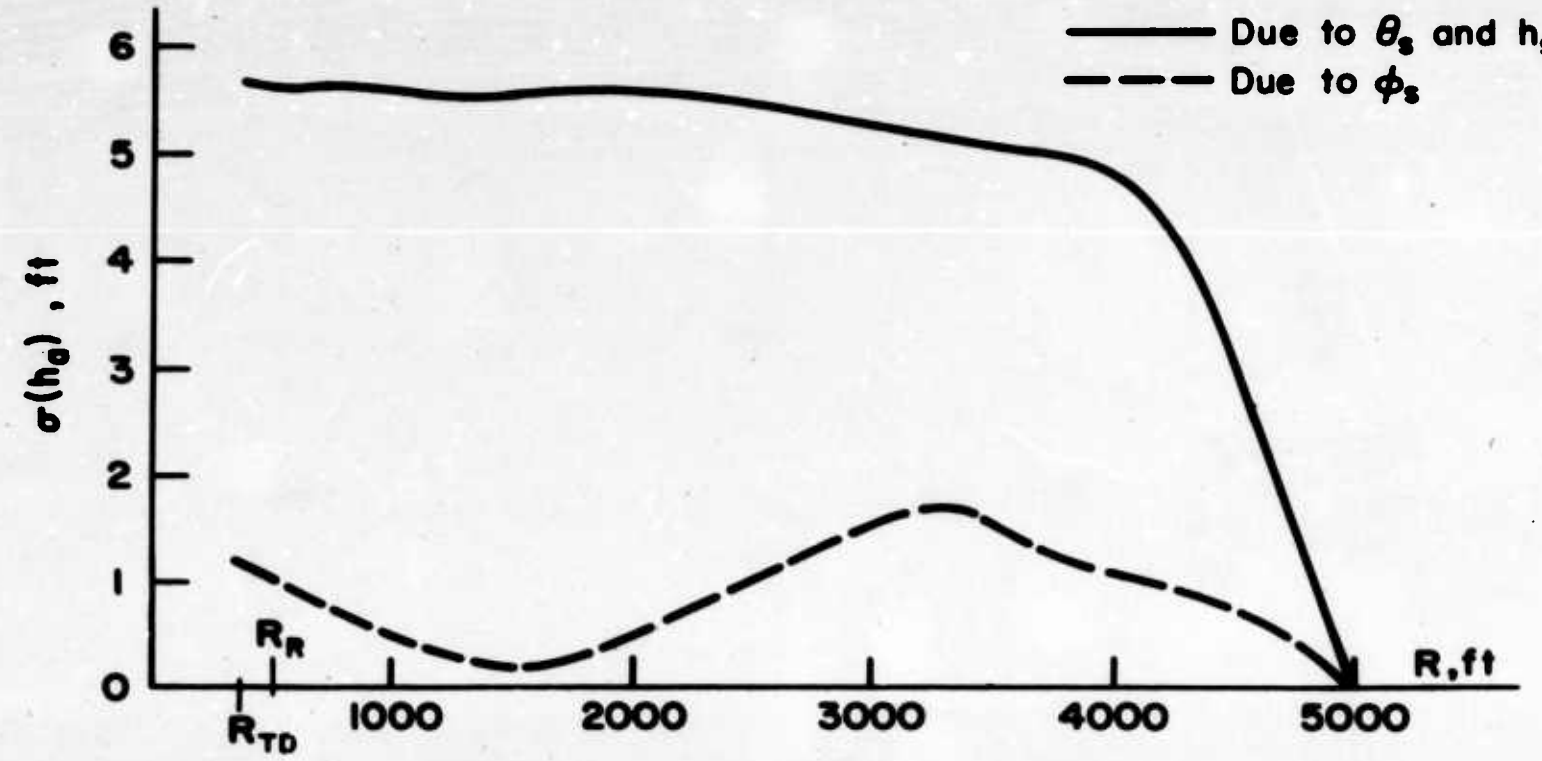

a) $\sigma(h_a)$ vs R with K = 1.0

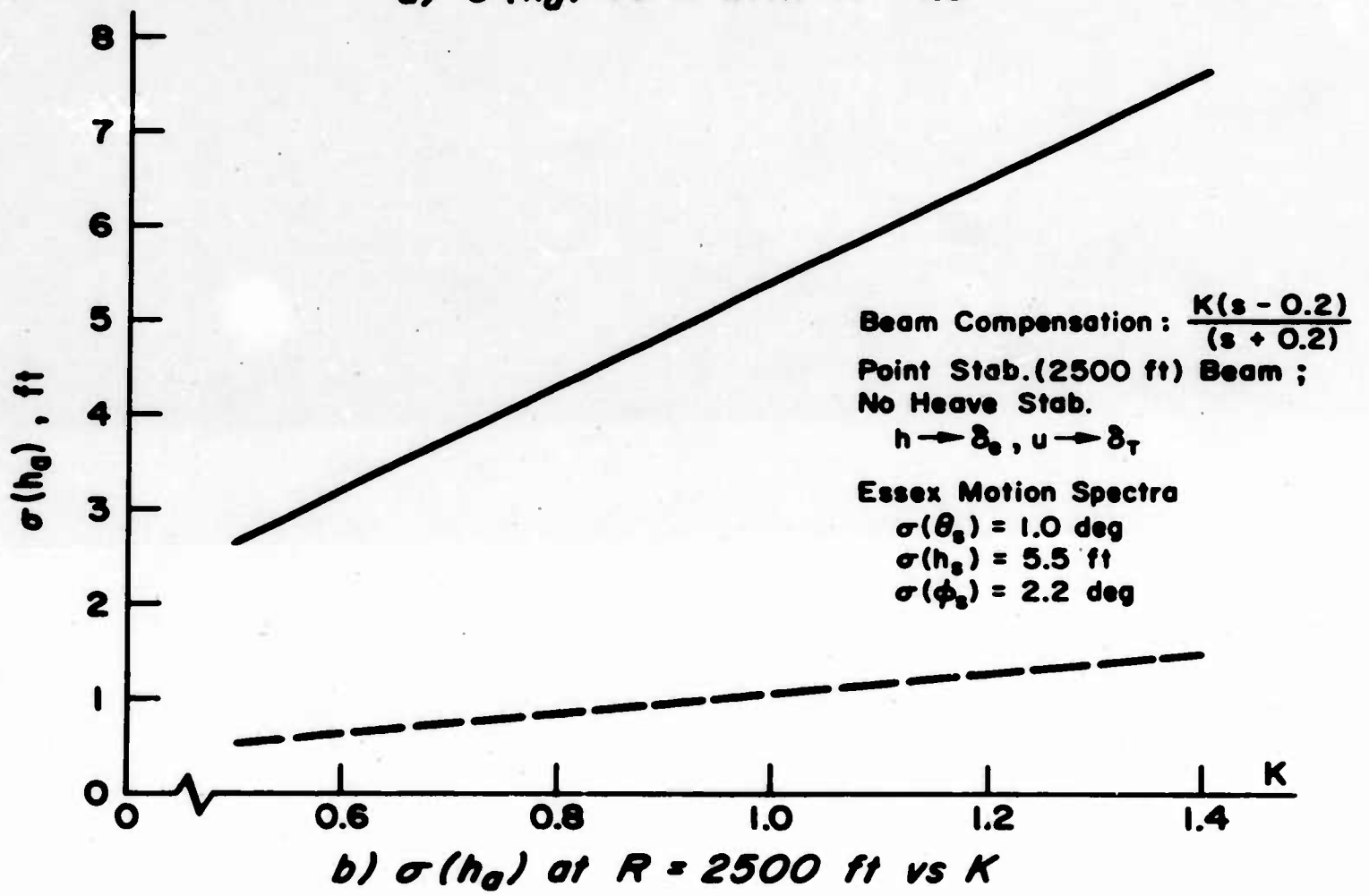

b) $\sigma(h_a)$ at R = 2500 ft vs K

Figure 11. Aircraft Altitude Excursions in the Groove Resulting from Pilot's Tracking the Compensated Beam

SECTION IV

ANALYSIS OF SHIP-MOTION-INDUCED LANDING DISPERSIONS

Certain simplifications were made to system time-varying elements which aid in understanding the results described in Sections II and III concerning ship-motion-induced components of landing dispersions. A constant-coefficient approximation of the point-stabilized FLOLS in combination with the transfer functions of the pilot/aircraft and ship motion inputs is shown to yield performance comparable to that of the more elaborate time-varying system. This simplification permits direct synthesis of beam motion compensation requirements to effectively reduce landing dispersions. Additional approximations are made to ship pitch and heave motions, assuming them to be correlated sinusoids of fixed phase relationship, which then permit comparison of relative phasing of deck, beam, and aircraft motions at a fixed frequency for the various FLOLS configurations considered. While the latter analogy of ship behavior is not strictly valid, it does qualitatively illustrate those factors relating the merits of various FLOLS stabilization methods, and the desirability of tracking versus averaging of ship-induced beam motion.

The effect of ship roll is neglected here since its contribution to landing dispersions has been determined to be relatively small, and therefore not a significant influence on the relative performance characteristics of competing systems.

A. CONSTANT-COEFFICIENT APPROXIMATIONS TO THE TIME-VARYING SYSTEM

As has been pointed out previously, the mathematical description of the system requires the use of linear equations with time-varying coefficients. The precise and economical evaluation of terminal errors from such equations demands methods such as the adjoint technique which do not afford physical insight into the interactions of the system elements. Even though the constant-coefficient approximation may appear inadequate for obtaining terminal errors, it would still be worth the insight it

allows. It also enables the use of the more powerful analytic tools which have been developed for studying and optimizing such systems.

To understand the approximation being made, it is necessary to look in detail at the interrelationship between the beam plane geometry and the pilot/airframe as it moves down the flight path. The beam motion equation, given in Fig. 1 of the text, mathematically represents this interrelation for a given FLOLS stabilization method, and neglecting ship roll this equation reduces to:

$$h_B = \underbrace{B_{h_s}^{h_B}(h_s) + B_{\theta_s}^{h_B}(\theta_s)}_{\text{Beam Translation}} + \underbrace{A_{\theta_s}^{h_B} \cdot R \cdot \theta_s}_{\text{Beam Rotation}} \qquad (4)$$

The beam rotation term in Eq 4 is range-sensitive, whereas the beam translation term is not. The two components of beam motion and their sum are illustrated in Fig. 12 as functions of range for the point-stabilized FLOLS, assuming sinusoidal pitch/heave motion characteristics. At any fixed range the beam simply moves up and down linearly with the ship motion inputs. But when the time-varying range of the pilot/airframe combination is considered, the beam rotation term introduces a variable gain into the equations of motion. However, even at the ramp where the rotational component is large, the magnitude of the translational component is typically five times that due to rotation. The total beam motion (Fig. 12c), therefore, closely resembles the translation component alone, i.e., is not greatly affected by range, and its envelope is representable by a constant-coefficient approximation.

The "best" approximation is that corresponding to the actual beam characteristics at some frozen range, which also yields the best agreement with the terminal dispersions computed using the more complete time-varying mathematical description.

Several fixed-range solutions were obtained with the aid of a digital computer; these solutions are compared with that of the exact time-varying system, obtained previously using the adjoint analog computer method, in Table X. This comparison shows that the touchdown dispersion parameters,

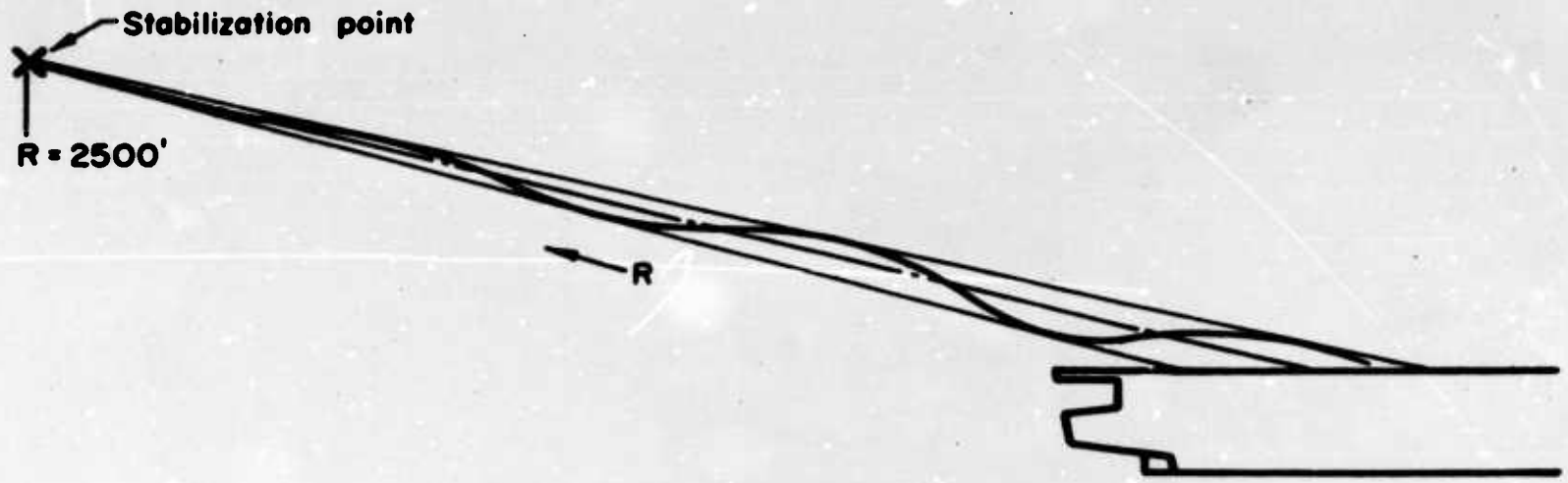

a) Rotation

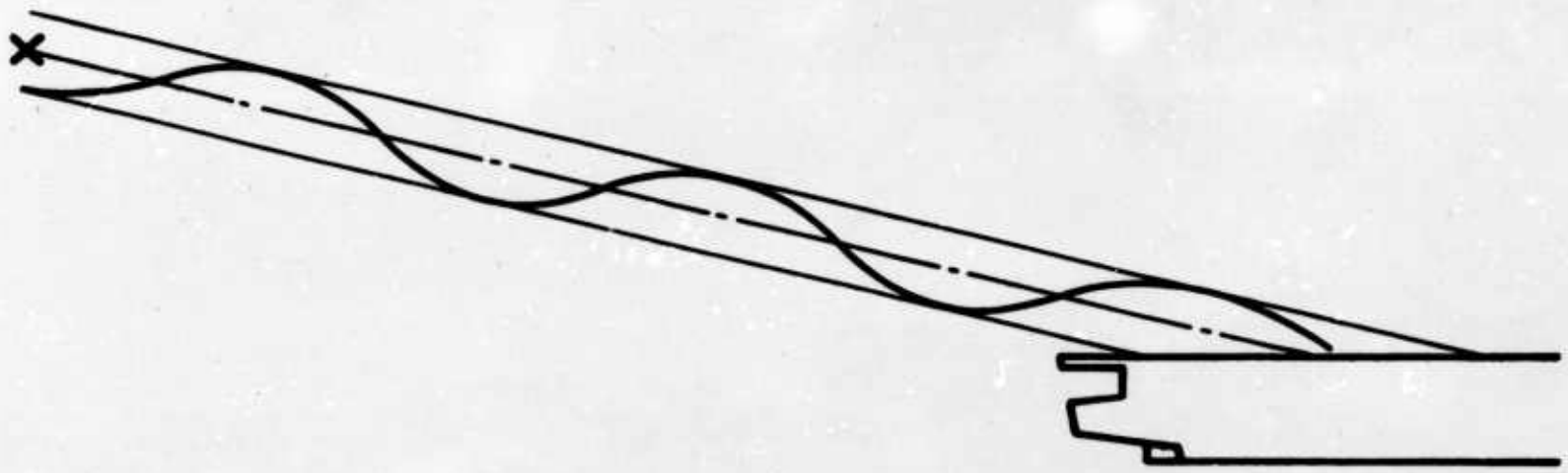

b) Translation

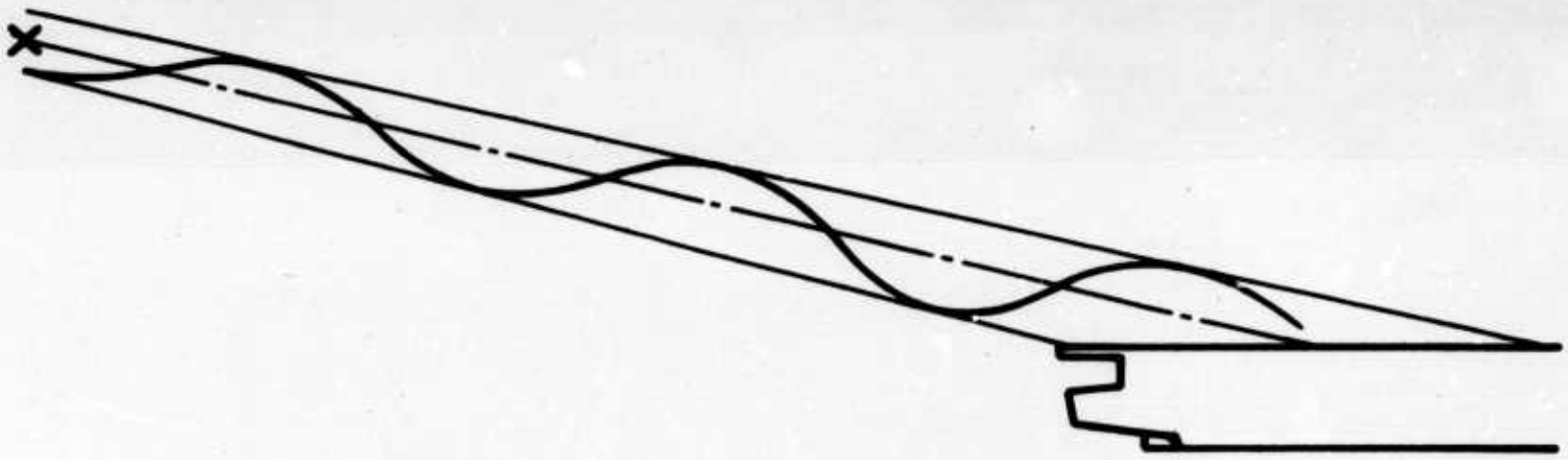

c) Composite of rotation and translation

Figure 12. Beam Motion Components for the Point-Stabilized FLOLS

TABLE X

COMPARISON OF APPROXIMATE CONSTANT-COEFFICIENT AND EXACT TIME-VARYING SOLUTIONS FOR THE POINT-STABILIZED FLOLS

LANDING DISPERSION*.....	$\sigma(\Delta h_R)$ (ft)	$\sigma(\Delta h_{TD})$ (ft)	$\sigma(\Delta V_I)$ (ft/sec)
Approximate fixed-range solution, using beam characteristics evaluated at:			
R = 500 ft (ramp).....	5.85	5.67	5.45
R = 1500 ft (midway between ramp and stabilization point).....	6.36	5.98	5.49
R = 2500 ft (stabilization point)....	6.83	6.28	5.71
Exact time-varying solution.....	6.3	5.7	5.4

*Using Essex motion spectra: $\sigma(\theta_s) = 1^o$; $\sigma(h_s) = 5.5$ ft
Piloting technique: $\theta, h \rightarrow \delta_e$, $u \rightarrow \delta_T$

Δh_{TD} and ΔV_I, are quite accurately reproduced with beam motions corresponding to those at the ramp (R = 500 ft); while height dispersion over the ramp, Δh_R, is best reproduced with beam characteristics corresponding to a range midway between the ramp and the stabilization point (R = 1500 ft). The suitability of these "best fit" ranges depends, of course, on the ratio of $\sigma(\theta_s):\sigma(h_s)$; for values different than those used in the above comparisons, other ranges will be more appropriate.

B. SYNTHESIS OF BEAM-COMPENSATION REQUIREMENTS

With the preceding background, we can now confidently use analytical techniques to improve our understanding of the basic elements of the problem. Consider, for the sake of simplicity, only the dispersion of the touchdown point, Δh_{TD}. Figure 13 is a simplified block diagram relating applicable transfer functions of system elements necessary for the computation of Δh_{TD}. The touchdown dispersion is conveniently expressed in power spectral density terms, as given by Eq 5.

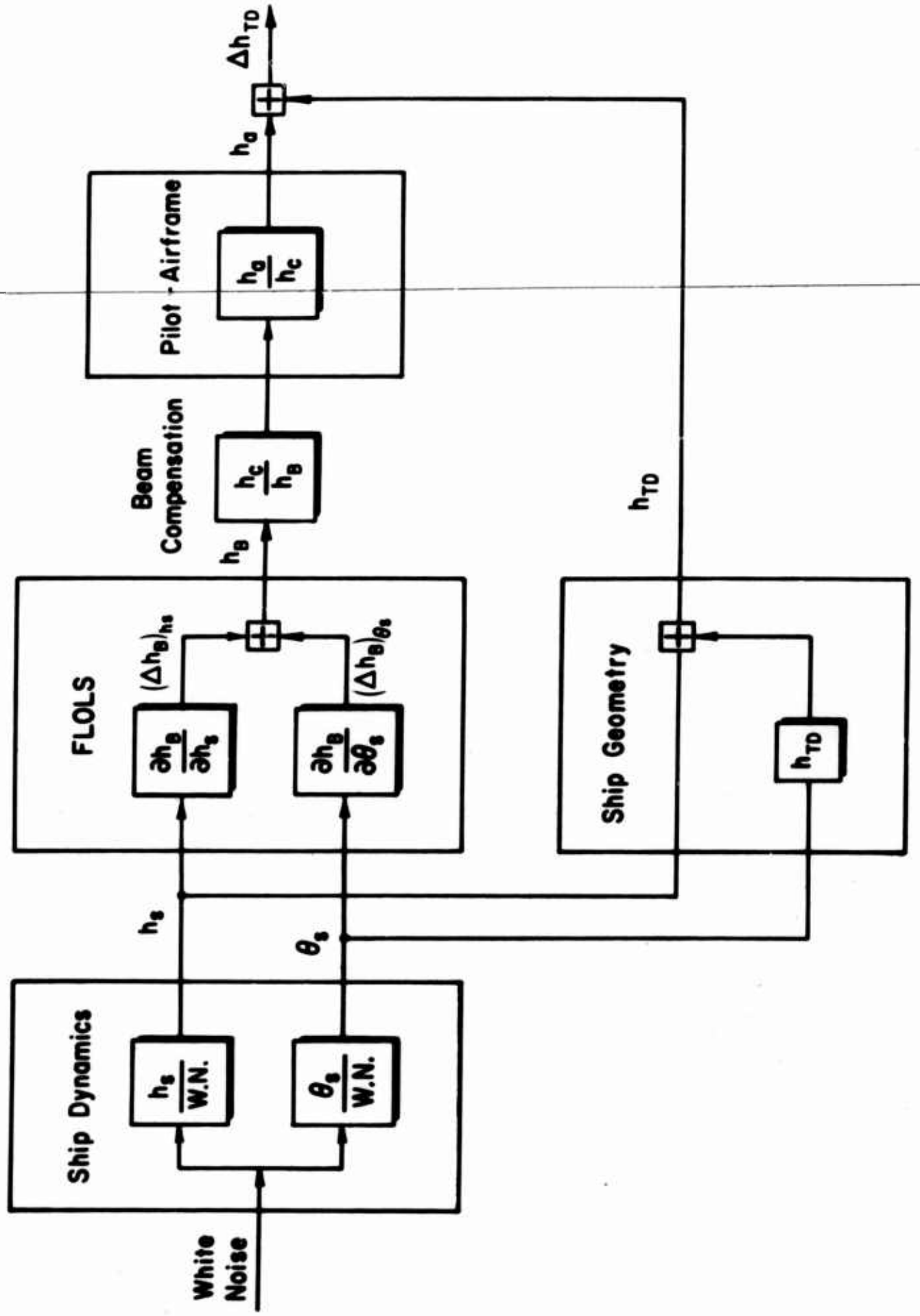

Figure 13. Simplified System Block Diagram Used for Computation of Δh_{TD}

$$\Phi_{\Delta h_{TD}} = \left[\left(\frac{h_a}{h_c}\right)\left(\frac{h_c}{h_B}\right)\right]^2\left[\left|\frac{\partial h_B}{\partial \theta_s}\right|^2 \Phi_{\theta_s} + \left|\frac{\partial h_B}{\partial h_s}\right|^2 \Phi_{h_s}\right] - \Phi_{h_s} - \left|L_{TD}\right|^2 \Phi_{\theta_s} \qquad (5)$$

where Φ is the symbol for power spectral density

For the numerical example, which follows, the characteristics used are those for the uncompensated point-stabilized FLOLS (using frozen-range characteristics corresponding to R = 500 ft and for $h_c/h_B = 1$) and the Essex ship motion spectra given in Appendix A. The closed-loop pilot/vehicle transfer function, when evaluated with Appendix A values of airframe characteristics and pilot gains (for $\theta,h \rightarrow \delta_e$, $u \rightarrow \delta_T$ control), is given by Eq 6.

$$\left.\frac{h_a}{h_c}\right]_{\substack{\theta,h\rightarrow\delta_e \\ u\rightarrow\delta_T}} = \frac{-0.16(s + 0.13)(s + 4.31)(s - 3.58)}{(s + 0.11)\left[s^2 + 2(0.41)(0.5)s + (0.5)^2\right]\left[s^2 + 2(0.19)(3.46)s + (3.46)^2\right]} \qquad (6)$$

A convenient method for illustrating the solution of Eq 5 is to present graphs of the individual spectral components and the vector summations involved. This process is shown in Fig. 14. The solution is performed in four parts, separately solving the following relationships:

Figure 14a: Beam motion..... $h_B = \frac{\partial h_B}{\partial h_s} h_s + \frac{\partial h_B}{\partial \theta_s} \theta_s$ (7)

Figure 14b: Touchdown point motion.... $h_{TD} = h_s - L_{TD}\theta_s$ (8)

Figure 14c: Aircraft motion..... $h_a = \left[\frac{h_a}{h_c}\right]^2 h_B$ (9)

Figure 14d: Dispersion of the aircraft touchdown point..... $\Delta h_{TD} = h_a - h_{TD}$ (10)

As shown in Fig. 14d, a fairly large Δh_{TD} value results principally because of the lagging phase of aircraft motion relative to the motion of the touchdown point (i.e., $\measuredangle h_a/h_{TD} \doteq -45^\circ$ at the central motion

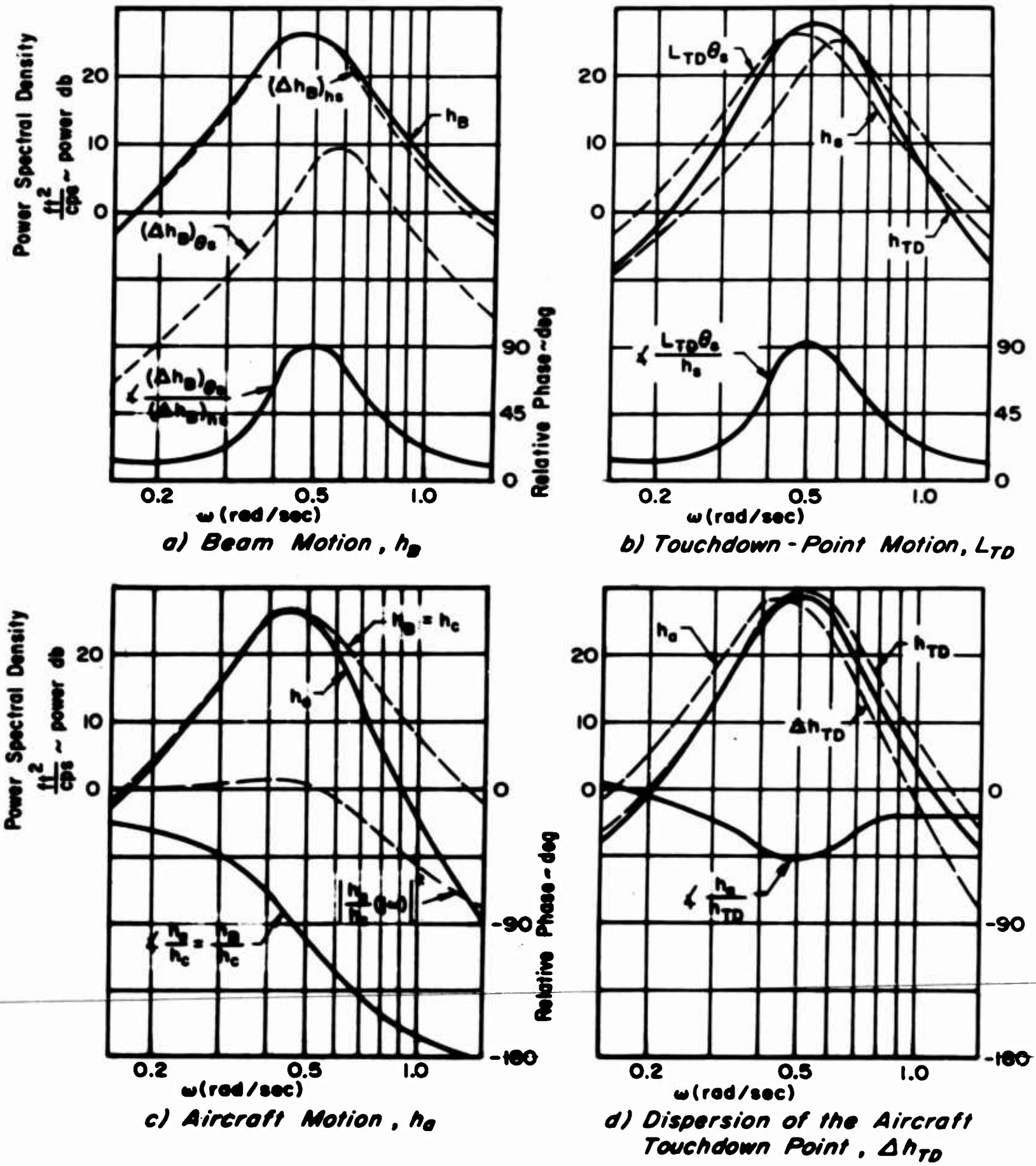

Figure 14. Spectral Representation of Aircraft Touchdown Dispersion Factors for the Uncompensated Point-Stabilized Beam

frequency, $\omega_s \doteq 0.5$ rad/sec). This phase lag comes about as a result of pilot/aircraft lags in following beam motion as indicated in Fig. 14c (i.e., $\measuredangle h_a/h_c = \measuredangle h_a/h_B \doteq -100^\circ$ at $\omega_s = 0.5$). Requirements for beam motion compensation, to reduce Δh_{TD}, are implied in this cause/effect relationship. Thus it is desirable to introduce phase lead compensation, h_c/h_B, which will effectively reduce the h_a/h_{TD} phase lag. Also, since the h_a and h_{TD} power spectra (Fig. 14d) are fairly well matched as a function of frequency, it is desirable to maintain $h_a/h_B = 1$ in the frequency region of interest. The equalization network, h_c/h_B, given in Eq 11 meets this requirement, and is used to illustrate the synthesis procedure in Fig. 15.

$$\frac{h_c}{h_B} = K\left[\frac{\tau s - 1}{\tau s + 1}\right] \tag{11}$$

The time constant, τ, of Eq 10 is adjusted in Fig. 15a to advance the phase of h_a/h_B by about 45°*; i.e., to compensate the $\measuredangle h_a/h_{TD} \doteq -45^\circ$ lag shown in Fig. 14d. The result of the beam phase compensation is shown in Fig. 15b, indicating a net reduction of the Δh_{TD} power density of approximately 12 db at the central ship-motion frequency, $\omega_s = 0.5$. This improvement corresponds to reduced $\sigma(\Delta h_{TD})$ by a factor of 2, as determined previously from computations with the adjoint method [note that the $\sigma(h_{TD})$ can be computed analytically as well by taking the area integral of the linear plot of the Δh_{TD} power spectral density].

C. RELATIVE PHASING OF DECK, BEAM, AND AIRCRAFT MOTIONS FOR VARIOUS FLOLS STABILIZATION METHODS

Using simple harmonic respresentation of deck motion spectra and constant-coefficient approximations to the range-sensitive geometry described above, phase vectors can be constructed to represent the motions of the deck, beam, and aircraft in the manner illustrated in Fig. 16. Previously utilized Essex ship motion spectra are approximated with the sinusoidal functions described in Fig. 16a. Motions of the ramp, h_R, and

*Evaluation of h_c/h_B from Eq 11 for $\tau = 5.0$ and $s = j\omega_s = j0.5$ yields $K \measuredangle +43.6^\circ$.

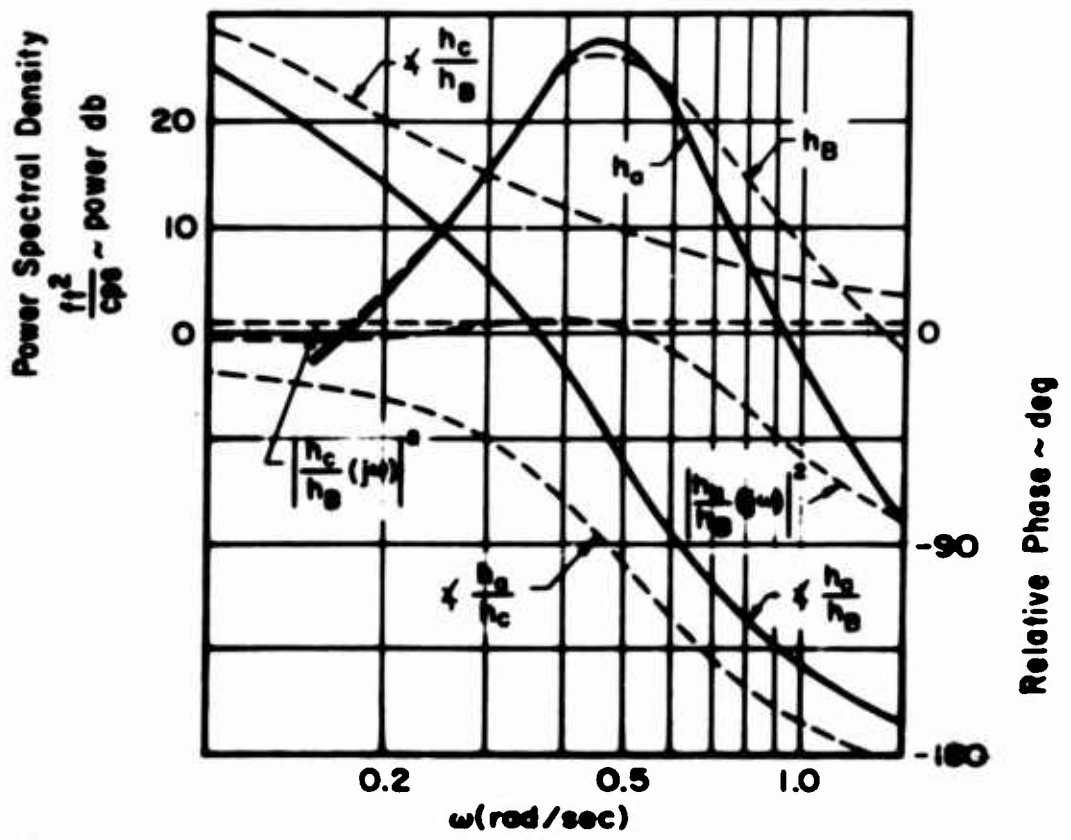

a) Beam Phase Compensation To Counteract The Pilot/Aircraft Lag

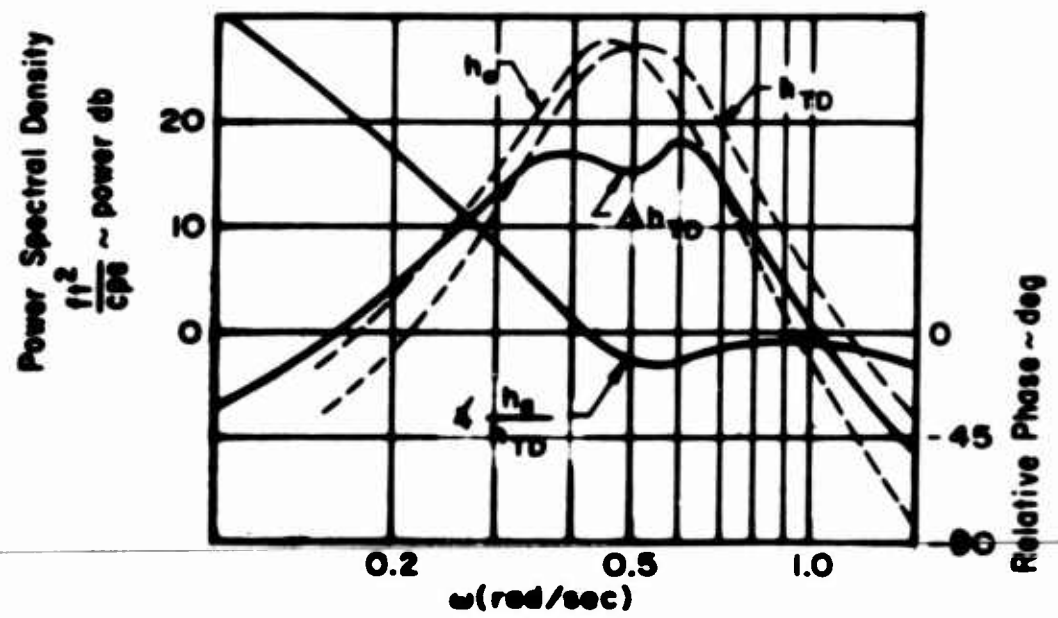

b) Resulting Δh_{TD} With Beam Phase Compensation

Figure 15. Spectral Representation of the Synthesis Procedure for Compensating the Beam Motion Phase

touchdown point, h_{TD}, are simply related to pitch and heave motions by the illustrated deck geometry and phase vectors.

Vertical displacement of the beam, h_B, is considered for the point-stabilized FLOLS in Fig. 16b. Phase vectors are constructed for the resulting beam motion at the ramp to approximate its effects on landing dispersions. The phasing of beam motion is additionally dependent on the location of the FLOLS relative to the ship pitch axis, and on the particular FLOLS stabilization logic utilized. The location of the FLOLS is usually forward of the pitch axis and, for the case illustrated, beam translation due to pitch, $(\Delta h_B)_{\theta_S}$ is in phase with θ_S. Other FLOLS configurations can be similary treated: e.g., in the case of synchronizing beam motion with touchdown point motion (Configuration 1NH), the phase of $(\Delta h_B)_{\theta_S}$ is changed by 180° and its magnitude adjusted to make the total beam phase vector equal to h_{TD}; beam stabilization against heave motion simply removes the h_S vector component from h_B, leaving $(\Delta h_B)_{\theta_S}$ as the total beam motion; and so on, as illustrated subsequently.

The aircraft vertical motion vector, h_a, is considered in the manner indicated in Fig. 16c, and simply relates the magnitude and phase lag of the pilot/aircraft flight path deviation in following the ship-induced beam motion, h_B. For the latter purpose, the closed-loop pilot/aircraft system is evaluated from Fig. 14c at the approximate dominant ship motion frequency, $\omega_S \doteq 0.5$ rad/sec, resulting in the phase vectors (or phasors) shown.

Finally, the deck, beam, and aircraft phasors are mated according to the four basic FLOLS stabilization methods considered, as shown in Fig. 17. For each case illustrated, the relative phasing of deck motions (solid phasors) is fixed. Of particular interest here is the phasing of the aircraft motion, h_a, in relation to the ramp, h_R, and touchdown point, h_{TD}, recognizing that landing dispersions, $\sigma(h_{TD})$ and $\sigma(h_R)$, are proportional to the lengths of the line segments connecting the tips of appropriate (h_a to h_{TD} and h_a to h_R) phasors, in the manner indicated for the point-stabilized FLOLS. On this basis it is obviously desirable to have the h_a phasor located between h_{TD} and h_R as in the case shown for the "compensated meatball," and additionally have its length proportional to the average

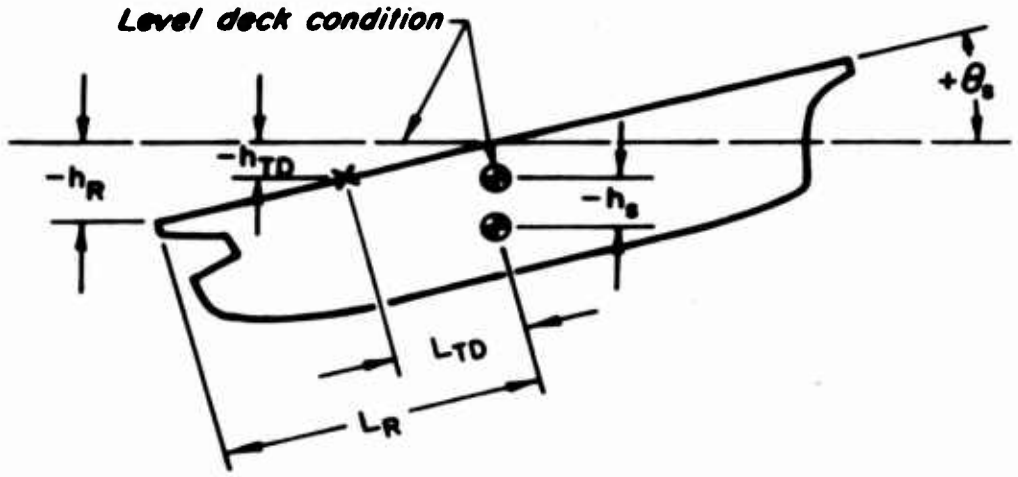

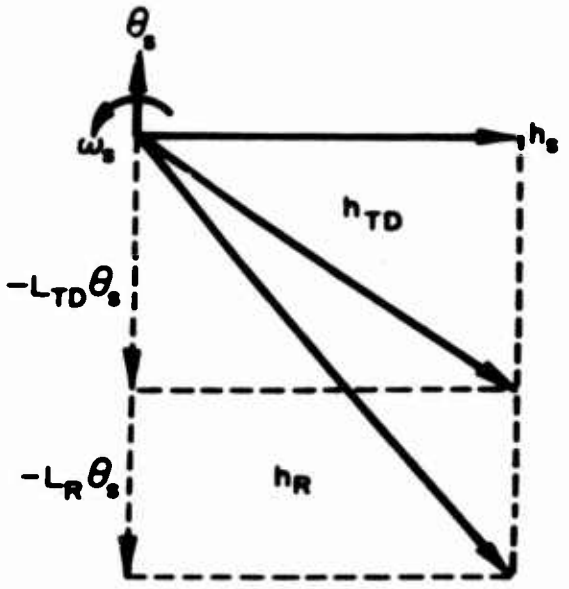

$h_s(t) \doteq 7.8 \sin \omega_s t$ $\qquad h_R(t) = h_s(t) - L_R\theta_s(t)$

$\theta_s(t) = 1.4 \sin(\omega_s t + 90°)$ $\qquad h_{TD}(t) = h_s(t) - L_{TD}\theta_s(t)$

(a) Relative phasing of deck motions

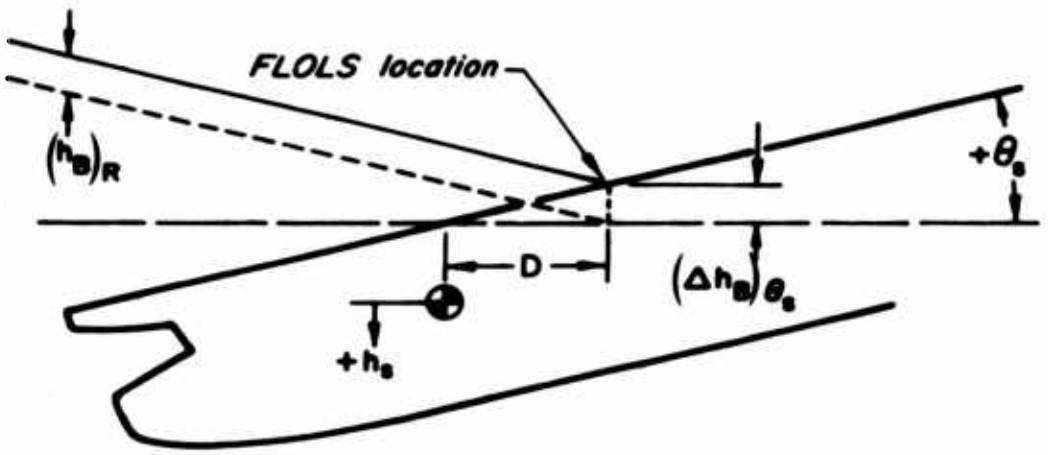

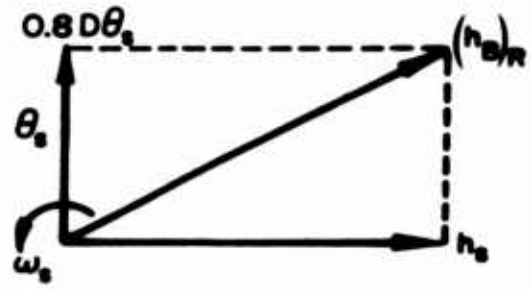

$(h_B)_R = \left[h_s + (\Delta h_B)_{\theta_s}\right]_{Ramp}$; $\quad (h_B)_R(t) \doteq h_s(t) + 0.8D\theta_s(t)$

(b) Phasing of beam relative to pitch and heave motions at the ramp; point -stabilized FLOLS (configuration 2NH)

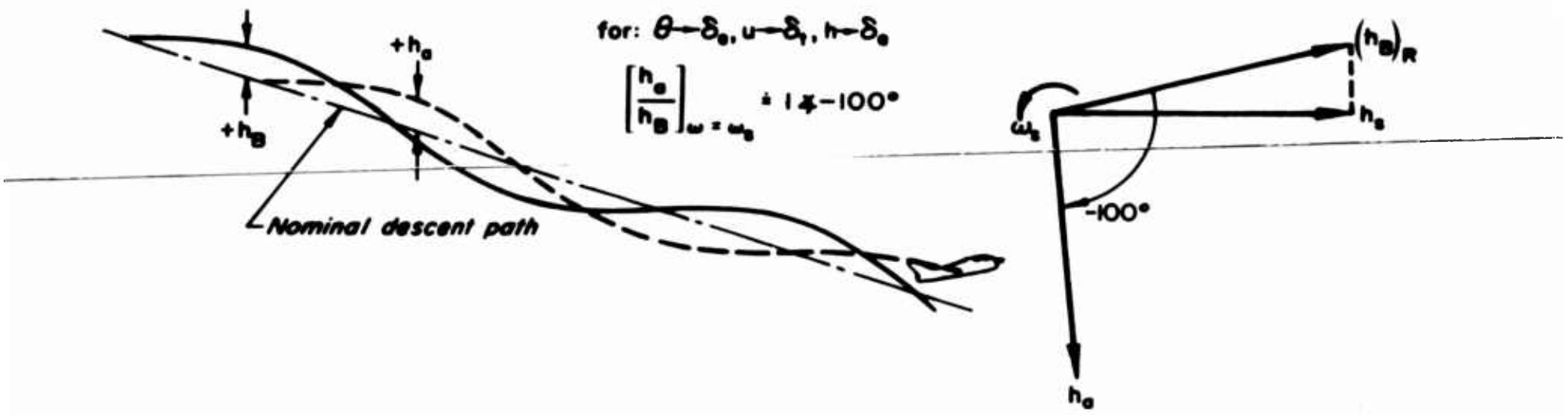

(c) Aircraft phase lag in following beam motions

Figure 16. Illustration of Phase Vector Construction of Deck, Beam, and Aircraft Vertical Motions

ANGLE STABILIZATION *(Configuration 1NH)*	POINT STABILIZATION *(Configuration 2NH)*
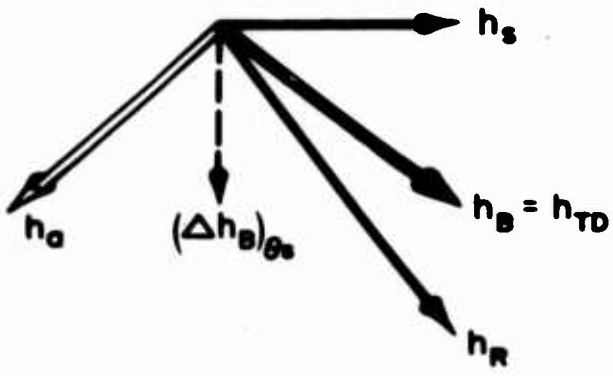	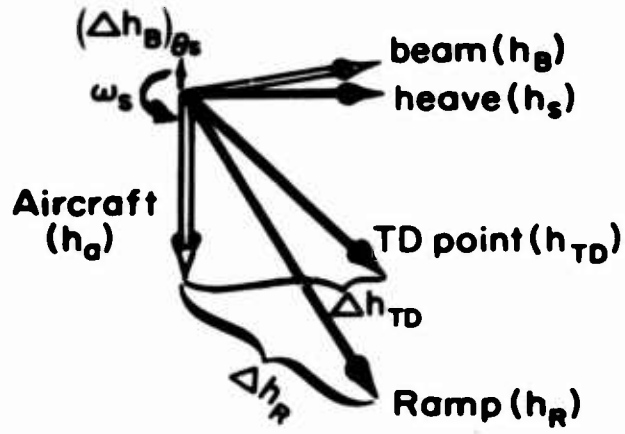
LINE AND POINT STABILIZATION *(Configuration 3NH)*	**COMPENSATED MEATBALL** *(Configuration 4NH)*
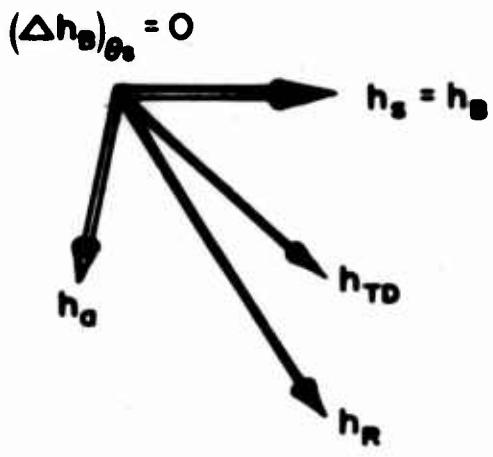	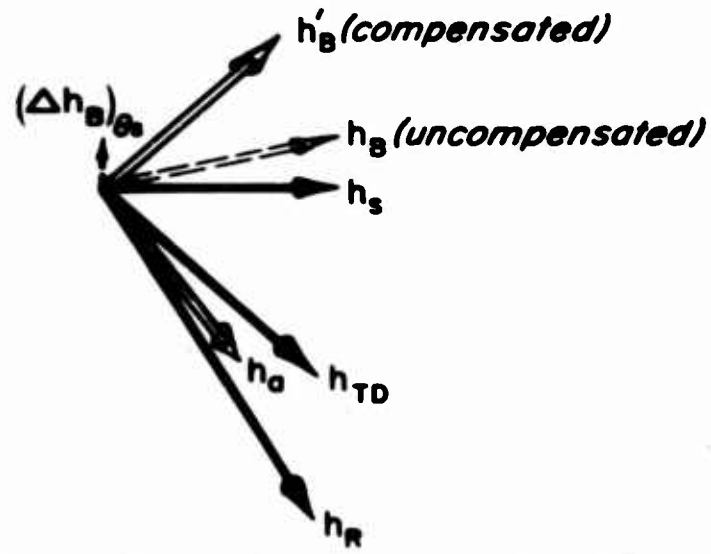 *Note: Phase of h_B is advanced to h'_B by FLOLS servo compensation network*

Figure 17. Illustration of Relative Phasing of Deck, Beam, and Aircraft Vertical Motions for Various FLOLS Stabilization Methods

h_{TD} and h_R phasor magnitudes. By the same logic, other FLOLS configurations illustrated can be ranked according to their indicated phasor relationships, and reasons for their inadequacies are readily apparent. Briefly reviewing these characteristics for the four FLOLS configurations illustrated in Fig. 17, it is seen that:

1. Angle stabilization is characterized by the greatest disparity between aircraft and deck motions. This condition is brought about by the synchronized motion of the beam and touchdown point (h_B in phase with h_{TD}), which adversely lags aircraft motion, h_a, relative to motions of the deck (h_R and h_{TD}). Under such conditions better performance is probably attainable with pilot-averaging of the beam motion ($h_a = 0$). Stabilizing the beam against heave motion further lags the aircraft phasors with respect to h_R and h_{TD}, and thus increases landing dispersions.

2. Point stabilization ranks second best to the compensated-meatball FLOLS, since a significant component of aircraft motion is in phase with ramp and touchdown point motions, thereby reducing landing dispersions to some extent over beam-averaging ($h_a = 0$) conditions. Stabilizing the beam against heave advances the h_a phasor; however, the remaining beam motion, $h_B = (\Delta h_B)_{\theta_S}$, is too small tc be of any consequence, and its phase is advanced even farther (note that from the latter consideration height dispersions at the ramp would be more adversely increased than those over the touchdown point).

3. Line-and-point stabilization ranks intermediate to the first two systems described above because of correspondingly intermediate phasing of the h_a phasor. Stabilizing the beam against $(\Delta h_B)_{\theta_S}$ does slightly reduce the magnitude of beam motion, but also retards the phase of h_B. Stabilizing the beam against heave effectively yields performance equivalent to the beam-motion-averaging technique (i.e., $\Delta h_R = h_R$, $\Delta h_{TD} = h_{TD}$).

4. The compensated-meatball system is basically the point-stabilized configuration described above, but with phase lead compensation added to advance the phase of h_B to h_B' as indicated. The amount of phase lead supplied is intended, as shown, to reduce phase differences between aircraft and deck motions, and thereby reduce landing dispersions.

These qualitative results are consistent with the measured landing dispersion values presented in Section II. Thus, this simplified dynamic description of the system provides invaluable insight into the complex interplay of elements. The analytical method thus can provide a simple picture of and a logical basis for synthesizing equalization requirements.

Another possibility indicated by the simplified analysis is the control of beam phase through dynamic variation (as opposed to a fixed-parameter equalization network) of pitch and roll correction factors in accordance with continuously measured magnitude and phase of heave relative to pitch. Thus pitch- and heave-induced components of beam motion could be controlled directly to produce fixed phasing between beam and deck motions. Total beam motion amplitude can be similarly and simultaneously controlled to induce aircraft vertical flight path excursions always coincident with the vertical motion of a point on the deck located midway between the ramp and the touchdown point.

SECTION V

DISCUSSION AND CONCLUSIONS

The mathematical model descriptive of carrier landing has been shown to yield theoretical performance consistent with that actually experienced in terms of vertical landing dispersions and resulting bolters, waveoffs, and accidents. Examination of this model has permitted delineation of principal problem causes, as well as postulation of improvements. Specific conclusions derived from the modeling, performance evaluation, and analyses activities performed in the course of this study are discussed below.

1. The currently operational point-stabilized FLOLS yields landing performance which is as good as or better than other conventional beam-stabilization methods.

"Other" conventional stabilization methods investigated include the "angle"-stabilized and "line-and-point"-stabilized FLOLS. The angle method predates the point-stabilized FLOLS in usage and was shown to yield greatly inferior performance to the newer method. The line-and-point-stabilized FLOLS is currently undergoing sea trial evaluations as a possible replacement for the point-stabilized FLOLS; analyses have indicated slightly inferior landing performance under conditions of "meatball-chasing."

2. The "meatball-averaging" piloting technique advocated by Naval doctrine yields best over-all landing performance in conjunction with the presently operational point-stabilized FLOLS.

Pilot's tracking of ship-motion-induced deviations of the conventionally stabilized FLOLS beam does not improve system performance over the meatball-averaging technique, in spite of the necessarily greater pilot tracking effort and greater resulting aircraft motions in the groove. Yet pilots seem to possess an innate tendency for meatball-chasing, and at certain times of truly compensatory display (e.g., on dark moonless nights) they have no choice but to track all meatball motions. Accordingly, it appears

desirable to evolve stabilization systems which characteristically induce the least beam motion. In this respect, the experimental line-and-point-stabilization method yields slightly reduced FLOLS beam motion over the point-stabilized FLOLS, but actual motion differences are probably not discernible by the pilot because of considerable beam motion due to ship heave. Large beam motions predominantly result from ship's response to low frequency swell waves, either in calm seas or in combination with large sea waves. The incidence of combined swell and sea waves seems more probable than either alone, so considerable heave motion of the beam will generally occur during normal carrier air operations.

3. Additional stabilization of the FLOLS beam against ship heave motion can theoretically eliminate beam-chasing.

By additionally stabilizing the optical landing system against heave motion in conjunction with the line-and-point-stabilization scheme, a totally immobile beam and commanded flight path result, which should theoretically eliminate beam-chasing. The more stable FLOLS beam reduces the piloting control effort involved, but it does not improve landing performance over that obtained with the conventional point-stabilized FLOLS. Stabilization of the beam against ship heave is otherwise detrimental to landing performance for stabilization schemes other than the line-and-point method.

4. Significant reduction of landing dispersions and accidents is attainable with the compensated-meatball FLOLS.

This system derives from the conventional point-stabilized FLOLS, but has compensation added to advance the beam motion phase. The beam so compensated enables the pilot to more closely synchronize the aircraft flight path with the vertical motion of the ramp and touchdown point. Mechanization requirements seem slight, requiring relatively simple modifications to the present operational recovery system; and in view of the potentially high payoff (analyses have indicated a reduction in accident rate by as much as 40:1 over the conventional meatball-averaging technique), this FLOLS modification deserves additional study with respect to operational suitability and more optimum filter design, i.e., one less

susceptible to variation in ship motion spectra and aircraft dynamic characteristics.

5. Landing dispersions are most significantly and equally affected by atmospheric turbulence and ship motions, and to a much lesser extent by unstabilized FLOLS beam motion.

One obvious approach to improving performance is to reduce the intensity of rough-air and ship motions, as might be possible by streamlining the ship superstructure and using ship pitch stabilizers. Ship motion prediction can also theoretically eliminate deck motion effects on landing dispersions by suitably anticipating deck conditions at the instant of touchdown. These solutions, however, require considerable development of operationally suitable methods and equipment which are not easily implemented. Other more easily attainable improvements involve tighter control of flight path to combat rough-air effects, and the synchronization of aircraft vertical motions with those of the deck to reduce their relative motion effects on the landing, as is accomplished with the "compensated-meatball" scheme.

6. Actual pilot tracking performance with the currently operational landing system is already as good as is theoretically possible.

This is a corollary to the above observation, and is inferred from the good correlation of actual landing dispersions with those computed in conjunction with a theoretically optimum human pilot model.

7. Absence of the real horizon can seriously degrade landing performance.

An easily accessible pitch attitude reference is required for acceptable landing performance, and is normally available in the form of the natural horizon. Loss of this primary reference, as might occur on dark moonless nights, can be responsible for a significant deterioration in performance (analyses have indicated five times greater probability of an accident under certain environmental conditions).

8. Despite the apparent success of the mathematical model of the carrier landing system, there remain uncertainties which prevent its confident use; these should be resolved through future model refinement activities.

The mathematical model of the complete carrier approach and landing system developed in this study permits rapid assessment of the potential performance improvement accruing from changes to the system and its inputs. In spite of this apparent success, there remain areas of uncertainty in the present model which preclude its confident use in computing absolute performance improvements accompanying a system modification. However, a preliminary subjection of the uncertain areas to changes in assumptions shows that reasonable (as presently understood) changes do not affect relative improvements in performance. Thus, the present model can be used with moderate confidence to pinpoint system or input changes which have large potential payoff in improving performance. However, to more definitely identify desirable and recommended system changes:

a. The system model must be improved to eliminate as far as possible the performance-sensitive uncertainties in the present preliminary model.

b. The current set of promising system changes must be subjected to a more thorough analytic examination based on the revised model.

c. Changes yielding substantial improvement with the revised model must be further scrutinized in terms of operational consequence, feasibility, and economical redesign of the present system.

The most pressing uncertainty in the model is that associated with the assumed character of the air wake. Preliminary results from other concurrent studies have qualitatively shown that the air wake behind a carrier is strongly influenced by ship's pitching motions. Basic data which can describe the time/space character of the vertical, horizontal, and spanwise gradient components of air wake flow are needed for this phase of model improvement.

Additional areas of uncertainty exist in piloting methods and LSO influences on landing dispersions. Advanced piloting control techniques over and above simple compensatory tracking (e.g., learned or precognitive

maneuvers) may be used to combat the effects of the wake immediately aft of the ramp; and the LSO's go/no-go decision function apparently averts a considerable number of accidents. Both precognitive piloting techniques and LSO influences on landing performance should be considered in future model refinement activities.

REFERENCES

1. Vaughan, W. S., Jr., Terrence S. Luce, and Wallace F. Rollins, Aircraft Carrier Lighting Aids to Night Recovery of Jet Aircraft, A State-of-Art Review, Human Sciences Research, Inc., Rept. HSR-RR-63/14-Lt, July 1963. (Report CONFIDENTIAL)

2. Review of Fleet Carrier Landing Doctrine; Report of, Naval Air Test Center Rept. 5213, FT2222-186, 5 October 1962.

3. AN/SPN-10 Carrier Landing System, Ship Motion Instrumentation Programs, Bell Aircraft Corp. Rept. 60003-012, April 1959. (Report CONFIDENTIAL)

4. Final Report on Project OP/V203, Evaluation of the Optical Glide Path Indicator System, Commander, Operation Development Force Letter Ser 01156, 19 November 1955. (Letter CONFIDENTIAL)

5. Project TED No. PTR AC-210.2; Carrier Landing Aids and Techniques, Letter Report No. 1, Final Report, Naval Air Test Center Rept. PTR AC-210.2, FT35-25, 2 February 1953.

6. Fresnel Lens Optical Landing System Mk 6 Mod 0, Technical Manual, Installation, Service, Operation and Maintenance Instructions, NavWeps 51-40ABA-1, 15 July 1962.

7. Final Report on an Improved Stabilization Design for the Fresnel Lens Optical Landing System, Control Instrument Company, Inc., Rept. DEV-8140, 1959.

8. Nelson, J. H., and J. L. Shipley, Shipboard Evaluation of Two Degrees of Freedom Concept of Fresnel Lens Optical Landing System, Report No. 1, Final Report, Problem Assignment No. RSSH-99/018 (WepTask No. RA123P000/201-1/F012-15-002), Naval Air Test Center, 4 May 1961.

9. Aircraft Landing System Compatibility Study, F8U-2NE, AN/SPN-10, Bell Aerosystems Company Rept. 60003-080, November 1962. (Report CONFIDENTIAL)

10. Aircraft Recovery Bulletin No. 61-12 for Mark 6 Mod 0 Fresnel Lens Optical Landing System, BuWeps NAEL-SE-431, 30 November 1962.

11. McRuer, D. T., and E. S. Krendel, Dynamic Response of Human Operators, WADC-TR-56-524, October 1957.

12. Elkind, J. I., "A Survey of the Development of Models for the Human Controller," Guidance and Control—II, ed. R. C. Langford and C. J. Mundo (Progress in Astronautics and Aeronautics, Vol. 13) Academic Press, New York, 1964, pp. 623-643.

13. McRuer, D. T., E. S. Krendel, and D. Graham, Adaptive and Optimalizing Behavior of the Human Operator in Compensatory Tracking, Systems Technology, Inc., Paper No. 29, 1964.

14. Ashkenas, I. L., and D. T. McRuer, The Determination of Lateral Handling Quality Requirements from Airframe/Human-Pilot System Studies, WADC-TR-59-135, June 1959.

15. McRuer, D. T., I. L. Ashkenas, and C. L. Guerre, A Systems Analysis View of Longitudinal Flying Qualities, WADD-TR-60-43, January 1960.

16. Jex, H. R., and C. H. Cromwell, Theoretical and Experimental Investigation of Some New Longitudinal Handling Quality Parameters, ASD-TR-61-26, March 1961.

17. Durand, T. S., and H. R. Jex, Handling Qualities in Single-Loop Roll Tracking Tests: Theory and Simulator Experiments, ASD-TDR-62-507, November 1962.

18. Ashkenas, Irving L., and Duane T. McRuer, "A Theory of Handling Qualities Derived from Pilot-Vehicle System Considerations," Aerospace Engineering, Vol. 21, No. 2, February 1962.

19. Cromwell, C. H., and I. L. Ashkenas, A Systems Analysis of Longitudinal Piloted Control in Carrier Approach, Systems Technology, Inc., TR-124-1, June 1962.

20. Ashkenas, I. L., and T. S. Durand, "Simulator and Analytical Studies of Fundamental Longitudinal Control Problems in Carrier Approach," Proc. AIAA Simulation for Aerospace Flight Conference, August 1963.

21. Rapp, Fred L., Determination of Optimum Approach Speeds for Carrier Landings, BuWeps Naval Weapons Bulletin No. 3-61, September 1961.

22. Abrams, C. R., Comparison of Two Automatic Throttle Controllers for the F8U-2N Aircraft, Naval Air Development Center Rept. NADC-ED-L6292, 30 November 1962.

23. Zbrozek, J. K., The Relationship Between the Discrete Gust and Power Spectra Presentations of Atmospheric Turbulence, with a Suggested Model of Low Altitude Turbulence, Royal Aircraft Establishment Tech. Note Aero. 2682, March 1960.

24. Hydrodynamic Effects Influencing Aircraft Carrier Landing Operations, Oceanics, Inc., forthcoming report, Contract Nonr-4186(00).

25. Lanning, J. H., and R. H. Battin, Random Processes in Automatic Control, McGraw-Hill Book Co., New York, 1961.

26. Markowitz, S. A., and F. G. Negro, Statistical Presentation of Fleet Operational Landing Parameters for Models F8U-1, F9F-8P, F3H-2N, A4D-1, and A3 Aircraft Aboard the USS Saratoga (CVA-60) in the Mediterranean Sea Area, Naval Air Material Center Rept. NAMATCEN-ASL-1035, 31 August 1961.

27. Waldron, S., The Effect of Ship Length, Ship Motions and Landing Geometry Upon the Safety of Carrier Operations, Office of the Chief of Naval Operations, Naval Warfare Analysis Group, Study No. 20, 16 October 1961.

28. Giordano, M. J., and P. S. Linder, Derivation of Roll and Pitch Correction Factors for the Point-in-Space Stabilization Used with Either the Mirror or Fresnel Lens Optical Landing System, Naval Air Material Center Rept. NAEL-ENG-6865, 12 April 1962.

29. Quinn, R. B., Analysis of Stabilization of Optical Landing System Against Ship Roll and Pitch, BuWeps Rept. R-5-62-39, October 1962.

30. Williams, A. J., The Influence of Ship Motions on the Recovery of Naval Aircraft, Royal Aircraft Establishment Tech. Note Naval 16, November 1956.

31. Lindquist, Dean C., A Statistical Evaluation of Airplane Structural Landing Parameters in Mirror-Aid Landing Operations Aboard Aircraft Carriers, BuAer Airframe Design Division Rept. AD-224-1, April 1959.

32. Perry, Barbour Lee, The Computation of Effective Display Sensitivity in Aircraft Landing, May 22, 1963. (Enclosure 1 to BuWeps Letter RSSH-51/54:TP dtd 4 December 1963.)

33. Hoy, W. W., A Method for Establishing Landing Design Criteria for Carrier-Based Airplanes, Chance Vought Corp. Rept. 2-53400/2R367, 1 August 1962.

APPENDIX A

SYSTEM MODEL FORMS AND VALUES

The model forms and values used in computing landing performance for various carrier landing systems are summarized in this appendix. Each system element is separately described with respect to its simulation and variations tested on the analog computer.

A. AIRFRAME

The conventional linearized equations describe the airframe's longitudinal perturbations about a straight-and-level operating condition. Several derivatives contributing insignificantly to the aircraft response are neglected here. These include $X_{\dot{w}}$, X_q, $Z_{\dot{w}}$, Z_q, and $M_{\dot{w}}$. The additional assumption of straight-and-level flight is justified on the basis of the relatively small, $\gamma_o \doteq 4^o$, glide slope used for carrier approach and landing. A conventional stability axis system was used. The inputs considered were (1) elevator and throttle deflections, and (2) horizontal and vertical air turbulence; these are subsequently described.

$$
\begin{aligned}
(s - X_u)u \quad & -X_w w \quad + g\theta \;=\; X_{\delta_e}\delta_e + \frac{X_{\delta_T}}{(T_e s + 1)}\,\delta_T + X_u u_g + X_w w_g \\
-Z_u u + (s - Z_w)w \quad & -U_o s\theta \;=\; Z_{\delta_e}\delta_e + \frac{Z_{\delta_T}}{(T_e s + 1)}\,\delta_T + Z_u u_g + Z_w w_g \\
-M_u u \quad & -M_w w + (s^2 - M_q s)\theta \;=\; M_{\delta_e}\delta_e + \frac{M_{\delta_T}}{(T_e s + 1)} + M_u u_g + M_w w_g
\end{aligned}
\qquad \text{(A-1)}
$$

$$
\theta = q/s \quad ; \quad \dot{h}_a = s h_a = -w + U_o s\theta \quad ; \quad \alpha = w/U_o
$$

The particular aircraft used for this study was the F4D-1 in power-approach configuration at an airspeed of 120 knots. The dimensional

stability derivatives, aircraft transfer functions, and coupling numerators appropriate to the multiple-loop piloted control system are listed in Table A-I.

TABLE A-I

CHARACTERISTICS OF THE F4D-1 AT 120 KNOTS

A. DIMENSIONAL STABILITY DERIVATIVES

X_u	$= -0.055$	Z_u	$= -0.31$	M_u	$= 0.000$
X_w	$= -0.103$	Z_w	$= -0.89$	M_w	$= -0.030$
X_α	$= -20.9$	Z_α	$= -180$	M_α	$= -6.07$
$X_{\delta e}$	$= -7.50$	$Z_{\delta e}$	$= -31.3$	$M_{\dot{\alpha}}$	$= 0.000$
$X_{\delta T}$	$= 1.0\, T_{\delta T}/m$	$Z_{\delta T}$	$= -0.23 T_{\delta T}/m$	$M_{\delta e}$	$= -3.74$
		α_o	$= 13.1^\circ$	$M_{\delta T}$	$= 0.000$

$U_o = 202$ ft/sec ; $T_{\delta T} = 4000$ lb/in.

$m = 468$ slugs ; $T_e = 0.5$ sec (thrust lag)

B. TRANSFER FUNCTIONS

$$\Delta = \left[s^2 + 2(0.10)(0.21)s + (0.21)^2\right]\left[s^2 + 2(0.31)(2.58)s + (2.58)^2\right]$$

$$N_{\theta\delta e} = -3.74(s + 0.033)(s + 0.66)$$

$$N_{u\delta e} = -7.50(s - 4.19)(s + 0.50)(s + 4.86)$$

$$N_{w\delta e} = -31.3(s + 24.8)\left[s^2 + 2(0.12)(0.22)s + (0.22)^2\right]$$

$$sN_{h\delta e} = 31.3(s - 3.57)(s - 0.043)(s + 4.31)$$

$$(s + 2.0)N_{\theta\delta T} = 0.12(s + 1.40)$$

$$(s + 2.0)N_{u\delta T} = 17.0(s - 0.033)\left[s^2 + 2(0.32)(2.60)s + (2.60)^2\right]$$

$$(s + 2.0)N_{w\delta T} = -3.92s(s + 0.71)(s + 1.40)$$

$$s(s + 2.0)N_{h\delta T} = 3.92(s + 1.40)\left[s^2 + 2(0.14)(2.46)s + (2.46)^2\right]$$

$$N_{\theta ug} = 0.0093s$$

$$N_{uug} = -0.055(s + 0.88)\left[s^2 + 2(0.028)(2.48)s + (2.48)^2\right]$$

$$N_{wug} = -0.31s^2(s + 0.71)$$

(Continued on p. 71)

(Table A-I concluded)

$$sN_{h_{u_g}} = 0.31s\left[s^2 + 2(0.14)(2.46)s + (2.46)^2\right]$$

$$N_{\theta_{w_g}} = -0.03(s + 0.055)$$

$$N_{u_{w_g}} = -0.103s(s + 3.44)(s - 2.73)$$

$$N_{w_{w_g}} = -0.89(s + 7.49)\left[s^2 + 2(0.11)(0.21) + (0.21)^2\right]$$

$$sN_{h_{w_g}} = 0.89(s + 1.03)\left[s^2 + 2(-0.27)(0.57)s + (0.57)^2\right]$$

C. COUPLING NUMERATORS

$$s(s + 2.0)N^{\theta\ h}_{\delta_e\delta_T} = -14.7(s + 1.40)$$

$$(s + 2.0)N^{\theta\ u}_{\delta_e\delta_T} = -63.8(s + 0.65)$$

$$(s + 2.0)N^{w\ u}_{\delta_e\delta_T} = -562.0(s + 23.6)(s - 0.036)$$

$$s(s + 2.0)N^{h\ u.}_{\delta_e\delta_T} = 562.0(s + 4.33)(s - 3.62)$$

$$sN^{\theta\ h}_{\delta_e u_g} = -1.16s$$

$$(s + 2.0)N^{u\ w}_{\delta_T u_g} = -5.50s(s + 0.71)$$

$$(s + 2.0)N^{u\ \theta}_{\delta_T u_g} = 0.16$$

$$s(s + 2.0)N^{u\ h}_{\delta_T u_g} = 5.50\left[s^2 + 2(0.14)(2.46)s + (2.46)^2\right]$$

$$sN^{\theta\ h}_{\delta_e w_g} = -2.39(s + 0.034)$$

$$s(s + 2.0)N^{u\ h}_{\delta_T w_g} = 15.6(s + 0.96)(s - 0.25)$$

B. PILOT

The pilot's longitudinal control of an aircraft making a carrier approach is discussed in Refs. 19 and 20. The pilot's transfer functions and the two piloting techniques used in this study were indicated by the work referenced above. The pilot's outputs are given by Eq A-2 and A-3.

$$\delta_e = (K_{\delta_e\theta})\theta_\epsilon + (K_{\delta_e h})h_\epsilon \qquad \text{(A-2)}$$

$$\delta_T = (K_{\delta_T h})h_\epsilon + (K_{\delta_T u})u_\epsilon \qquad \text{(A-3)}$$

The nominal gain values used correspond to those determined appropriate in the above references, unless otherwise noted, and are given in Table A-II.

TABLE A-II

NOMINAL PILOT GAINS

	PILOTING TECHNIQUE	
	Altitude Control with Elevator	Altitude Control with Throttle
$K_{\delta_e}\theta$	−1.62 rad/rad	−1.62 rad/rad
$K_{\delta_e}h$	−0.0051 rad/ft	0
$K_{\delta_T}h$	0	0.0016 in./ft
$K_{\delta_T}u$	0.0176 in./ft/sec	0

Note that the altitude loop gain, $K_{\delta_e}h$ or $K_{\delta_T}h$, was held constant as a function of range. This in effect assumes that the pilot correctly deciphers and proportionately controls absolute height error, h_ϵ, despite the range-sensitive FLOLS optical gain.

C. SHIP MOTIONS

Ship motions result from a combination of swell and sea wave inputs acting on the ship. Wave inputs have been defined as stationary Gaussian processes and the ship dynamics characterized by linear equations of motion. The method employed to simulate carrier motions as inputs to the rest of the system consisted of shaping filter approximations to the power spectra of these motions for given conditions of sea state and swells. Ship motion power spectra were obtained either from direct measurement (Ref. 3, for the Essex motions) or from theoretical models (Ref. 24, for the Forrestal motions). The Essex motion spectra used are illustrated in Fig. A-1, together with their fitted transfer function characteristics.

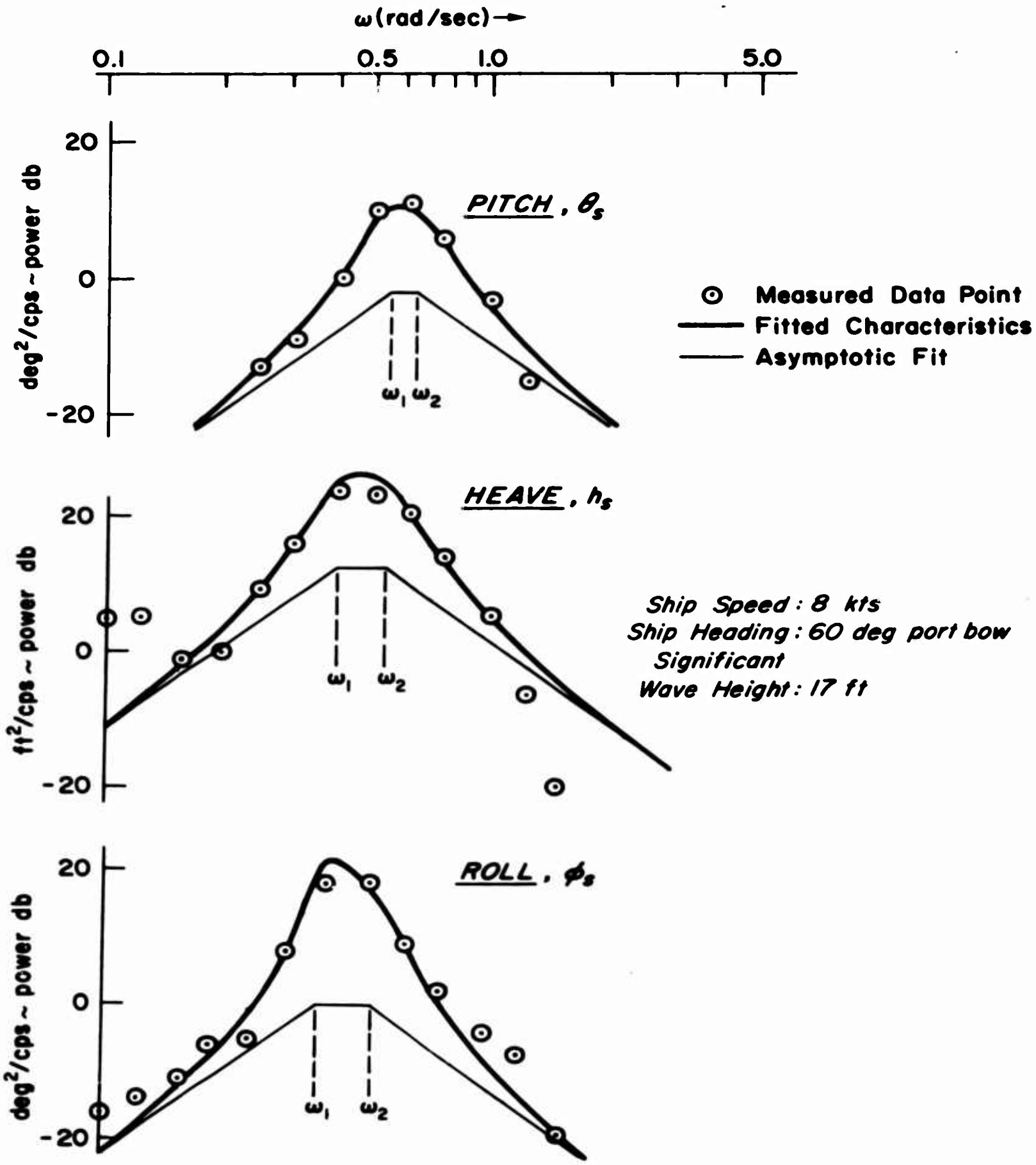

Figure A-1. Power Spectra of Essex Ship Motions Used in the Analyses

The general form of the transfer function models (fits to the spectra) was deduced from theoretical considerations, i.e., the longitudinal equations of motion for the ship in a seaway. The phase angle between pitch and heave as a function of frequency was deduced from various sources (e.g., Ref. 30), which indicated that pitch should lead heave by 45° to 90° in the dominant region of the motion spectrum. The natural frequencies (ω_1 and ω_2; also numerator) of the pitch and heave transfer function fits were first selected to roughly fit the spectra amplitude ratio data while at the same time providing for the proper phase lead of pitch over heave. Damping ratios (ζ_1 and ζ_2) were then adjusted to more closely match the shape of the amplitude ratio characteristics illustrated in Fig. A-1.

After several reiterations of this process, both amplitude ratio and phase characteristics were obtained which matched the data fairly well. Corresponding pitch/heave phase characteristcs are illustrated in Fig. A-2 using the same transfer functions as for Fig. A-1. Similar approximations were made to the two sets of Forrestal motions used in this study; these, as well as the Essex transfer functions, are summarized in Table A-III.

D. GUSTS

Both horizontal, u_g, and vertical, w_g, random gusts were employed. Figure A-3 shows the generalized gust spectrum forms adopted in the study,

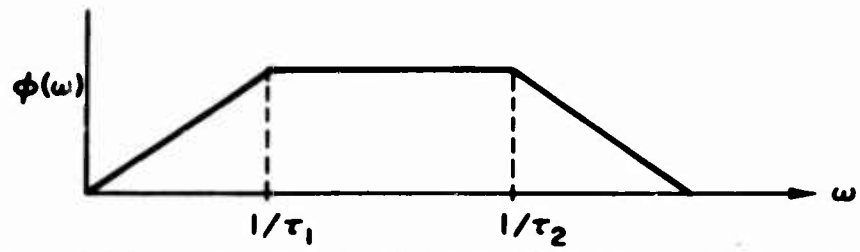

Figure A-3. Generalized Gust Spectrum Form Used in the Analyses

which were fitted by the following white-noise shaping filters:

$$\frac{u_g}{W.N.} = \frac{\sigma(u_g)\sqrt{2\left(\frac{1}{\tau_{u_1}} + \frac{1}{\tau_{u_2}}\right)s}}{\left(s + \frac{1}{\tau_{u_1}}\right)\left(s + \frac{1}{\tau_{u_2}}\right)} \qquad \text{(A-4)}$$

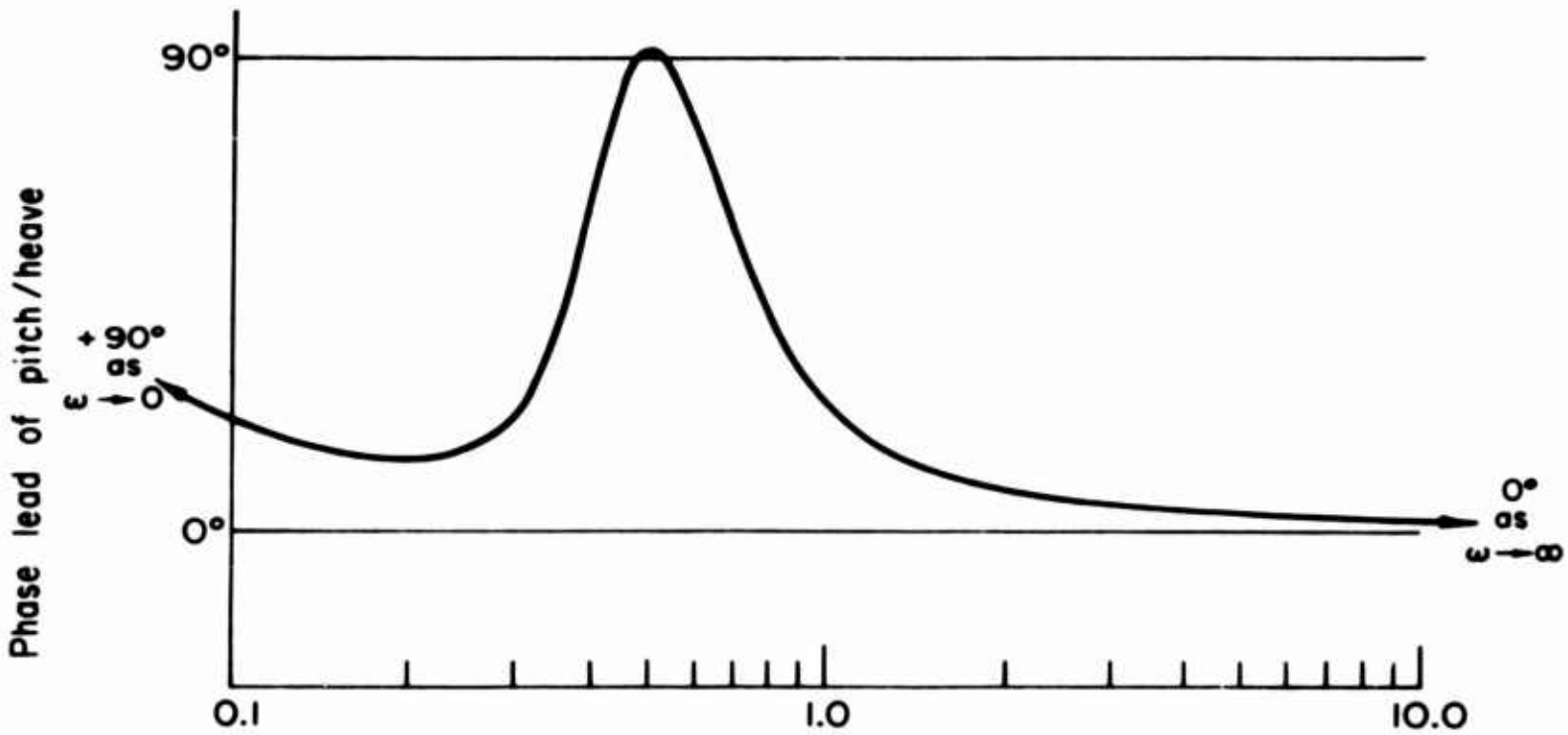

$$\frac{\theta_s}{h_s}(s) = \frac{s\left[s^2 + 2(.2)(.4)s + (.4)^2\right]}{(s + .04)\left[s^2 + 2(.3)(.64)s + (.64)^2\right]}$$

Figure A-2. Phase Characteristics of Pitch Relative to Heave Using Transfer Function Approximations to Essex Motions

TABLE A-III

SUMMARY OF TRANSFER FUNCTION APPROXIMATIONS TO SHIP MOTIONS: RESPONSE OPERATORS TO WHITE NOISE INPUTS

SHIP AND ENVIRONMENTAL CONDITIONS	PITCH, θ_s/W.N.	HEAVE, h_s/W.N.	ROLL, φ_s/W.N.
ESSEX Speed: 8 knots Heading: 60° port bow Significant wave height: 17 ft Predominantly swell waves	$\sigma(\theta_s) = 1.0^\circ$ $\dfrac{0.00583s^2}{\Delta}$ $\zeta_1 = 0.2 \quad \zeta_2 = 0.3$ $\omega_1 = 0.55 \quad \omega_2 = 0.64$	$\sigma(h_s) = 5.5$ ft $\dfrac{1.16s(s + 0.04)}{\Delta}$ $\zeta_1 = 0.2 \quad \zeta_2 = 0.2$ $\omega_1 = 0.4 \quad \omega_2 = 0.55$	$\sigma(\varphi_s) = 2.2^\circ$ $\dfrac{0.00416s^2}{\Delta}$ $\zeta_1 = 0.12 \quad \zeta_2 = 0.12$ $\omega_1 = 0.37 \quad \omega_2 = 0.5$
FORRESTAL Speed: 10 knots Heading: 30° port or starboard Significant wave height: 17 ft Sea waves from Sea State 6	$\sigma(\theta_s) = 0.75^\circ$ $\dfrac{0.00262s^2}{\Delta}$ $\zeta_1 = 0.15 \quad \zeta_2 = 0.25$ $\omega_1 = 0.6 \quad \omega_2 = 0.8$	$\sigma(h_s) = 0.93$ ft $\dfrac{0.312s^2}{\Delta}$ $\zeta_1 = 0.15 \quad \zeta_2 = 0.25$ $\omega_1 = 0.465 \quad \omega_2 = 0.8$	Not used
FORRESTAL Speed: 10 knots Heading: —— Significant wave height: 15 ft Swell waves only	$\sigma(\theta_s) = 0.71^\circ$ $\dfrac{0.0773s^2}{(s+1)^2\left[s^2 + 2(0.1)(0.4)s + (0.4)^2\right]}$	$\sigma(h_s) = 4.4$ ft $\dfrac{1.21s}{(s+1)^2\left[s^2 + 2(0.1)(0.4)s + (0.4)^2\right]}$	Not used
$\Delta = \left[s^2 + 2\zeta_1\omega_1 s + \omega_1^2\right]\left[s^2 + 2\zeta_2\omega_2 s + \omega_2^2\right]$			

$$\frac{w_g}{W.N.} = \frac{\sigma(w_g)\sqrt{2\left(\frac{1}{\tau_{w_1}}\right)+\left(\frac{1}{\tau_{w_2}}\right)}\ s}{\left(s+\frac{1}{\tau_{w_1}}\right)\left(s+\frac{1}{\tau_{w_2}}\right)} \qquad \text{(A-5)}$$

A wide range of high ($1/\tau_{u_2}$, $1/\tau_{w_2}$) and low ($1/\tau_{u_1}$, $1/\tau_{w_1}$) frequency break points were evaluated to find their effect on landing dispersions.

E. KINEMATICS AND TERMINAL ERROR EQUATIONS

The vertical displacements of the deck touchdown point, h_{TD}, and of the ramp, h_R, are given by

$$h_{TD} \doteq h_s - L_{TD}\theta_s - Y_{TD}\varphi_s \qquad \text{(A-6)}$$

$$h_R \doteq h_s - L_R\theta_s - Y_R\varphi_s \qquad \text{(A-7)}$$

where L_{TD}, L_R, Y_{TD}, and Y_R are defined in Fig. A-4. The vertical velocity of the touchdown point, h_{TD}, is

$$\dot{h}_{TD} \doteq \dot{h}_s - L_{TD}\dot{\theta}_s \qquad \text{(A-8)}$$

The instantaneous vertical separation between the aircraft and the ramp is given by the terminal error equation for ramp clearance,

$$\Delta h_R \doteq h_a - h_R \qquad \text{(A-9)}$$

Similarly, the touchdown height error is given by

$$\Delta h_{TD} \doteq h_a - h_{TD} \qquad \text{(A-10)}$$

Aircraft altitude, h_a, in both Eq A-9 and A-10 is referenced to that inertial path defined by a $\beta_o = 4^o$ beam and given ship speed, U_s (under steady deck conditions), in the manner illustrated in Fig. A-5. The impact velocity results from the combined effects of the vertical velocities of the deck and the aircraft and the tilted position of the deck at time of impact. It is given by

$$\Delta V_I \doteq \dot{h}_{TD} - \dot{h}_a + U_R(\theta_s + \sin\psi_d\varphi_s) \qquad \text{(A-11)}$$

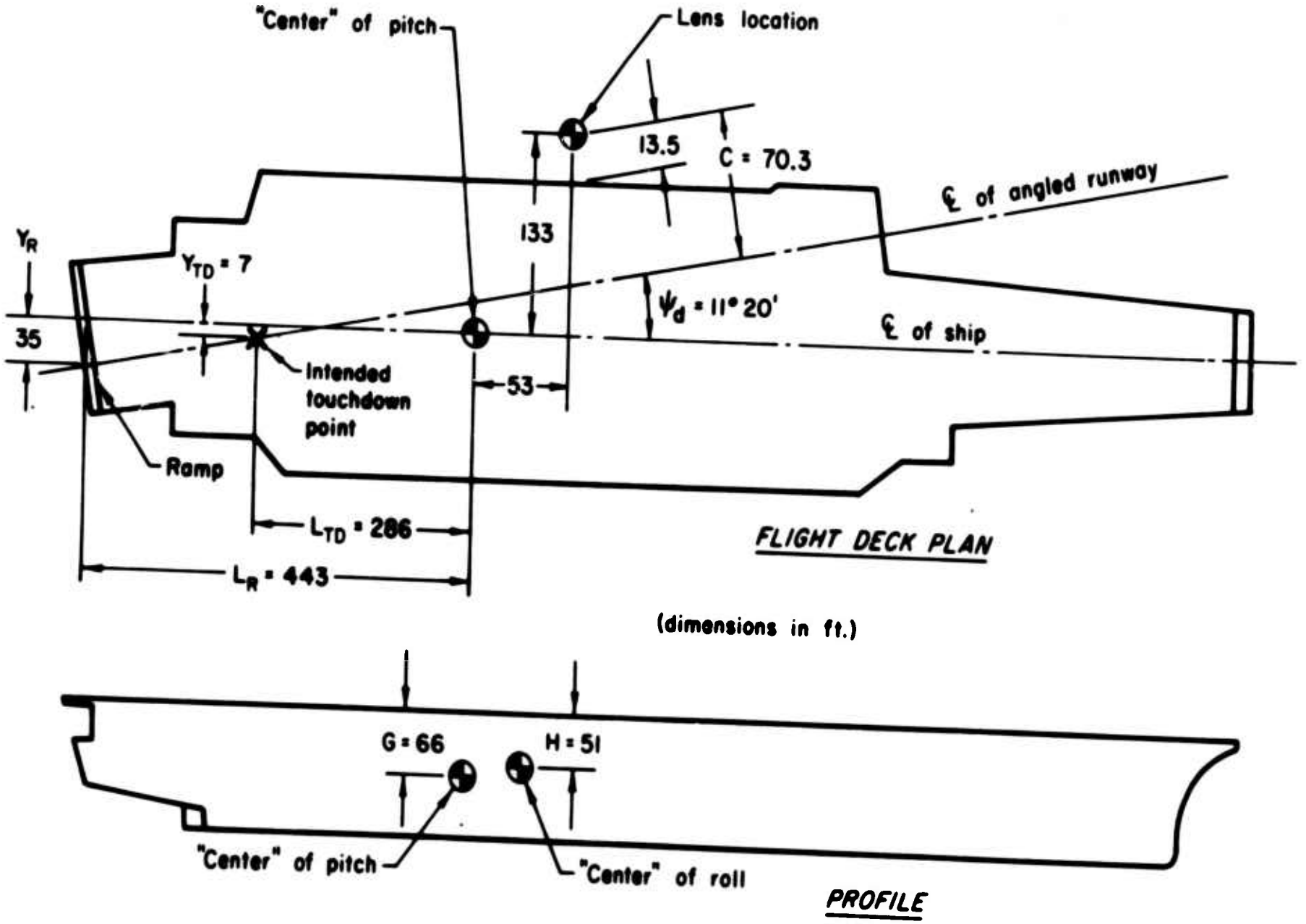

Figure A-4. Carrier Geometry

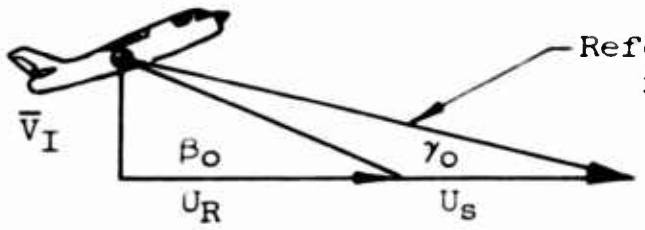

$$\gamma_o \doteq \frac{U_o - W - U_s}{U_o - W} \beta_o$$

Figure A-5. Definition of Reference Inertial Flight Path

In Eq A-11, $\dot{h}_a$ is the perturbation velocity about the nominal aircraft sink rate, $\bar{V}_I$ (illustrated in Fig. A-5), and U_R is ground speed, which is given by

$$\begin{aligned} U_R &\doteq U_o - (W + U_s) \\ &\doteq U_o - \text{WOD} \end{aligned} \qquad \text{(A-12)}$$

A 30 knot WOD (wind-over-the-deck) was used in the evaluations.

F. FLOLS

For the purposes of this study the aircraft's motion was restricted to a single vertical plane, that through the nominal (unperturbed) angled deck centerline. Therefore the pilot will see a "roger meatball" whenever he is on the intersection line of this vertical plane and the beam plane, i.e., the plane defined by the fan-shaped beam of light produced by the Fresnel lens unit with reference to its datum bar. The error seen by the pilot is proportional to his vertical distance from this line of intersection (the "beam"). The FLOLS kinematics were considered with respect to height reference perturbations from a nominal (steady deck) descent path caused by beam motion. The beam motion in inertial space is a function of the ship's motion and the controlled lens position relative to the ship axes. The vertical displacement of the beam from the reference flight path, h_B, is given as a function of range by

$$\begin{aligned} h_B \doteq\ & \left[D + C \sin \psi_d - \beta_o G \cos \psi_d\right] \theta_s \\ &+ \left[C \cos \psi_d - B + \beta_o H \sin \psi_d\right] \varphi_s + h_s + C \cdot \varphi_L \\ &+ \left[\cos \psi_d (\theta_s) - (\beta_o \cos^2 \psi_d - \sin \psi_d) \varphi_s - \theta_L\right] R \end{aligned} \qquad \text{(A-13)}$$

The constants in Eq A-13 are determined by the applicable carrier geometry. For the case studied, the geometry of the USS Constellation (CVA-64) was used and is shown in Fig. A-4.

Substituting the numerical values given in Fig. A-4 into Eq 13 yields:

$$h_B \doteq 62.3\theta_s - 64.1\varphi_s + h_s + 70.3\varphi_L + \left[0.98\theta_s - 0.13\varphi_s - \theta_L\right]R \qquad \text{(A-14)}$$

The FLOLS logic, which specifies pitch and roll lens servo gains, θ_L and φ_L, as functions of θ_s, φ_s, and h_s, is dictated by the beam stabilization scheme chosen. Once this is specified, the beam equation has the form:

$$h_B = \left(\frac{\partial h_B}{\partial h_s}\right)h_s + \left(\frac{\partial h_B}{\partial \theta_s}\right)\theta_s + \left(\frac{\partial h_B}{\partial \varphi_s}\right)\varphi_s \qquad \text{(A-15)}$$

where

$$\frac{\partial h_B}{\partial h_s} = B_{h_s}^{h_B}$$

$$\frac{\partial h_B}{\partial \theta_s} = A_{\theta_s}^{h_B}(R) + B_{\theta_s}^{h_B}$$

$$\frac{\partial h_B}{\partial \varphi_s} = A_{\varphi_s}^{h_B}(R) + B_{\varphi_s}^{h_B}$$

The FLOLS kinematics were simulated in the manner indicated by Eq A-15. Thus, for example, in simulating beam stability against heave motion, the term $\partial h_B/\partial h_s$ is set to zero; conversely, in simulating unstabilized heave motion, $\partial h_B/\partial h_s = 1.0$ is used. The various FLOLS stabilization schemes described in the text are summarized in Table A-IV with respect to values of the partial derivatives of Eq A-15. Also given in Table A-IV are the FLOLS pitch and roll correction factors corresponding to the control logic used; these, however, were not necessary for the simulation, and are given for general interest.

Another point of interest is the FLOLS control logic for the compensated-meatball system. Note that, similar to the uncompensated system, the lens

pitch control is a function of ship pitch, θ_s, and roll, φ_s, only and that very little equalization is necessary for θ_s. The major portion of the meatball compensation is accomplished by rolling the lens. This is done purposely in order to preserve the beam motion envelope of the uncompensated-meatball system, as is discussed in the text.

TABLE A-IV

SUMMARY OF FLOLS STABILIZATION CONTROL LOGIC

FLOLS STABILIZATION CONFIGURATIONS			BEAM MOTION EQUATION $h_B = \frac{\partial h_B}{\partial h_s} h_s + \left(\frac{\partial h_B}{\partial \theta_s}\right)\theta_s + \left(\frac{\partial h_B}{\partial \varphi_s}\right)\varphi_s$					FLOLS LOGIC Note: θ_s and φ_s in deg; h_s in ft	
			$\frac{\partial h_B}{\partial h_s} = B_{h_s}^{h_B}$	$\frac{\partial h_B}{\partial \theta_s} = A_{\theta_s}^{h_B}(R) + B_{\theta_s}^{h_B}$		$\frac{\partial h_B}{\partial \varphi_s} = A_{\varphi_s}^{h_B}(R) + B_{\varphi_s}^{h_B}$			
			$B_{h_s}^{h_B}$ (ft/ft)	$A_{\theta_s}^{h_B}$ (ft/rad/ft)	$B_{\theta_s}^{h_B}$ (ft/rad)	$A_{\varphi_s}^{h_B}$ (ft/rad)	$B_{\varphi_s}^{h_B}$ (ft/rad)	Lens Pitch, θ_L (deg)	Lens Roll, φ_L (deg)
1. Angle-stabilized	NH	Beam has constant angle relative to horizon; translates with vertical motion of deck touchdown point	1	0	-286	0	-6.6	$0.98\theta_s - 0.1\varphi_s$	$-5.0\theta_s + 0.82\varphi_s$
	WH	Beam also stabilized against ship heave; translates with ship pitch/roll-induced vertical motion of deck touchdown point	0	0	-286	0	-6.6	$0.98\theta_s - 0.1\varphi_s$	$-5.0\theta_s + 0.82\varphi_s - 0.85h_s$
2. Point-stabilized	NH	Beam translates with heave and rotates about a point 2500 ft aft of ship due to ship pitch/roll-induced vertical motion of lens unit	1	-0.0255	62.3	-0.0259	63.4	$1.0\theta_s - 0.1\varphi_s$	0
	WH	Beam also stabilized against ship heave; just rotates about 2500 ft point	0	-0.0255	62.3	-0.0259	63.4	$1.0\theta_s - 0.1\varphi_s$	$-0.85h_s$
3. Point-and-line-stabilized	NH	Beam translates with ship heave	1	0	0	0	0	$0.98\theta_s - 0.1\varphi_s$	$-0.\theta_s + 0.91\varphi_s$
	WH	Beam fixed with respect to inertial space	0	0	0	0	0	$0.98\theta_s - 0.1\varphi_s$	$-0.\theta_s + 0.91\varphi_s - 0.85h_s$
4. Compensated-meatball	NH	Beam motion similar to that of Configuration 2NH, but with phase lead added	$\frac{h_B \text{ (Configuration 4NH)}}{h_B \text{ (Configuration 2NH)}} = \frac{1.1(s - 0.2)}{(s + 0.2)}$					$0.9\frac{(s/0.19)+1}{(s/0.2)+1}\theta_s$ $-1.12\frac{(s/1.32)+1}{(s/0.2)+1}\varphi_s$	$(-1.71h_s - 1.8\theta_s + 1.9\varphi_s)\frac{-(s/4.2)+1}{(s/0.2)+1}$

APPENDIX B

ANALOG COMPUTER MECHANIZATION

An analog computer was used to generate data necessary to the analytic study of the carrier approach and landing problem. Two separate and distinct simulations were set up on the computer, a conventional or real-time system simulation and an adjoint system simulation.

A. REAL-TIME SIMULATION

A schematic representation of the real-time simulation is shown in Fig. B-1. The mechanization is conventional and utilizes the models of system elements described in Appendix A. Instead of using white noise sources as inputs to ship motions and atmospheric turbulence filters, sine waves of appropriate amplitude and frequency (given in Fig. B-1) were used to simulate the filters directly. In the case of ship motions, a single sine wave was used to describe pitch and heave (with phase of pitch leading heave by 90°), and a separate sine wave was used to simulate ship roll. While the real-time simulation was sparingly employed (i.e., used principally to perform checks on results obtained from the adjoint simulation), it proved to be an invaluable aid in designing, setting up, and checking the adjoint simulation.

B. ADJOINT SIMULATION

The carrier approach and landing system is classified as a time-varying linear system with random inputs. As such, neither analytic techniques nor a conventional analog simulation is of practical use in obtaining the statistical properties of the random outputs. The adjoint method (Ref. 25) was used in conjunction with the analog computer to obtain these statistical measurements, the results from which are used throughout the text. The computer mechanization for this simulation is schematically represented in Fig. B-2. This mechanization employs the more complete mathematical models of system elements, i.e., previously described approximations used for the

SHIP MOTIONS

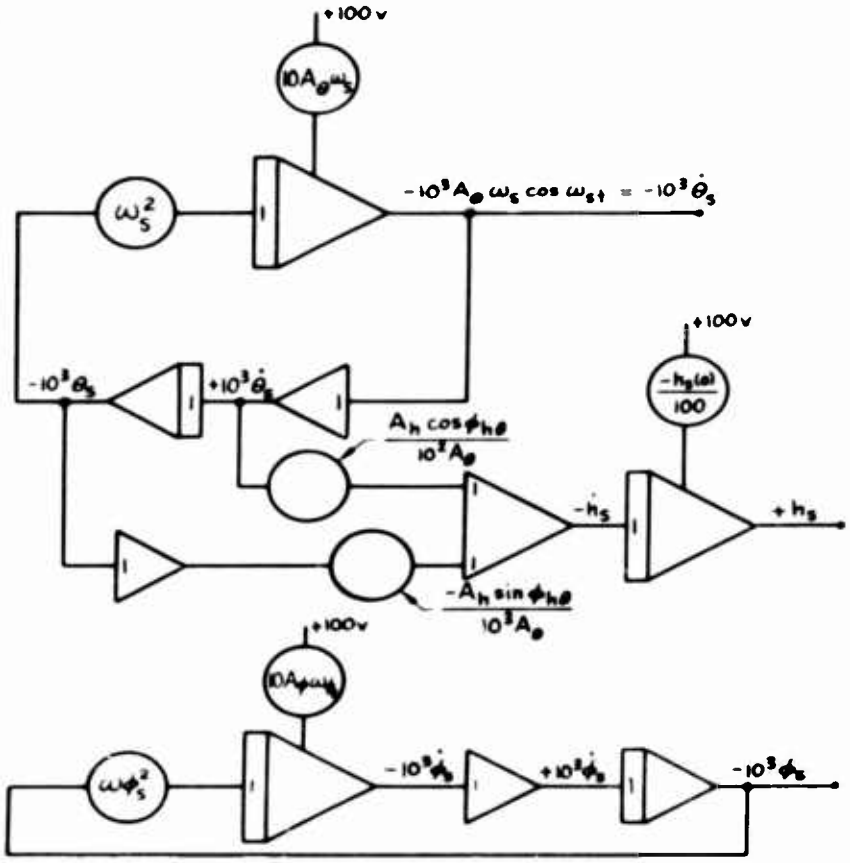

RANDOM GUSTS

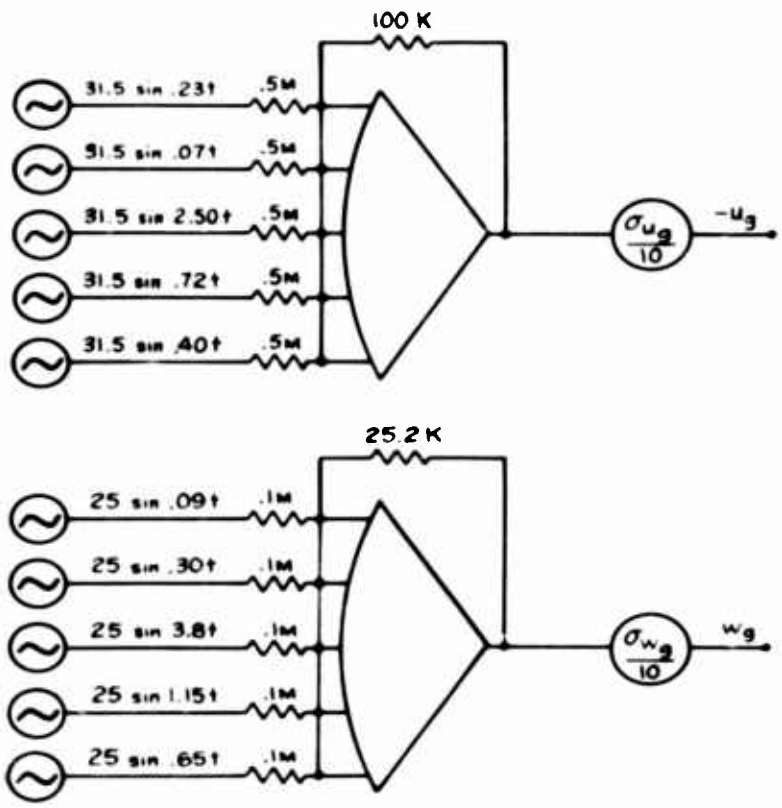

FLOLS

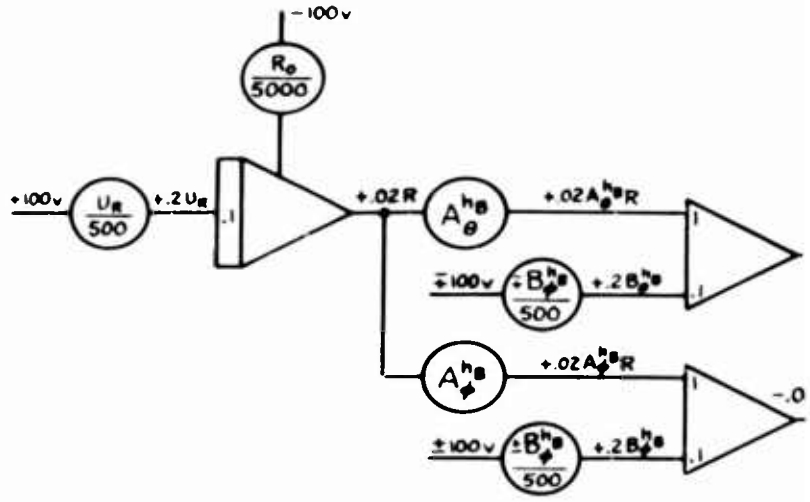

KINEMATICS AND TERMINAL E

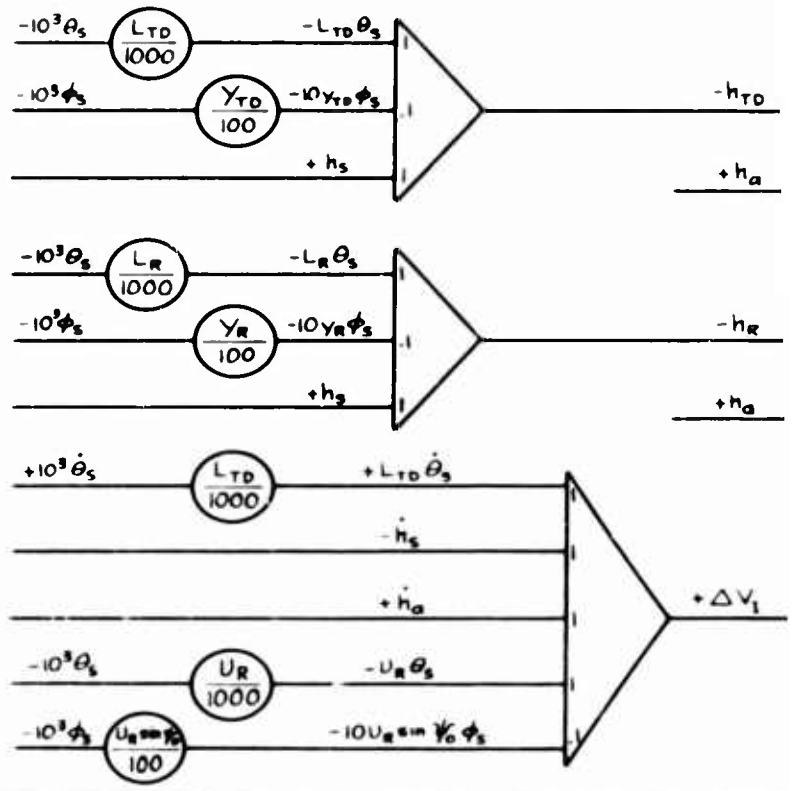

PILOT

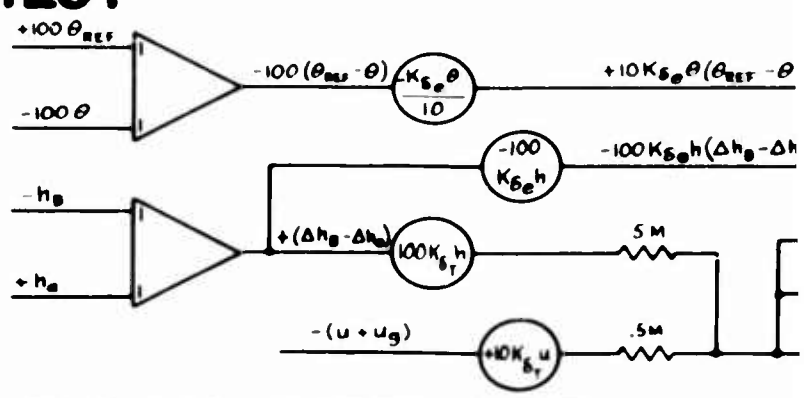

Figure B-1. Analog Computer Mechanizati

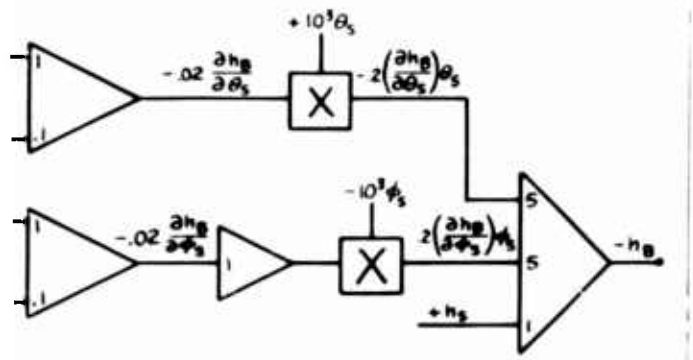

NAL ERROR EQUATIONS

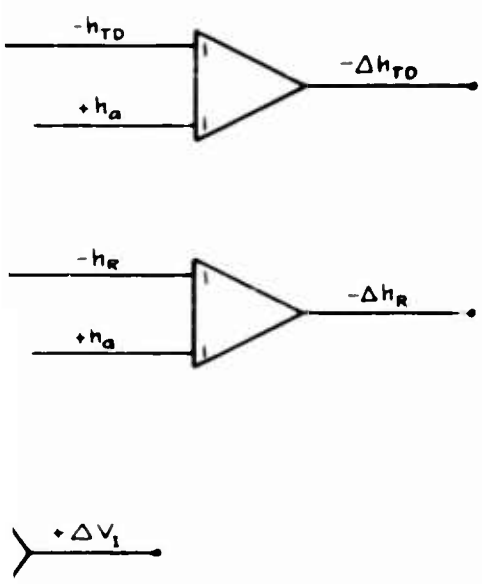

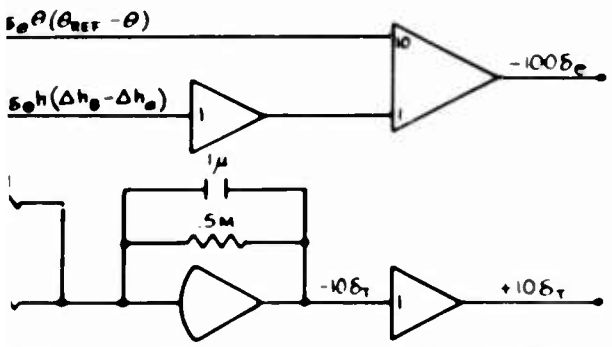

AIRFRAME

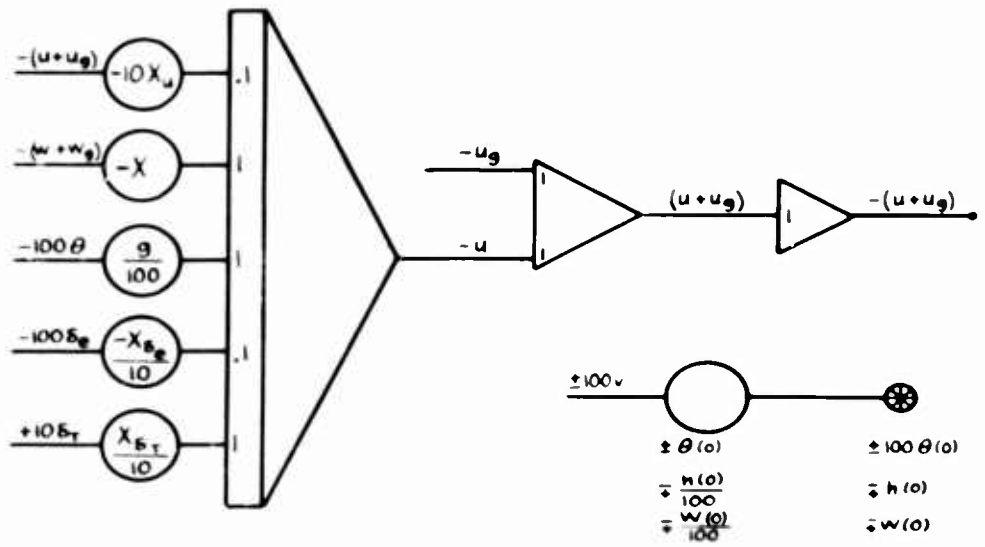

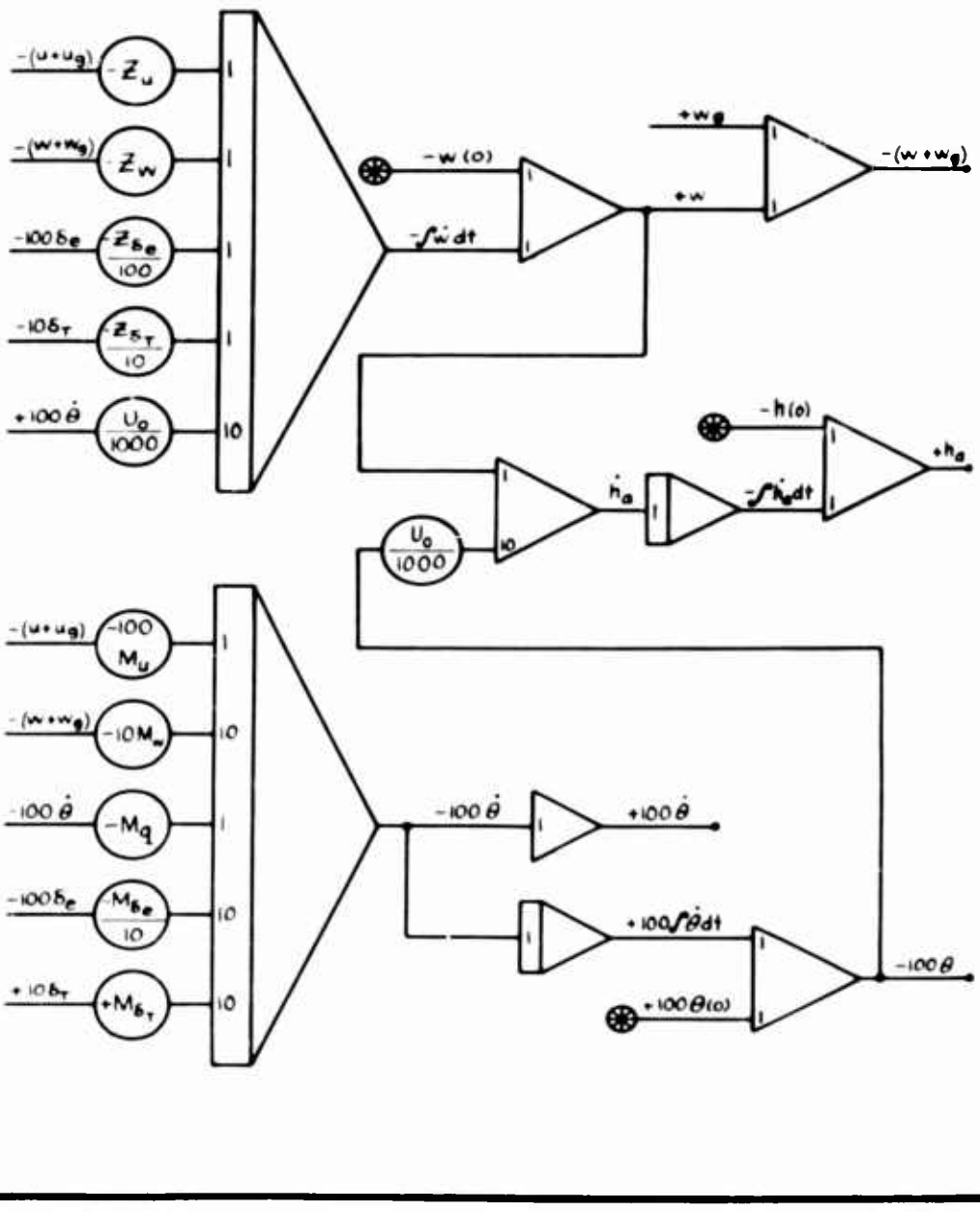

anization of Real-Time Simulation

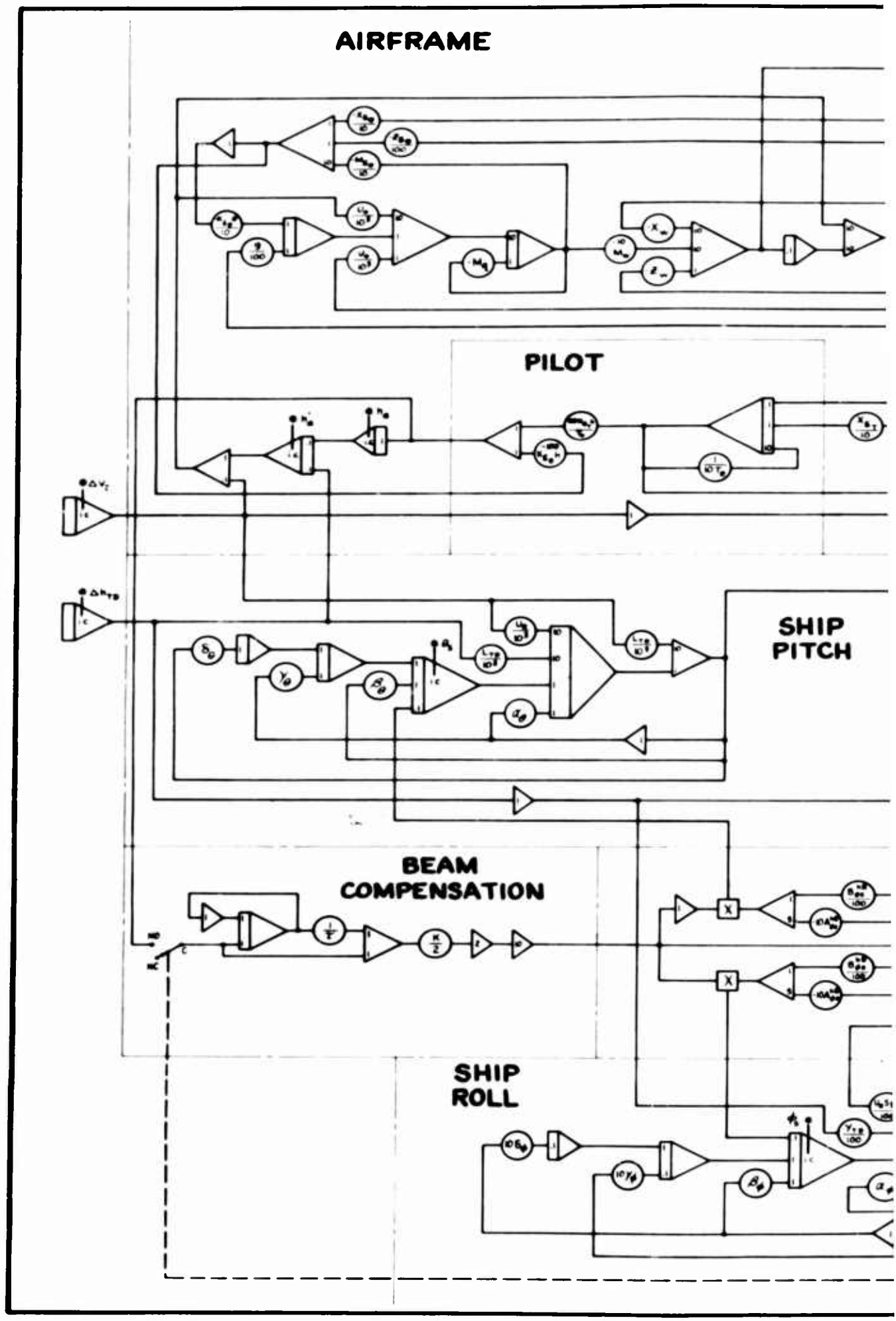

Figure B-2. Analog Compute

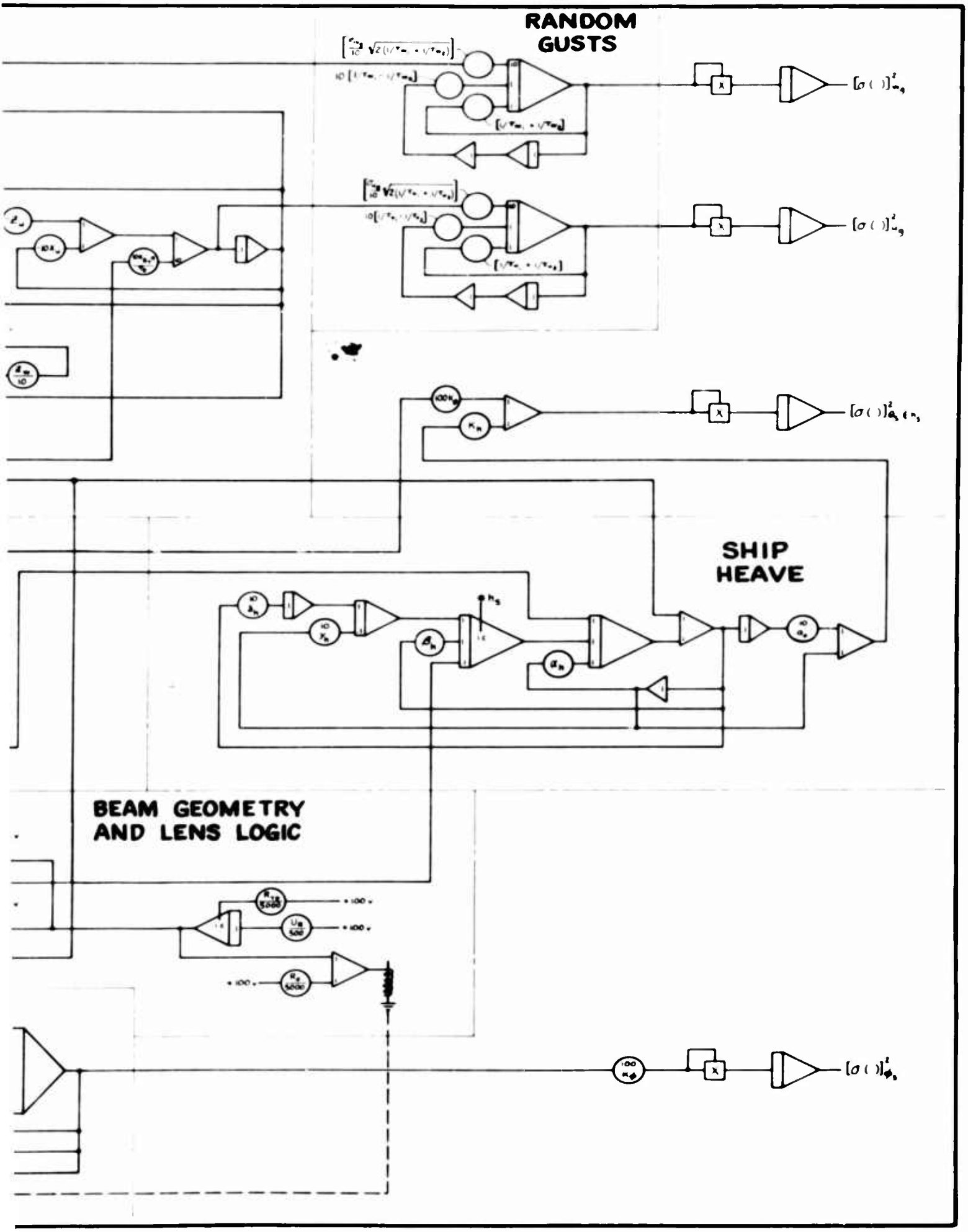

lechanization of Adjoint Simulation

real-time simulation were not necessary with the adjoint method. The significance of Fig. B-2 may appear vague owing to the lack of directly observable physical ties to the real system. Accordingly, the adjoint technique and the method used for constructing it from the real-time simulation are briefly reviewed.

Let us first review the problem of determining the response of a time-varying system to a random disturbance. The impulse response, $w(t,t_1)$, of a linear time-varying system is a function of two time variables:

1. The time, t_1, at which the impulse is introduced
2. The time, t, at which the response is measured

In contrast, the impulse response of a linear constant-coefficient system is a function of only one variable, the time <u>difference</u> between the application of an impulse and the measurement of the response.

The ensemble mean-square response,* $\widetilde{|\epsilon(t)|^2}$, of a system at time t, due to a unit white noise input applied continuously from $-\infty$ to t, is given by

$$\widetilde{|\epsilon(t)|^2} = 2\pi \int_{-\infty}^{t} \left[w(t,t_1)\right]^2 dt_1$$

where $w(t,t_1)$ = the response at time t to a unit impulse applied at time t_1

If the random disturbances of the time-varying system can be represented by unit white noise passed through a linear shaping filter, then w is the impulse response of the shaping filter and the system. Suppose we wish to evaluate $\widetilde{[\epsilon(t)]}^2$ using the above formula. $w(t,t_1)$ can be obtained from direct measurements of the impulse response on an analog computer.

If a unit impulse is introduced at time t_1, the simulated system gives $w(t,t_1)$ as a function of t. Thus, since the variable of integration is t_1, it would appear necessary to take a number of impulse responses for various

---

*The ensemble average is the value of a parameter at time t, averaged over a large number of runs with random initial conditions and noise, but all having the same statistical parameters. In time-varying problems, the ensemble average for a given time is not the same as the time average for a given run.

values of t_1, cross-plot the results, and integrate the kernel of the equation numerically or graphically, as sketched in Fig. B-3. Thus, for the example sketched, several analog computer runs would be required to generate the information required to obtain $\left[\widetilde{\epsilon(t)}\right]^2_{t=3}$ and the whole process would have to be repeated for other values of t. This procedure is clearly uneconomic. Fortunately it may be replaced by a procedure which generates $w(t,t_1)$ as a <u>continuous</u> function of t_1 for each t required.

The technique used to generate $w(t,t_1)$ as a continuous function of t_1 is the adjoint method, described in Ref. 25. The basic theory is explained in a heuristic fashion by appealing to the principle of reciprocity encountered in linear systems. A familiar example of this principle occurs in structural influence coefficients, i.e., a concentrated load applied at Point A produces a deflection at Point B equal to that which would be produced at Point A by the same load applied at Point B.

Extending this idea to the present context, a unit impulse applied to a linear system at time t_1 and producing an output at t given by $w(t,t_1)$ would yield the same response as the response at time t_1 to a unit impulse applied at time t, provided the latter response is measured at the original input terminal, the impulse is applied at the original output terminal, and time is run backward. To exploit this idea it is necessary to form an analog computer circuit which is related to the original simulator circuit (real-time simulation) by a simple set of rules which will be given later. The resulting circuit is called the adjoint circuit. Squaring the adjoint output for the system sketched in Fig. B-3 produces a time history identical to the graph of w^2 versus t_1 but reversed in time. Integrating this squared time history between zero and 3 sec yields $\left[\int_0^t |w(t,t_1)^2\right]_{t=3}$ in a single run.

As noted above, this integral can be evaluated using the adjoint analog. The simplest way to obtain the system adjoint analog diagram is to first form the real-time system analog diagram. Then by the application of a few rules the adjoint can be obtained. The following rules summarize the process of constructing the adjoint circuit from the real-time system analog:

1. The outputs of a summer or integrator in the system analog become the inputs to that summer or integrator in the adjoint analog; the inputs in the system analog become the outputs in the adjoint.

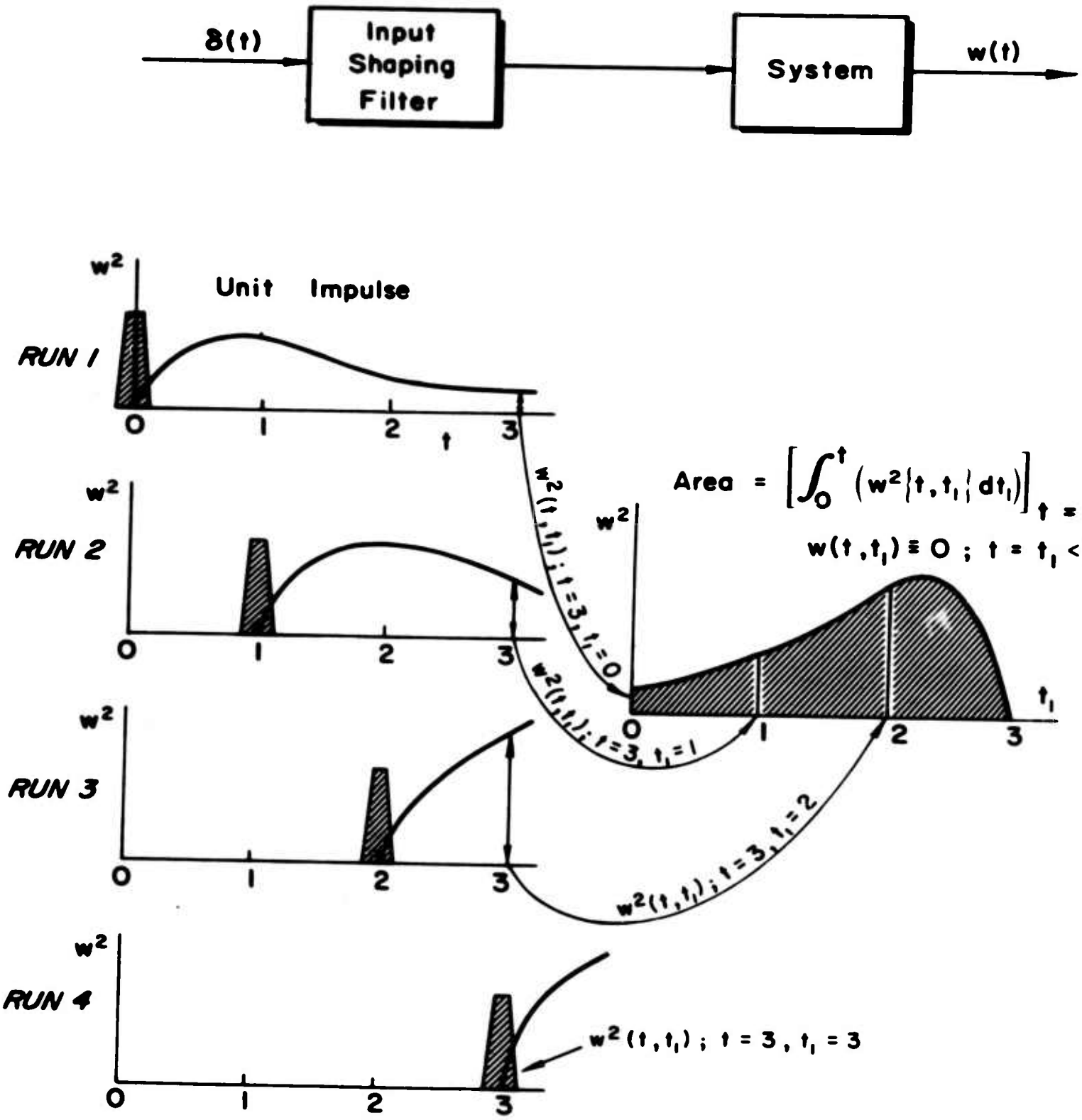

Figure B-3. Steps Required to Calculate Mean-Squared Response by the Direct (Nonadjoint) Method

2. The input and output are exchanged on all pots.

3. Pots which were used to represent time-varying coefficients are replaced by multipliers driven by the coefficient as a function of the new variable $\tau = t_2 - t$, i.e., time-varying coefficients are started at their final values and run backward.

4. A unit impulse, which is the input called for, is put into the integrator from which the output of interest was taken in the system analog. Since the integral of a unit impulse is a unit step, instead of generating an actual impulse a step can be put on the output of the integrator. This usually can be accomplished by putting an initial condition on the integrator. The step should not exist on the output of the integrator until the machine is put into the operate mode, unlike some initial conditions for which it is desired to have the value at the integrator output before the problem begins to run.

5. The adjoint weighting functions are measured, in the adjoint analog, at the points where the corresponding inputs in the system analog were introduced. The components necessary to square, scale, and/or integrate the weighting functions are added.

6. The simulation can be "cleaned up" to eliminate unnecessary components and get realizable pot settings by using amplifier gains other than unity.

APPENDIX C

SAMPLE CALCULATION OF PERFORMANCE INDICES

System 3WH of Table I
for "moderate" environmental condition;
$h \rightarrow \delta_e$ piloting technique

1. Computation of landing dispersions, from Table VI,

$$\sigma(h_R) = 5.15 \text{ ft}$$

$$\sigma(V_I) = 3.14 \text{ ft/sec}$$

$$\sigma(h_{TD}) = 4.74 \text{ ft}$$

2. Computation of ideal β_o for $P_{h_R} = P_{V_I}$

$$\text{Ideal } \beta_o = \frac{\left[(V_I)_{\text{ultimate}}\right]\sigma(h_R)}{\left[\bar{x}_{TD}\sigma(V_I) + (U_o - U_s - W)\sigma(h_R)\right]} \text{ rad}$$

Assume the following nominal conditions:

$$(V_I)_{\text{ultimate}} = 21 \text{ fps} \qquad \text{(Ref. 31)}$$

$$\bar{X}_{TD} = 234 \text{ ft} \qquad \text{(Ref. 6)}$$

$$U_o = 202 \text{ ft/sec}$$

$$U_s + W = \text{WOD} = 52 \text{ ft/sec}$$

$$\text{Ideal } \beta_o = \frac{5.15}{\frac{\sigma(V_I)}{\sigma(h_R)} + 0.641} = 4.1^\circ$$

3. Computation of margins

$$(h_R)_M = \bar{h}_R = \bar{x}_{TD}\beta_{o_{(ideal)}}$$

$$= 234\left(\frac{4.1}{57.3}\right) = 16.77 \text{ ft}$$

$(V_I)_M$ not required for ideal β_o (since $P_{h_R} = P_{V_I}$)

$(x_{TD})_M$ = distance from intended touchdown point to last wire

= 60 ft (Ref. 6)

4. Computation of probabilities

a. Probability of h_R not exceeding $(h_R)_M$ in any given pass is $(1 - P_{h_R})$

$$(1 - P_{h_R}) = F\left[\frac{(h_R)_M}{\sigma(h_R)}\right]$$

$$= F[3.29]$$

$$= 0.99949$$

b. Probability of V_I not exceeding $(V_I)_M$ in any given pass is $(1 - P_{V_I})$, where

$$(1 - P_{V_I}) = (1 - P_{h_R}), \text{ see Step 2}$$

c. Probability of x_{TD} not exceeding $(x_{TD})_M$ is $(1 - P_{x_{TD}})$

$$(1 - P_{x_{TD}}) = F\left[\frac{(x_{TD})_M}{\sigma(x_{TD})}\right]$$

$$\sigma(x_{TD}) \doteq \frac{1}{\beta_o}\,\sigma(h_{TD})$$

$$\doteq 4.74\,\frac{57.3}{4.1}\,\frac{\text{rad}}{\text{deg}} = 66 \text{ ft}$$

$$(1 - P_{x_{TD}}) = F(0.91)$$

$$= 0.819$$

5. Computation of maximum arrest rate per pass (P_L), assuming ideal LSO, i.e., $(h_{LSO})_M \doteq 0$

$$P_L = (1 - P_{h_R})(1 - P_{V_I})(1 - P_{x_{TD}})$$
$$= (0.99949)^2(0.837)$$
$$= 0.837$$

6. Computation of minimum number of required passes per landing ($P_{P/L}$)

$$P_{P/L} = \frac{1}{P_L} = 1.22$$

7. Minimum number of bolters and waveoffs per landing ($P_{B,W}$)

$$P_{B,W/L} = 1 - P_{P/L}$$
$$= 1 - 1.22$$
$$= 0.22$$

8. Computation of accident rate per landing due only to $\sigma(h_R)$ and $\sigma(V_I)$ dispersions ($P_{A/L}$)

$$P_{A/L} = \left\{1 - \left[(1 - P_{h_R}P_{h_{LSO}})(1 - P_{V_I}P_{V_{LSO}})\right]\right\}P_{P/L}$$
$$\doteq \left(P_{h_R}P_{h_{LSO}} + P_{V_I}P_{V_{LSO}}\right)P_{P/L}$$

Assume $$P_{h_{LSO}} = P_{V_{LSO}} = 0.1$$

(i.e., assumed is that pilot and LSO waveoffs effectively prevent 90 percent of each type of potential accident)

Then for $P_{h_R} = P_{V_I}$

$$P_{A/L} = 0.2\, P_{h_R}P_{P/L}$$
$$= 0.2(0.00051)(1.22)$$
$$= 1.25 \times 10^{-4}$$

In general, for relative assessment of competing systems,

$$\frac{P_{A/L}\ _{\text{System 1}}}{P_{A/L}\ _{\text{System 2}}} = \frac{\left[(P_{h_R}P_{h_{LSO}} + P_{V_I}P_{V_{LSO}})(P_{P/L})\right]_{\text{System 1}}}{\left[(P_{h_R}P_{h_{LSO}} + P_{V_I}P_{L_{LSO}})(P_{P/L})\right]_{\text{System 2}}}$$

and if assumed that

$$P_{h_{LSO}} = P_{V_{LSO}} = K$$

i.e., the LSO function is independent of the landing dispersion functions, then

$$\frac{(P_{A/L})_{\text{System 1}}}{(P_{A/L})_{\text{System 2}}} = \frac{\left[(P_{h_R} + P_{V_I})(P_{P/L})\right]_{\text{System 1}}}{\left[(P_{h_R} + P_{V_I})(P_{P/L})\right]_{\text{System 2}}}$$

and with ideal β_o (i.e., $P_{h_R} = P_{V_I}$)

$$\frac{(P_{A/L})_{\text{System 1}}}{(P_{A/L})_{\text{System 2}}} \doteq \frac{(P_{h_R}P_{P/L})_{\text{System 1}}}{(P_{h_R}P_{P/L})_{\text{System 2}}}$$